

# High-Power Laser Propagation: Thermal Blooming

DAVID C. SMITH, MEMBER, IEEE

*Invited Paper*

**Abstract**—This paper presents a tutorial review of the self-induced thermal distortion of laser radiation propagating in absorbing media. The distortion of the laser beam is the result of heating of the path by absorption of a small fraction of the laser beam power by the medium which changes the index of refraction and therefore distorts the beam. Thermal-blooming effects can limit the laser powers which can be effectively propagated through the atmosphere, or in media which absorb laser power such as industrial or laboratory environments, liquid or gas cells, or even laser active media themselves. In this paper, we review the steady-state thermal blooming of CW beams including laboratory-simulation experiments and computer-code results. The thermal distortion of pulsed-laser radiation is also covered including single-pulse thermal distortion and the distortion of a train of laser pulses. In these discussions, we derive and identify the scaling laws and determine the important nondimensional parameters so that the results can be interpreted and applied to other propagation conditions. The thermal-blooming problem can be complicated by a number of circumstances, such as the geometry of the propagation path, and these special cases are also reviewed. Among those covered are: the influence of stagnation zones, transonic flow, the kinetic cooling effect, molecular and aerosol absorption and relaxation, laser-beam jitter, and atmospheric turbulence. In addition, the techniques utilized to minimize blooming, such as laser-beam shaping, and adaptive-optics phase correction, are also discussed.

## I. INTRODUCTION

HERMAL BLOOMING of laser beams is the result of the nonlinear interaction of laser radiation with the propagation path which is heated by absorption of a fraction of the radiation itself. The term thermal blooming, was initially applied to the expansion or "blooming" of a CW beam propagating in a stationary liquid, but the term is now generally used to describe all self-induced thermal distortion of laser radiation. Most interest in thermal blooming stems from the desire to propagate laser-radiation energy through the atmosphere. Even though the attenuation by the atmosphere can be low in the so-called atmospheric windows, the thermal distortion can still be severe for sufficiently high laser powers. Since the distortion depends on the laser-beam intensity itself, there will always be thermal distortion in the atmosphere for sufficiently intense laser beams.

When a laser beam is propagated through a medium, a fraction of the laser energy is absorbed by the medium. This absorbed power heats the medium and alters the index of refraction of the path, and leads to a distortion of the beam itself. This is thermal blooming. There are many different types of thermal blooming, but generally the steady-state blooming can be characterized by the form of heat transfer which is balancing the absorbed laser power. Steady-state blooming can involve the distortion which arises from index changes when the laser power absorbed is balanced by thermal conduction, natural convection, or forced convection due to transverse flow or beam motion. Thermal conduction is

generally a poor form of heat transfer, and results in rather severe distortion of the beam. If sufficient time exists to establish natural convection, and the heating is sufficient, buoyancy or natural convection can transport away the absorbed laser power. This problem is somewhat complicated by the interaction of the buoyant forces and the fluid mechanics of the flow. For viscous materials the convection is determined by a balance between viscous drag and buoyancy. For less viscous materials, i.e., most gases, the balance is between the inertial force of convection and buoyancy.

By far the most important CW case occurs with the wind-dominated condition or beam motion relative to the air caused by slewing. In this case the distortion of CW laser beams takes on a characteristic shape which has become associated with thermal distortion. The beam forms a crescent-shaped pattern with the narrow portion of the crescent in the wind direction and more spreading in the direction transverse to the wind. The intensity pattern is bent into the wind as a result of the thermal distortion. The geometry of wind-dominated blooming and an actual photograph of a distorted beam pattern are shown in Fig. 1. The strength of the distortion is characterized by the parameter  $N$  which will be discussed in detail. These qualitative observations can be explained in terms of the density gradients set up by the absorption. As the wind moves through the beam, the temperature increases because of the absorption. In steady state, the density of the air decreases as the air moves across the beam. Light is refracted toward the more dense medium since the speed of light is least there; this explains the refraction of the beam into the wind. For a bell-shaped intensity contour the downwind portion of the beam will be refracted into the upwind portion; this tends to narrow the beam profile in the wind direction. The gradients in temperature transverse to the wind for the general bell-shaped contour all decrease outward and cause the beam to spread symmetrically about the axis, parallel to the wind, and centered on the beam. This gives a qualitative explanation of CW blooming in a wind-dominated case.

One question often asked concerning thermal blooming is the laser-wavelength scaling. Based on experimental observations and computer-code results, we find that the wavelength appears in two ways: 1) the ability of focus, i.e., the Fresnel number, and 2) the absorption of the atmosphere. The Fresnel number dependence is really the size of the beam or the geometric focusing capability and not really diffraction effects *per se*. (The exception to this is the collimated-beam, large-Fresnel-number case which will be discussed later). The atmospheric absorption dependence on laser wavelength is most important. Lasers for propagation through the atmosphere are chosen to lie in an atmospheric window as depicted in Fig. 2 [1]. Even though transmission is good, the distortion depends critically upon how much is absorbed; even 1 part per million per centimeter (ppm/cm) can cause severe distortion for kilowatt power levels. The absorption has significant

Manuscript received November 30, 1976; revised May 26, 1977.

The author is with the United Technologies Research Center, East Hartford, CT 06108.

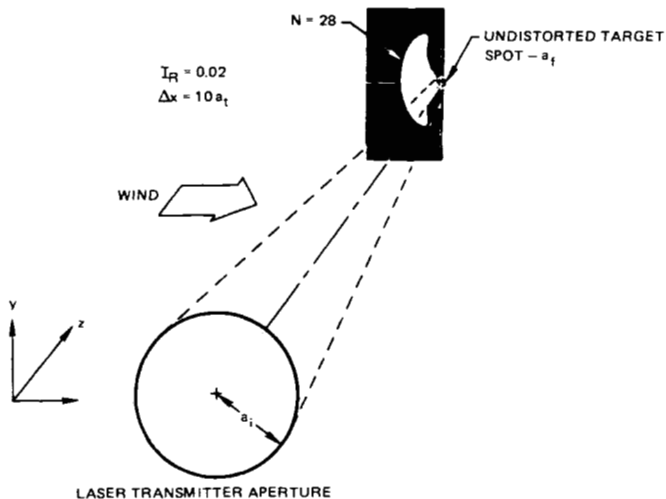


Fig. 1. Schematic diagram of the thermal blooming of a CW laser beam with transverse flow and slew. The intensity contour in the focal plane is an actual contour obtained in laboratory simulation experiments.

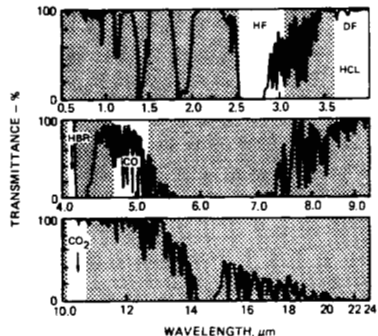


Fig. 2. Broad-band atmospheric transmission as a function of wavelength from [1]. Data was taken over a 10-km path; the light sections denote the wavelength ranges where there are potential high-power lasers.

structure as demonstrated by the numerical modeling of McClatchey and Selby [2] as shown for the 3–5  $\mu\text{m}$  in Fig. 3; the location of some DF chemical laser lines are also shown in the Fig. 3 [3]. Measurements have confirmed this structure. The  $\text{CO}_2$ -laser radiation, a very important, high-power, and efficient laser, is subject to less structure in the atmospheric absorption, the dominant absorbers being  $\text{CO}_2$  molecules and water vapor. For atmospheric conditions designated as mid-latitude summer and the P(20)  $\text{CO}_2$  vibrational-rotational transition, the absorption is  $2.4 \times 10^{-6} \text{ cm}^{-1}$  with  $0.8 \times 10^{-6} \text{ cm}^{-1}$  due to  $\text{CO}_2$  and the remainder due to water [3].

One avenue for overcoming thermal distortion is to use a short-duration laser pulse. Even if the kinetics of the absorption are instantaneous, and the absorbed power is converted into translational energy, it takes a finite time to change the density of the propagation path. This time is associated with the acoustic transit time across the beam. Thus laser pulses whose duration is shorter than the acoustic transit time across the beam suffer less distortion than those whose duration is longer and contain the same energy. This short-pulse distortion is referred to as  $t$ -cubed blooming since the distortion is found to increase as the cube of the laser-pulse duration. For atmospheric transmission we are tempted to make the pulse as short as possible to avoid thermal blooming and thus transmit

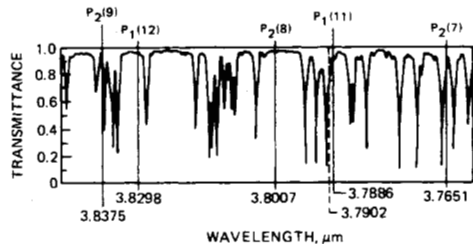


Fig. 3. High resolution transmission from [2] in the wavelength regime of the DF chemical laser showing the significant structure in atmospheric absorption. Some of the DF laser transitions are also shown from the spectroscopic data [3].

a given laser-pulse energy without suffering thermal distortion. However, another nonlinear problem is encountered called gas breakdown, which is a function of the laser-beam intensity. Breakdown is the ionization of the air path because of the interaction of the intense radiation with the gas, and leads to almost total laser-beam absorption. Thus for a fixed energy flux the shortness of the pulse is limited by the threshold for gas breakdown. For microsecond-duration pulses this limit is of the order of a  $10\text{J/cm}^2$  for  $10.6-\mu\text{m}$  wavelength laser sources propagating in realistic atmospheres [4]. Gas breakdown is another severe propagation problem which will be reviewed in a subsequent article [5]. Short laser pulses can reduce the influence of thermal blooming, but the shortness of the laser pulse required to transmit a given laser energy is limited by other considerations. Thus an obvious ploy is to use multiple-pulse lasers where each pulse is sufficiently long to avoid gas breakdown, and sufficiently short to minimize the individual pulse blooming. The repetition rate is then determined by the limits of thermal blooming caused by overlap or the residual heating due to previous pulses. In this article, we examine the problem of multiple-pulse thermal blooming where each pulse itself is not bloomed but the residual effect of previous pulses can cause blooming of subsequent pulses. This problem is complicated by the effects of strong focusing or laser-beam slewing where the clean-out of the density gradients of previous pulses is strongly dependent on the position along the propagation path. The distortion of multiple pulse lasers thus depends on the focusing and slew rates.

There are many extenuating circumstances that can influence the thermal blooming of high-power laser beams. These include the kinetics of the laser absorption, the effects of atmospheric turbulence, laser-beam jitter, as well as particular circumstances of the propagation path, such as stagnation zones or regions of zero relative velocity between the beam and the atmospheric path, as well as transonic flow where shock waves or large density changes are possible due to heat addition. Most of these areas have been investigated and are also discussed in this article. Of particular significance for  $\text{CO}_2$ -laser radiation propagation through the atmosphere is the potential for kinetic cooling where the absorption of laser-beam power leads to the cooling of the atmosphere with the potential for thermally induced focusing, as opposed to thermally induced blooming.

Kinetic cooling is a transient effect which can be important in a number of cases involving atmospheric propagation of  $\text{CO}_2$  laser radiation [6]–[10]. (The kinetics of the absorption, both molecular and aerosol, may be important for other high-power laser transitions, but the cooling effect appears to be unique to the  $\text{CO}_2$  laser).

The kinetic cooling occurs when CO<sub>2</sub> molecules in the atmosphere absorb the 10.6-μm wavelength radiation (the inverse of the laser transition), and the absorbed energy is stored in the 001 CO<sub>2</sub>-vibrational level and the ν = 1 first vibrational level of N<sub>2</sub> manifold. The lower absorbing level is repopulated by equilibrating collisions with CO<sub>2</sub> ground-state atoms at the expense of translational energy, thereby cooling the gas. This cooling lasts until the laser energy, which was absorbed and stored in the upper level, relaxes, via collisions, to the ground state and heats the gas. This collisional-relaxation time is critically dependent on altitude (pressure) and composition of the atmosphere, particularly water vapor [10]. Typical kinetic cooling times range from several milliseconds at sea level to several tenths of seconds above 10-km altitude (see [6, Fig. 4]). In order for the kinetic cooling effect to be important, this time must be long compared to the time required to transport the air across a beam diameter, i.e., a characteristic thermal distortion time. Under these conditions, beam focusing can occur as shown in the theoretical calculations of Wallace and Camac [7] resulting from the cooling and density increase as demonstrated experimentally by Gebhardt and Smith [8] and Sica [10]. Kinetic cooling is one of the few examples where atmospheric propagation effects can be used to advantage.

A brief historical review of the early work on thermal blooming is appropriate. The early investigations of blooming were concerned primarily with low-power visible laser radiation interacting with absorbing liquids. In the mid 1960's the papers on thermal blooming were mostly reports of qualitative observations and defining the problem in terms of heat-transfer mechanisms and time regimes. References [11]–[27] represent some of the earlier papers on thermal blooming. One of the first reports on thermal blooming was that of Leite *et al.* in 1964 [11] where they reported the thermal distortion caused by various liquids inserted in the cavity of a He-Ne laser. They used the effect to measure the absorption coefficient of liquids, pointing out a practical use of the effect. Gordon *et al.* [12] presented a theoretical description of the transient behavior of thermal blooming in liquids with thermal conduction as the dominant heat transfer mode. Leite *et al.* [14] pointed out the nonlinearity of the blooming and of its possible use as a power limiter. The effects of thermal lensing aberrations as well as the derivation of natural convection flows in absorbing liquids was given by Whinnery *et al.* [15]. Inaba and Ito [18] showed photographs of thermally distorted CO<sub>2</sub> laser beams propagated through liquid CS<sub>2</sub>, and showed the crescent-shaped pattern and correctly identified this pattern as due to convection-heat transfer. Akhmanov *et al.* [21] presented a paper where they derived the expression for the angular deflection of a laser beam caused by natural convection. The first thermal distortion of laser radiation with a wind was reported by Gebhardt and Smith [24] with measurements of the beam deflection and decrease in beam intensity as a function of transverse wind velocity. Smith [27] published the first CO<sub>2</sub>-laser thermal blooming in gases with conduction and natural convection, and derived the convection velocity for gaseous absorbers. Since that time, there have been a large number of papers published on thermal blooming and they are more appropriately discussed in the body of the text.

Self-induced thermal distortion is a serious problem for the propagation of high-average power CW, single- and multiple-

pulse-laser radiation through absorbing gases. As an example, with no cross-flow or path conditioning, thermal blooming can cause significant beam spread at a power level of 300 W over a propagation path of 10 m for a linear absorption of 10<sup>-5</sup> cm<sup>-1</sup> (This would correspond to, for example, air contaminated with  $\frac{1}{3}$  ppm SF<sub>6</sub> for the P(20) CO<sub>2</sub>-laser transition). Thus for this example the linear loss of 0.1 percent is hardly measurable, but the blooming loss is important. To emphasize the importance of understanding the blooming, we note that the application of a 5 mi/h cross wind increases the power level where blooming becomes important to 100 kW for the same conditions as above. We will show in this paper the scaling laws for thermal blooming for the different operational modes from which one can determine the importance of this effect for laboratory scale devices, industrial devices for material processing, or applications involving atmospheric propagation. The discussion and experimental data is usually presented for CO<sub>2</sub> lasers, but the nondimensional parameters and conclusions can, in general, be applied to any laser wavelength.

## II. STEADY-STATE PERTURBATION SOLUTIONS

The self-induced thermal distortion is a highly nonlinear problem since the distortion depends on the laser intensity itself. A simple method for determining the magnitude of the effect and a physical feel for the problem is to treat the problem as a perturbation and calculate the thermal distortion based on the original undistorted beam. In this section, several perturbation solutions to the general thermal-blooming problem are treated for the different cases. A convenient division of the thermal-blooming problem is steady state and transient blooming. The steady state is then subdivided into different cases depending on the dominant heat transfer process; conduction, natural convection or forced convection.

In this section, we will present the steady-state-perturbation solution for a collimated beam, ignoring for the time being the effects of diffraction. These types of solutions are of value in obtaining a physical feel for the problem and obtaining an order-of-magnitude estimate of the severity of the effect from nondimensional analysis.

### A. Governing Equations

From the conservation of energy, the intensity  $I$  is given by

$$\operatorname{div}(\vec{I}\vec{s}) = -\alpha I \quad (1)$$

where  $\vec{s}$  is the unit vector denoting the direction of propagation and  $\alpha$  is the linear loss due to absorption in the medium. The vector  $\vec{s}$  is determined by the index of refraction of the medium through the following equation [28]

$$d/ds(\operatorname{grad} S) = \operatorname{grad} \mu \quad (2)$$

where  $S$  is the eikonal and  $\mu$  is the index of refraction. The eikonal is related to the unit vector  $\vec{s}$  by

$$\mu\vec{s} = \operatorname{grad} S. \quad (3)$$

Equation (1) can be expanded to give

$$\vec{s} \cdot \operatorname{grad} I + I \operatorname{div}(\vec{s}) = -\alpha I. \quad (4)$$

From the definition of  $S$  and (3), we get

$$\operatorname{div} s = \operatorname{div} \frac{\operatorname{grad} S}{\mu}.$$

Substituting into (4), we get

$$\frac{\text{grad } S}{\mu} \cdot \text{grad } I + \frac{I}{\mu} \text{div grad } S = -\alpha I$$

and using (2)

$$\frac{I}{\mu} \int \text{grad } \mu \cdot d\vec{s} \cdot \text{grad } I + \frac{I}{\mu} \text{div} \int \text{grad } \mu \cdot d\vec{s} = -\alpha I.$$

For this particular problem it is convenient to divide the derivatives into axial derivatives, i.e., in the direction of propagation and transverse derivatives.

$$\nabla = \frac{\partial}{\partial z} \hat{z} + \nabla_t \hat{r}$$

and in all cases of interest the integration along a ray  $d\vec{s}$  can be approximated by  $dz'$ ; this is the so-called paraxial-ray approximation and is almost always valid for thermal blooming and similar type problems

$$\int \nabla_t \mu dz \cdot \nabla_t I + \int \nabla_z \mu dz \nabla_z I + \frac{I}{\mu} \int \nabla_t^2 \mu dz = -\alpha I.$$

This equation can be rewritten in integral form

$$\frac{I(r, z)}{I(r, 0)} = \exp \left[ -\alpha z - \int_0^z \left( \nabla_t + \frac{\nabla_t I}{I} \right) \cdot \int_0^{z'} \frac{\nabla_t \mu}{\mu_0} dz'' dz' \right]. \quad (5)$$

This solution gives the change in intensity of an initially collimated beam propagating through a medium with a variable index of refraction. In deriving it, the main assumptions involved were ray optics, neglect (i.e., neglect diffraction effects) of index gradients in the axial direction and the paraxial ray approximation.

The thermal distortion of laser beams arises because the absorbed laser power in the medium changes the index of refraction and therefore changes the beam intensity itself as given by (5). The relationship between absorbed laser power and index of refraction will now be given. The density of the gas is related to the index of refraction by the Dale Gladestone law

$$\mu - 1 = K\rho \quad (6)$$

where  $K$  is a constant for a particular gas and is equal to  $\frac{2}{3}$  the polarizability of the molecule or atom.

The gas density is related to the temperature and pressure through the perfect gas law

$$P = \rho RT \quad (7)$$

where  $P$  is the gas pressure,  $R$  the gas constant, and  $T$  the temperature. The temperature change is determined from the energy-balance equation and for steady state constant pressure case is related by

$$\rho c_p \vec{v} \cdot \text{grad } T - K \nabla^2 T = \alpha I \quad (8)$$

where  $v$  is the gas velocity,  $K$  the thermal conductivity, and  $c_p$  is the specified heat at constant pressure

$$\text{grad } \mu = K \text{grad } \rho = \text{grad } T \left( \frac{\partial \mu}{\partial T} \right) = \text{grad } T \mu_T \quad (9)$$

where  $\mu_T$  is the rate of change of the index of refraction of the gas with respect to temperature at constant pressure. Thus

with the above equations the problem is completely specified in the ray optics limit for steady state thermal distortion.

### B. Thermal Conduction Dominated

For experimental conditions where there is no relative motion between the beam and the gas and no natural convective velocities are established, the steady state solution is determined when the thermal conduction balances the laser power absorbed by the gas. For order of magnitude analysis, equation (8) can be written in the form

$$\rho' c'_p v' \frac{\Delta T}{L'} - \frac{k \Delta T}{L'^2} = \alpha I$$

where the primes denote characteristic values of the parameters. Comparison of the convection term with the conduction term requires that the velocity obey the inequality

$$v' < \frac{k'}{\rho' c'_p L'}$$

in order for thermal conduction to dominate where  $L$  is the characteristic dimension of the problem, normally taken to be the beam radius.

For circularly symmetric beams, the problem has radial symmetry and the temperature is determined by the solution to the energy equation

$$\frac{k}{r} \frac{\partial}{\partial r} \left( r \frac{\partial T}{\partial r} \right) = \alpha I$$

and from (9)

$$\nabla^2 \mu = \nabla^2 T \mu_T.$$

The perturbation solution of this problem for an initially Gaussian beam was first treated by Smith [27] where the solution is given by

$$I(r, z) = I(r, 0) \exp \left( -\alpha z + \frac{\mu_T P e^{-r^2/a^2} \left( z - \frac{1}{\alpha} (1 - e^{-\alpha z}) \right)}{\pi k \mu a^2} \right).$$

It is convenient to write the intensity in the form

$$I(r, z) = I(r, 0) \exp (-\alpha z - D_c e^{-r^2/a^2}) \quad (10)$$

where

$$D_c = \frac{-\mu_T P}{\pi k \mu a^2} \left( z - \frac{1}{\alpha} (1 - e^{-\alpha z}) \right) - \frac{-\mu_T P \alpha z^2}{2 \pi k \mu a^2}, \quad \alpha z \ll 1. \quad (11)$$

For most gases and solids  $\mu_T$  is negative and thus the thermal distortion causes a decrease in the on-axis intensity as the beam is propagated through the medium. Some materials have a positive  $\mu_T$  and thus the beam is focused by the medium. Examples of material with positive  $\mu_T$  are germanium and water below 4°C. The nondimensional parameter  $D_c$  determines the magnitude of the thermal distortion and fully characterizes the thermal blooming for the collimated beam. The parametric behavior of the thermal blooming of CO<sub>2</sub>-laser radiation in gases has been examined by Smith, and Fig. 4 shows the radial profile obtained as well as a schematic of the experimental apparatus. Smith also examined the dependence of the thermal blooming on path length, absorption coefficient, and laser power, and showed qualitative agree-

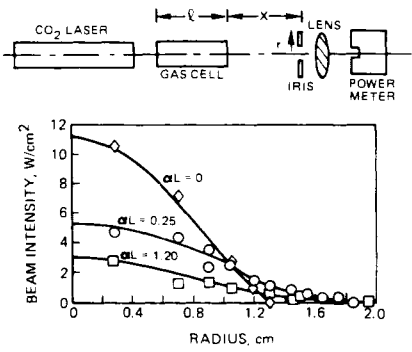


Fig. 4. Schematic of the experimental apparatus and data showing the steady-state thermal blooming caused by conduction and natural convection heat transfer. In the lower part, the intensity contours are shown as a function of the absorption coefficient of the gas [27].

ment with the theoretical predictions. Because of the buoyancy effect the thermal distortion was influenced by natural convection and Smith also showed this effect.

### C. Natural Convection

The gas heating caused by absorption of laser radiation can lead to buoyancy or natural convection currents; if they are present, the air path will be cooled by the introduction of cooler gases. Akmanov *et al.* [16] showed that natural convection leads to a deflection of the laser beam into the direction of flow, i.e., downwards. Experiments were also reported of natural convection in liquids by Whinnery *et al.* [15]. For the liquid case the natural convection velocity was derived based on a balance between the viscous forces of the liquid and the buoyant force caused by heating. The velocity is of the form

$$v = \frac{\beta g \Delta T_m \pi \omega_0^2}{16 \nu} \quad (12)$$

where  $\nu$  is the liquid viscosity,  $g$  the acceleration of gravity,  $\omega_0$  the laser-beam size,  $\beta$  is the expansion coefficient of the medium, and  $\Delta T_m$  is the maximum temperature rise. For gases, the viscous forces are less important and the natural convection velocity was determined by Smith [27] to be the balance between inertial forces and buoyant forces and is given by

$$v_{NC} = \left( \frac{2\alpha Pg}{\mu c_p T} \right)^{1/3}. \quad (13)$$

The appropriate velocity for order of magnitude estimates of natural convection is determined by the size of the Reynolds number

$$Re = \rho V l / \mu. \quad (14)$$

If the velocity is such that the Reynolds number is greater than one, then inertial forces are more important than viscous forces. Thus an *a priori* check on the buoyant velocity can be made. The thermal distortion caused by natural convection is complicated because the flow is not uniform and must be evaluated point by point in the laser beam. A detailed treatment of this problem was carried out by Livingston [28]. However it has been found that natural convection can be treated as uniform and the distortion predicted is very similar to that encountered by forced convection with the magnitude given by the above derived velocities.

### D. Forced Convection or Wind

The most commonly occurring thermal distortion and the problem that has received the most attention is the thermal distortion of a laser beam propagating in a medium with transverse flow or a slewed beam. For this case the distortion is no longer symmetric because of the asymmetry introduced by the one-dimensional wind velocity or slew motion. For the sake of perturbation analysis we will first treat the problem for a collimated beam with a uniform wind  $v$  in the  $x$ -direction. For this case the energy equation is

$$\rho c_p v \frac{\partial T}{\partial x} = -\alpha I$$

which can be integrated to give

$$T - T_0 = \frac{\alpha}{\rho c_p v} \int_{-\infty}^x I dx' \quad (15)$$

and the intensity expression is given by

$$\frac{I(r, z)}{I(r, 0) \exp(-\alpha z)} = \exp \left\{ \frac{-\mu_T \alpha}{\mu \rho c_p v} \int_0^z \int_0^{z'} \left[ \frac{\partial I}{\partial x} + \frac{1}{2} \frac{\partial^2 I}{\partial y^2} \right. \right. \\ \left. \left. \cdot \int_{-\infty}^x I dx' + \frac{1}{2} \frac{\partial I}{\partial y} \int_{-\infty}^x \frac{\partial I}{\partial y} dx' \right] dz' dz'' \right\}.$$

For an initially Gaussian beam the derivatives and integrals can be evaluated

$$\frac{I(x, y, z)}{I(x, y, 0) \exp(-\alpha z)} = \exp \left\{ \frac{-2I_0 \mu_T \alpha}{\mu \rho c_p v a} \left[ \frac{x}{a} e^{-(x^2+y^2)/a^2} \right. \right. \\ \left. \left. + \frac{\sqrt{\pi}}{2} e^{-y^2/a^2} (1 - 2y^2/a^2)(1 + \operatorname{erf} x/a) \right. \right. \\ \left. \left. \cdot \int_0^z \int_0^{z'} e^{-\alpha z} dz' dz'' \right] \right\} \quad (16)$$

where  $\operatorname{erf}$  is the error function. In keeping with our identification of nondimensional parameters we can write the intensity as

$$\frac{I(x, y, z)}{I(x, y, 0) \exp(-\alpha z)} = \exp \left\{ -N_c \left[ \frac{x}{a} e^{-(x^2+y^2)/a^2} \right. \right. \\ \left. \left. + \frac{\sqrt{\pi}}{2} e^{-y^2/a^2} \left( 1 - \frac{2y^2}{a^2} \right) \left( 1 + \operatorname{erf} \frac{x}{a} \right) \right] \right\} \\ N_c = \frac{-\mu_T I_0 \alpha z^2}{\mu \rho c_p v a} \left[ \frac{2}{\alpha z} - \frac{2}{(\alpha z)^2} (1 - e^{-\alpha z}) \right] \\ \approx \frac{-\mu_T I_0 \alpha z^2}{\mu \rho c_p v a}, \quad \alpha z \ll 1. \quad (17)$$

Plotted in Fig. 5 are the equal intensity contours for a distortion parameter of one. The dashed circle is the undistorted 0.4 initial intensity contour for reference. It is interesting to note that the laser beam has a tendency to focus in the wind direction and spread in the transverse dimension, for a collimated beam in the absence of diffraction effects. Fig. 5 shows that the beam takes on a crescent-shaped pattern which has become associated with thermal distortion and has been observed in many blooming experiments. Shown in Fig. 6 is the relative peak intensity as a function of the distortion

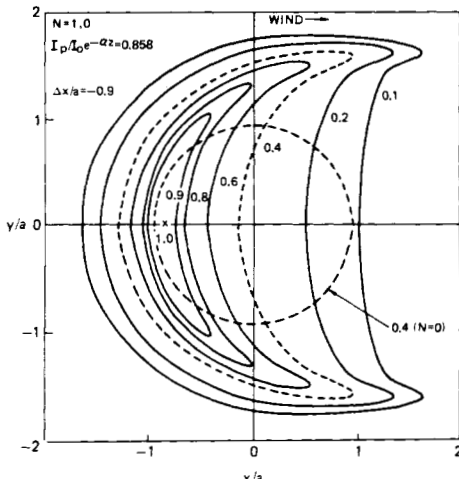


Fig. 5. Equal intensity contours of a steady state CW bloomed beam with a distortion parameter,  $N = 1$ , and the wind incident from the left. The initial Gaussian beam is collimated with the 0.4 intensity contour shown as the dashed circle.

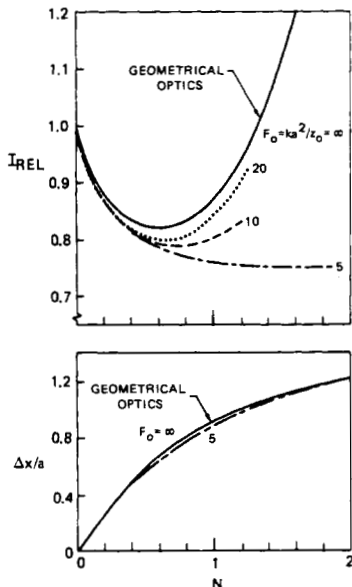


Fig. 6. The relative peak intensity and the deflection of the peak intensity into the wind as a function of the distortion parameter  $N$ . The solid curve is the computer code result neglecting diffraction spreading and the dashed curves, labeled by the Fresnel number, include diffraction spreading. The initial beam is a Gaussian, collimated beam [30].

parameter, where  $I_{REL}$  is the normalized intensity, normalized by the undistorted peak intensity [30]. In addition, the deflection of the peak intensity into the wind  $\Delta x$  normalized with respect to the  $e^{-1}$  radius is also shown. As noted in Fig. 6, the solid curves were calculated with geometrical optics, i.e., neglecting diffraction. The dashed curves were obtained by including diffraction effects as discussed below. In the geometrical optics limit, the theory predicts a caustic or infinite intensity for an  $N$  of  $\sim 2$ ; this caustic is of course prevented by diffraction spreading.

The first experimental evidence of the effects of wind on thermal blooming was presented by Gebhardt and Smith [31] and burn patterns of the distorted profiles obtained in their lab experiments are shown in Fig. 7. With no wind the crescent-shaped pattern is still observed but with a downward shift and is qualitative proof that the distortion caused by natural convection gives rise to the same type of distortion as

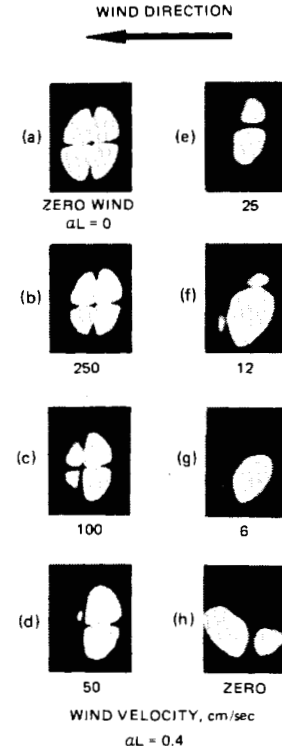


Fig. 7.  $\text{CO}_2$  laser beam burn patterns which show the distortion with varying wind velocities incident from the right [31].

that associated with a uniform wind. Each pattern is labeled by the wind velocity and shows the qualitative effects of wind on the strength of the thermal distortion.

Because of the tendency of the laser radiation to focus in the direction of the wind, diffraction effects will become more important the more severe the thermal distortion. The influence of diffraction was examined experimentally by Gebhardt and Smith [31] in laboratory simulation experiments where a collimated  $\text{CO}_2$  beam was propagated through a liquid cell containing  $\text{CS}_2$  which was translated perpendicular to the direction of propagation. Fig. 8 is a plot of intensity contours through the center of the beam where each is marked by the appropriate Fresnel number; the Fresnel number is a measure of the importance of diffraction and is based on the undistorted beam size and is given by

$$F = \frac{ka^2}{z}$$

where  $k$  is the wavenumber equal to  $2\pi$  divided by the laser wavelength,  $z$  is the path length, and  $a$  the  $e^{-1}$  laser-beam radius for a Gaussian beam. The data in Fig. 8 is for a constant distortion condition with  $N_c \sim 2$ . The dramatic change in thermal distortion with Fresnel number is obvious. The relative intensity and beam deflection for a series of experiments is shown in Fig. 9 where the data is plotted as a function of the distortion parameter  $N_c$  and each curve is marked by the initial Fresnel number. For large Fresnel numbers and a distortion parameter less than two, the agreement between the geometric-optics theory and experiment is very good. For the smaller Fresnel number cases the agreement is poor for severe distortion conditions. It is interesting to note that the beam deflection of the peak intensity is relatively insensitive to the Fresnel number as shown in Fig. 9(b).

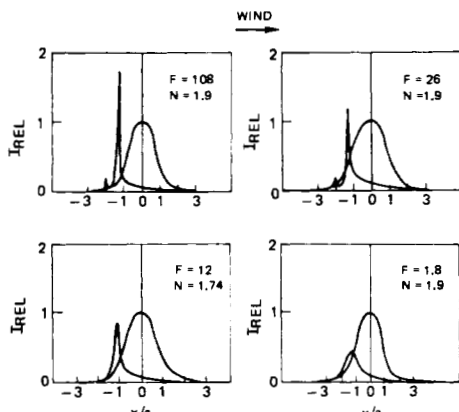


Fig. 8. Relative intensity contours taken through the center of the laser beam parallel with the wind direction with each contour labeled by the Fresnel number based on the initial Gaussian beam radius: the distortion number for all the cases was  $N_c \sim 2$  [30].

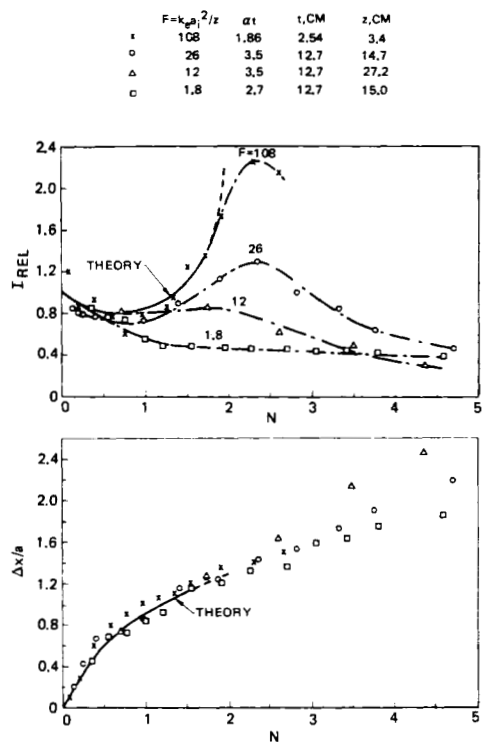


Fig. 9. The relative on axis intensity as measured experimentally as a function of the distortion parameter  $N_c$  and the Fresnel number. In the lower half the deflection of the peak intensity, normalized with respect to the  $e^{-1}$  initial beam radius is plotted as a function of  $N_c$ . The laser used in the experiments was CO<sub>2</sub>, and the absorbing medium was carbon disulfide [30].

For large Fresnel numbers ( $F > 20$ ) we see that the intensity actually increases with increased distortion for  $N > 2$ . This is the result of the focusing effect in the direction of the wind. For the very large initial Fresnel number cases, the degree of focusing in the wind direction is sufficient to overcome the transverse spreading and therefore the intensity is increased. A similar type of observation was made by Hull [32] where he used a visible laser beam in his blooming experiments. However, the intensification was observed at much lower Fresnel numbers than by Gebhardt and Smith, and this discrepancy remains unresolved. The data in Figs. 8 and 9 are of collimated beams and show that the effects of diffraction must be taken into account in calculating the thermal blooming.

Referring to Fig. 6, we see that the computer code results of Gebhardt and Smith [30] taking into account diffraction effects for the collimated-beam case, did predict, qualitatively, the experimental results shown in Fig. 9. For a focused beam, which is the most common situation, the influence of diffraction will be more important. The wave optics calculations of the thermal distortion of a CW beam with wind is discussed in detail in a following section.

#### E. Distortion Parameter for Focused and Slewed Laser Beam

The distortion parameter  $N_c$  for the collimated beam can be modified to take into account the effects of focusing and the influence of a variable wind velocity caused by beam slewing. This can be done by performing the double integration with respect to path length, taking into account both the variable beam size and wind or relative motion between the beam and the air. Again this modified  $N$  is derived based on a perturbation analysis where the distortion of the laser beam is calculated based on the initial undistorted profile.

The nondimensional distortion parameter in integral form is

$$N = N_c \left\{ \frac{2}{z^2} \int_0^z \frac{1}{Q(z')} \int_0^{z'} \frac{e^{-\alpha z''}}{\Omega(z'') Q^2(z'')} dz' dz'' \right\}$$

where  $Q(z)$  is the focusing factor equal to the beam radius at  $z$  divided by the initial beam radius  $a$ ; and  $\Omega$  is the transverse velocity at  $z$  divided by the initial velocity. We will approximate the focusing by the function

$$Q(z) = 1 - (1 - a_f/a_i) z/z_f$$

where  $z_f$  is the focus and  $a_f$  is the focal spot radius. This expression is valid within a few percent for large  $a_i/a_f$ . The distortion parameter for the focused beam,  $\alpha z \ll 1$  and uniform wind is

$$N_f = N_c (a_i/a_f) q (a_i/a_f)$$

where

$$q = \frac{2a_i/a_f}{(a_i/a_f - 1)} \left[ 1 - \frac{\ln a_i/a_f}{(a_i/a_f - 1)} \right].$$

In the range of Fresnel numbers from 1 to 10,  $q$  varies only from 1 to 1.6. In effect, then, focusing increases the distortion by the ratio of the strength of the focusing.

For a slewed laser beam the function  $\Omega(z)$  can be represented by

$$\Omega(z) = 1 + \frac{\omega}{v_0} z$$

where  $\omega$  is the slew rate and  $v_0$  is the initial velocity at the aperture.  $N$  for the slewed beam can also be calculated if we assume a collimated beam and again for  $\alpha z \ll 1$

$$N_\Omega = N_c \frac{2}{(v_f/v_i - 1)^2} \left[ \frac{v_f}{v_i} \ln \frac{v_f}{v_i} - \left( \frac{v_f}{v_i} - 1 \right) \right]$$

where  $v_f$  is the velocity transverse to the beam at the target. If we evaluate  $N$  for a velocity equal to the half-way point,  $N$  varies from this effective  $N$  from 1 to 3 as the ratio of  $v_f/v_i$  varies for 1 to 50. For qualitative estimates then slewing can be accounted for by using the velocity at the half-way point between the aperture and the target.

Each correction to  $N_c$  due to focusing, slewing, and the effect of finite  $\alpha z$  have been derived independent of the other

two. We will show that for most applications we can scale the thermal distortion by the single parameter  $N$ , consisting of the multiple of the correction factors.

$$N = N_c(a_i/a_f)q(a_i/a_f)f(v_f/v_i)g(\alpha z) \quad (18)$$

with

$$\begin{aligned} q &= \frac{2 a_i/a_f}{(a_i/a_f - 1)} \left[ 1 - \frac{\ln a_i/a_f}{(a_i/a_f - 1)} \right] \\ f &= \frac{2}{(v_f/v_i)^2} [v_f/v_i \ln v_f/v_i - (v_f/v_i - 1)] \\ g &= \frac{2}{\alpha z} \left[ 1 - \frac{1 - e^{-\alpha z}}{\alpha z} \right]. \end{aligned}$$

### III. WAVE OPTICS TREATMENT OF THERMAL BLOOMING

In the previous section the thermal distortion for a collimated beam with transverse wind neglecting diffraction effects was presented. A caustic was predicted by the geometric optics because of the focusing effects of the thermal lens in the direction of the wind. The presence of a caustic is counterbalanced by the effects of diffraction, and in order to predict the thermal distortion for distortion conditions greater than  $N$  equal to 2 (where the caustic occurs), it is required that the solution include the finite wavelength effects. (Reference [30] showed the importance of diffraction for collimated beams, but the numerical calculations were limited to small-distortion conditions.)

For the steady-state blooming with transverse wind, the energy equation and relationship of the index of refraction with density are of the same as before, equations (6) and (8). The relationship between the intensity and the index of refraction are written in the form

$$\begin{aligned} (\nabla S)^2 &= \mu^2 + \nabla^2 A/k^2 A \\ (2\nabla A \cdot \nabla S)/A + \nabla^2 S &= -\mu\alpha \end{aligned} \quad (19)$$

where the complex representation of the electric field has been assumed to be of the form

$$U = A \exp(i k S) \quad (20)$$

these equations are exact and involve no simplifying assumptions. The following assumptions are made in order to solve the problem numerically for the thermal blooming

$$\begin{aligned} \mu &= \mu_0 + \delta\mu \\ S &= \mu_0(z + \phi) \\ \frac{\partial}{\partial z}, \delta\mu, \text{ and } \phi &\approx 0. \end{aligned} \quad (21)$$

With these assumptions the two equations can be written in the following form

$$\left( \frac{\partial}{\partial z} + \vec{\theta} \cdot \nabla_t \right) \vec{\theta} = \frac{\nabla_t \mu}{\mu_0} + \frac{1}{4k^2 \mu_0^2} \nabla_t \left[ \frac{\nabla_t^2 I}{I} - \frac{1}{2} \left( \frac{\nabla_t I}{I} \right)^2 \right] \quad (22)$$

$$\frac{1}{I} \frac{\partial I}{\partial z} + \frac{\vec{\theta} \cdot \nabla_t I}{I} + \nabla_t \cdot \vec{\theta} = -\alpha. \quad (23)$$

The diffraction term is the second term on the right hand side in (22), and represents a force term which tends to bend the rays outward and spread the beam.

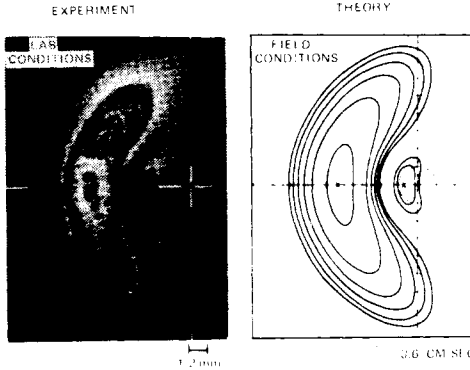


Fig. 10. Comparison of laboratory [36] and computer code results [35] under closely matching dimensionless scaling conditions. The equal intensity contours from the computer code are for 0.09, 0.14, 0.23, 0.36, 0.57, and 0.9 times the peak and the distortion parameter given by (18) is 16. In the laboratory scaled experiments, the Kalvar film photograph shows an inner bright contour which is roughly 0.5 times the peak irradiance and the distortion parameter is 13.

Numerical techniques to solve this problem have been applied by a number of authors [33]. At present computer codes have been developed by a number of authors for predicting the combined effects of diffraction and thermal blooming. The codes have been refined to such an extent as to take into account arbitrary initial intensity profiles and phases, slewing of the laser beam, as well as atmospheric turbulence combined with thermal distortion.

One of the first computer codes was developed by Wallace [34]. A more sophisticated code with more accurate predictions was developed by Bradley and Hermann [35] involving highly sophisticated numerical techniques to eliminate the problem of boundary reflections caused by numerical techniques as well as a coordinate system which was tailored to the distorted intensity pattern. These techniques result in computer computation with a high degree of reliability and were corroborated by experimental data. Shown in Fig. 10 is a comparison of the numerical results of Bradley and Hermann [35] with the experimental results of Gebhardt and Smith [36]. The conditions for the experiment and calculations were very similar and comparison of the intensity contours show excellent agreement.

Hayes *et al.* [37] compared the result of their wave-optics code with the results of Smith and Gebhardt [38] over a wide range of thermal distortion conditions and showed good agreement. Shown in Fig. 11 is the comparison of the peak intensity predicted by this numerical model with the experimental results. In Fig. 11,  $I_{REL}$  is the normalized peak intensity, normalized with respect to the undistorted value.

Fleck, Morris, and Feit [39] have recently completed a numerical analysis of the thermal distortion with a 4-D code incorporating both the three coordinate dimensions as well as transient effects. This sophisticated code can account for not only transient effects of multiple-pulse blooming, but also the transient behavior of thermal distortion due to stagnation zones and the effects of transverse flow. These effects are discussed in the following section.

The numerical results of the thermal distortion of the peak focal plane intensity as a function of laser power are shown in Fig. 12. The results point out very dramatically the influence of the nonlinearity of the propagation effects and point out the concept of a critical laser power for fixed propagation conditions. In the absence of thermal blooming, the intensity in

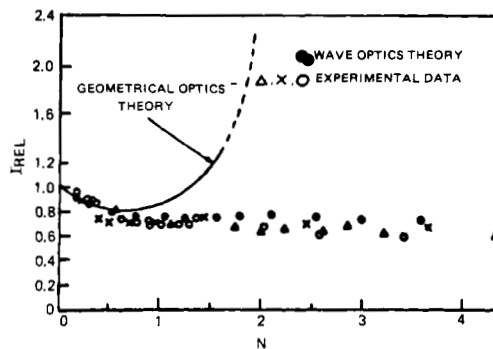


Fig. 11. Comparison of experimental laboratory data with computer code calculations of the thermal distortion [37]. The peak intensity, normalized by the undistorted peak, is plotted as a function of the nondimensional parameter,  $N$ , which was varied in the experiment by changing laser power and in the wave optics code by varying the wind speed.

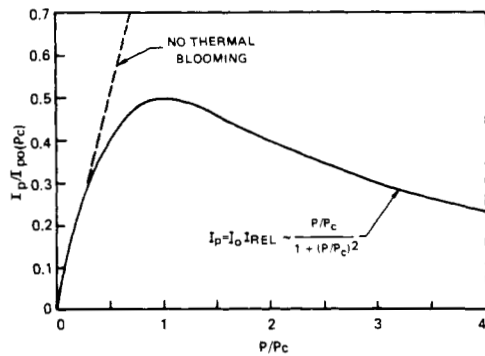


Fig. 12. Peak intensity as a function of laser power showing the non-linearity of thermal distortion and the concept of a critical power. The dashed line is the peak intensity as a function of power in the absence of blooming.

the focal plane increases linearly with increased laser power as shown by the dotted line in Fig. 12. Because of the nonlinearity of thermal blooming, the intensity in the focal plane reaches a maximum as a function of increased laser power. We have the concept of a critical laser power  $P_c$ , where the intensity reaches a maximum value, and for laser power above this value, the thermal distortion causes a decrease in the absolute intensity deliverable to the focal plane. The numerical results shown in Fig. 12 have been substantiated by laboratory simulation experiments.

Shown in Fig. 13 is a compilation of computer calculations for a wide variety of propagation conditions and laser beam shapes as a function of the single distortion parameter  $N$  as calculated by Gebhardt [40]. Table I identifies the initial conditions assumed in the computer calculations. Also shown in Fig. 13 is the empirical fit to the infinite Gaussian data using the single distortion parameter,  $N$  to characterize the distortion. A general trend in the data is also noted. There is less distortion for truncated Gaussians and even less for an initially uniform intensity beam than that suffered by the infinite Gaussian. In calculating  $N$  for beams other than Gaussian an assumption must be made concerning the proper beam size. For the clipped Gaussian, the radius of the aperture was  $2a_0$  and also for the uniform intensity profile where  $a_0$  is the beam radius used in calculating  $N$ . The donut mode was taken to be of the form  $I = [e^{-(r/D)} - e^{-(3.5r/D)}]^2$  where the beam radius now equals  $D/2\sqrt{2}$  and the beam was truncated at  $D$ .

SEE TABLE I FOR IDENTIFICATION OF SYMBOLS

- △ — ETC. — UNIFORM BEAM
- × — ANNULAR GAUSSIAN
- △ — ETC. — CLIPPED GAUSSIAN
- — INFINITE GAUSSIAN

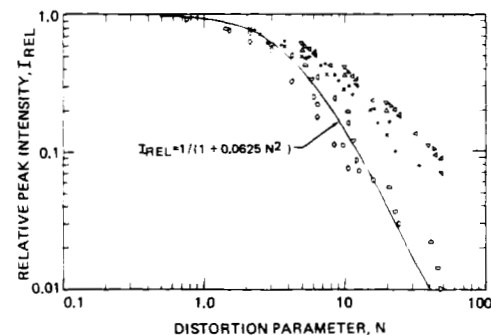


Fig. 13. Wave optics computer code results showing the relative peak intensity as a function of distortion parameter for various laser beam shapes: △—uniform, ×—annular, △—clipped Gaussian, ○—infinite Gaussian. The conditions for the calculations are given in Table I. The solid curve is an empirical fit to the code data [40].

TABLE I  
COMPUTER CODE INPUT DATA FOR THE RESULTS SHOWN IN FIG. 13

SYMBOL —NO.	BEAM SHAPE	$\beta$	$\lambda$	$D$	$\omega v_0$	$z$	$a$	$\epsilon$	$F$	$N_A$	$N_\omega$
△ -1	UNIFORM	3.34	3.8	0.8	2.38(-5)	1.6	0.039	7.76(-7)	25	0.1	3.8
△ -2		1.63	10.6	1.0	2.38(-5)	1.6	0.36		28	0.6	3.8
△ -3		4.79	3.8	0.8	0.37(-5)	4.0	0.084		7	0.7	1.5
△ -4		1.63	10.6	0.5	2.38(-5)	1.6	0.36		7	0.6	3.8
▽ -5		1.63		2.0					112	0.6	3.8
△ -6		2.76		2.0					66	0.6	3.8
△ -7		1.19		0.5					8.6	0.6	3.8
-8	DONUT	3.34	3.8	0.8			0.039		25	0.1	3.8
+ -9		1.63	10.6	1.0	0.37(-5)		0.36		28	0.6	3.8
* -10		4.79	3.8	0.8		1.0	0.094		7	0.7	1.5
○ -11	CLIPPED GAUSSIAN	1.0	10.6	1.57(-2)	8(-2)	11(-3)	4(+2)	9(+4)	18	0.4	8
○ -12		1.19		0.5	2.38(-5)	1.6	0.36	7.76(-7)	9.6	0.6	3.8
○ -13		1.63		1.0		1.6	0.36		28	0.6	3.8
○ -14		2.76		2.0		1.6	0.36		66	0.6	3.8
○ -15	INF. GAUSSIAN	1.0		1.57(-2)	8(-2)	11(-3)	4(+2)	9(+4)	18	0.4	8
○ -16		1.0		0.91(-2)	8(-2)	11(-3)	4(+2)	9(+4)	6	0.4	8

$\beta$  — BEAM QUALITY FACTOR  
 $\lambda$  — WAVELENGTH, MICRONS  
 $D$  — APERTURE DIAMETER, m ( $\approx 2\sqrt{2}a$ )  
 $\omega$  — SLEW RATE, RADIANS/SEC  
 $v_0$  — VELOCITY, CM/SEC  
 $z$  — RANGE, UM  
 $a$  — ABSORPTION COEFFICIENT, KM<sup>-1</sup>

$$\epsilon = \frac{\alpha}{\sigma T} \frac{1}{AD^2 v_0} \cdot \text{cm}^2/\text{W}$$

$$z = 1/4 \text{ GAUSSIAN INTENSITY RADIUS}$$

As can be seen in Fig. 13, each set of data for a particular beam shape follows a smooth function of the distortion parameter  $N$ . Thus for each shape it is possible to find an analytic expression similar to the one shown in Fig. 13 for the infinite gaussian. For the uniform intensity beam a good fit is found to be  $I_{REL} = (1 + 0.01 N^{1.2})^{-1}$  with the diameter of the aperture given by  $2a$ . We also note from the figure that the single parameter  $N$  shows little additional dependence on slew number, Fresnel number, or absorption number for the range of these parameters shown in Table I.

In summary, it appears that the numerical techniques developed to predict the thermal distortion of high-power laser radiation of CW laser beams are adequate for predicting the intensity that can be achieved in the focal plane of the laser. These predictions are for steady-state blooming in a uniform wind or slewed beams and are applicable for a wide variety of laser-beam conditions including infinite Gaussian, truncated Gaussian profiles, uniform intensities, and unstable resonator output beams. Certain conditions that could be encountered such as stagnation zones, transonic slewing conditions, the combined effect of blooming and turbulence, or blooming and beam jitter will be discussed in subsequent sections.

#### IV. LABORATORY SIMULATION EXPERIMENTS OF CW THERMAL BLOOMING

##### A. Scaling

In this section, we will describe the laboratory conditions which must be met in order to simulate atmospheric propagation of high intensity CW laser beams. Based on the perturbation solution, the distortion parameter  $N_c$  is the most important simulation parameter. We also derived modified versions of this parameter for large  $\alpha z$ , the influence of focusing and the effects of slewing or nonuniform transverse wind. It is not at all clear that the one single distortion parameter can be used, and for exact simulation it is required that these parameters be simulated separately and equally.

These nondimensional parameters are as follows:

$N_c$	distortion parameter based on initial beam parameters
$F$	$= ka^2/z$ Fresnel number
$\alpha z$	absorption length
$v_f/v_i$	slewing rate.

(24)

Based on the perturbation approach these effects can be combined into a single parameter given by (18). The experimental data are plotted in terms of this parameter  $N$ , and we will see how well the single parameter can be used to characterize the thermal blooming.

There are also additional restrictions on the experiment which must be met in order to simulate high-power laser propagation in the atmosphere. In the energy equation it was assumed that the density is constant; second that convection is the only form of heat transfer, and third that the thermal distortion has reached steady state. The first requirement can be satisfied in the laboratory experiment if we limit the temperature rise of the absorbing gas. The temperature rise is given by

$$\frac{\Delta T}{T} = \frac{\int_{-\infty}^{\infty} \alpha I dx}{\rho c_p v T}. \quad (25)$$

If the temperature rise on the center of the beam is kept less than 10 percent, then the change in density will be a secondary effect in the energy balance and this change can be neglected. This requires the following restriction on the laboratory experiment

$$\frac{\alpha a}{\rho c_p T v} \leq 0.1. \quad (26)$$

If this inequality is evaluated at the focus, this ensures that the temperature rise everywhere in the cell is small and would have no effect. This may be too stringent a requirement for simulation since the thermal lens is distributed along the entire path and this requirement can be relaxed somewhat.

For propagation in the atmosphere, a wind or transverse motion due to beam slewing is generally present and determines the temperature rise and thus the thermal distortion of the beam. For valid simulation we must also insure that this is the case and that other forms of heat transfer are negligible. In order to use moderate power lasers and still simulate distortion we can increase the absorptivity of the gas within the limit set by the temperature rise. We can also increase the distortion by using small size laser beams and low wind velocities. However the lower limit on beam size and labora-

tory wind velocities are set by the importance of thermal conduction and natural convection or buoyancy. As the beam is made smaller, conduction becomes more important relative to convection. According to Smith [27] convection dominates if

$$V > k/\rho c_p a \quad (27)$$

and for a gas cell the forced convection dominates natural convection if

$$V > V_{NC} = \left( \frac{\alpha Pg}{\rho c_p T} \right)^{1/3}. \quad (28)$$

The latter inequality can be relaxed if we orient the absorption cell in the laboratory experiment in the vertical plane thereby minimizing the buoyancy effects.

The steady-state restriction is easily met in the laboratory by ensuring that the measurements of laser-beam intensity are made after a few wind transit times across the beam. There is an additional transient effect on CW thermal blooming that can occur in the atmosphere under certain restrictive conditions and this is due to the kinetics of the absorption process. Thus far we have assumed that the absorption leads directly to gas heating with no delay. This is generally the case. An exception to this is the kinetic cooling effects which are discussed in detail in a following section.

##### B. Liquid Cell Thermal Distortion Experiments

Laboratory experiments to simulate high-power propagation of laser beams through the atmosphere enable us to conduct experiments under a wide variety of conditions which can not be done conveniently with moderate laser powers. The absorption in the laboratory cell can be increased such that the path length can be kept to a reasonable value (less than a meter). Along with this advantage multikilowatt beams can then be simulated with laser powers of a few watts. The beam diagnostics and parametric studies are then greatly simplified. Keeping in mind the simulation requirements in the previous section, an experimental apparatus as shown schematically in Fig. 14 can be used in simulation experiments.

The CO<sub>2</sub> laser is one of the most convenient lasers to operate at moderate power levels, giving stable, well defined beam modes with powers of tens of watts. A recirculating gas attenuator, described in detail in [41] is used to vary the laser power. The absorption cell, in this case a liquid cell filled with CS<sub>2</sub>, is scanned across the fixed laser beam, simulating a uniform wind. The detector can be either a gold-doped-germanium-type detector or a pyroelectric detector. Normally the detector is apertured with a pin hole which is small compared to the beam size. The detector in Fig. 14 is scanned across the beam on the same mechanism which scans the cell. The intensity contour is then displayed on an oscilloscope with the horizontal sweep of the scope driven by the translation of the cell. The absorption coefficient of CS<sub>2</sub> is typically 0.17 cm<sup>-1</sup>, the lowest of all liquids at 10.6-μm wavelength. In order to conduct experiments with reasonable values of  $\alpha z$  we are restricted to path lengths of a few centimeters. For the results reported here the cell length was 12.2 cm corresponding to an  $\alpha z$  of 2.2.

The two most important experimental parameters measured in the blooming experiments are the peak intensity and the deflection of the peak intensity. Fig. 15 shows the peak intensity of the laser beam normalized with respect to the intensity in the absence of blooming as a function of the

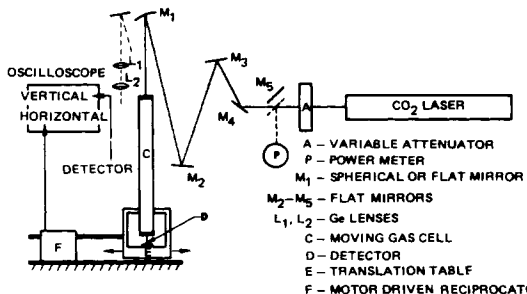


Fig. 14. Experimental apparatus for laboratory simulation of thermal blooming showing one configuration used to simulate a uniform cross wind. Both liquid and gas cells have been used.

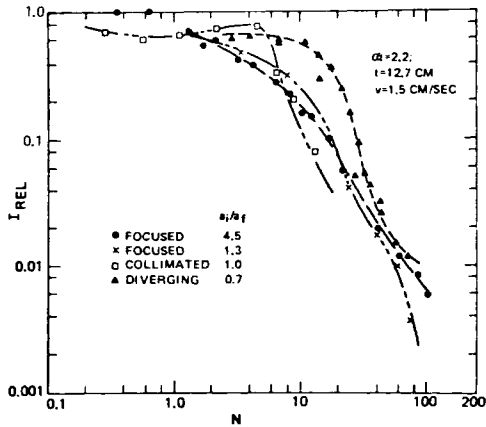


Fig. 15. Measured peak intensity of a CO<sub>2</sub> beam propagated through a carbon-disulfide cell with different degrees of focusing and plotted as a function of the distortion parameter  $N$  as given by (18). The peak intensity is normalized by the undistorted peak value [44].

distortion parameter  $N$ . The data are shown for different degrees of focusing and the curves were drawn through the data points. For these experiments the velocity was fixed at 1.5 cm/s and the distortion parameter was varied by varying the laser power and the focusing telescope. The two cases for the focused beams agree quite well with each other as shown in Fig. 15, indicating that the single parameter  $N$  is the proper scaling parameter. For the diverging beam, the relative intensity remains at a higher value even for large distortion parameters but eventually the data converges to the same general curve for  $N \sim 25$ . For the collimated beam, the data more closely follows the focused beam data and converge to the same curve at an  $N \approx 6$ . It does appear that the collimated and diverging beams must be considered as special cases and in general do not follow the same scaling as does the focused-beam case. Recall the difference in thermal distortion of collimated beams with different Fresnel numbers as shown in Fig. 9, especially for distortion parameters greater than one and less than four.

The deflection of the peak intensity into the wind is shown in Fig. 16 with the deflection  $\Delta x$  normalized by the undistorted laser-beam size at the detector. This data is for the same experiments as Fig. 15. The deflection of the peak intensity into the wind is independent of the degree of focusing. The intensity contours for the diverging beam have significant structure with several peaks and is less well-defined compared to the peaks observed for the focused beams. This may explain the discrepancy between the deflection of the diverging beam relative to the others as shown in Fig. 16.

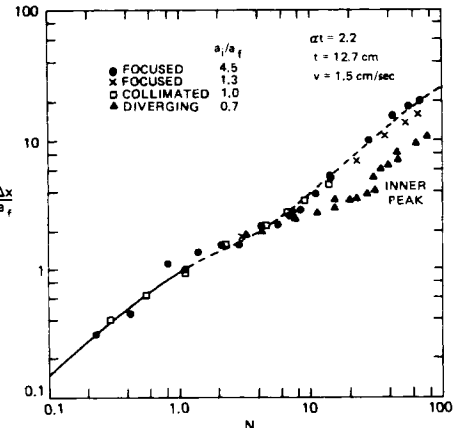


Fig. 16. Deflection of the peak intensity into the wind direction normalized by the initial  $a^{-1}$  laser beam radius. Experimental conditions are the same as those for Fig. 15 [44].

The advantage of using liquids for simulating the atmospheric path is that large distortions conditions can be obtained with small propagation paths and low laser powers. Laser powers of less than 10 W were used for the data shown in Figs. 15 and 16. However, there are disadvantages encountered when using liquids. The most important disadvantage is that the absorption coefficient is relatively fixed, and only large  $\alpha z$  conditions can be simulated. This introduces an additional experimental difficulty in that small laser beams must be used to obtain reasonable size Fresnel numbers. This introduces experimental errors in measuring beam sizes and also makes the experiments more difficult to align and maintain. For these reasons most laboratory experiments have used absorbing gases for thermal-blooming simulation.

### C. Gas Cell Experiments

In using gases for simulating long atmospheric paths, there are several options available. One can use a gas cell similar to the liquid cell and either translate the cell across the beam or translate the beam through the fixed cell. With the fixed cell, the laser beam is automatically scanned across the detector, which is sometimes an advantage. However, for photographing the beam, steady state is achieved when the cell is translated and photographs of the distorted beam can be made as well as power-in-the-bucket measurements.

Power-in-the-bucket measurements are made by collecting the laser power in various size apertures and measuring the power with a calorimeter; the apertures are usually centered on the shifted peak intensity. It is interesting to note that both power-in-the-bucket and peak intensity measurements show the same qualitative dependence on the experimental parameters. Thus the question of the relative importance of the peak intensity or average intensity is not too important in the thermal blooming problem. Another apparatus for simulating the absorbing medium which has proven useful is a closed cycle recirculating wind tunnel as depicted in Fig. 17. By using a wind tunnel, the thermal distortion is steady state and for experiments requiring long observation times, this can be a convenience. One good example is experiments involving the influence of laser-beam jitter on thermal blooming where the measured laser intensity must be averaged over the jitter frequency; a steady state wind condition makes this averaging straight forward. Uniform flow at low wind velocities (1 to 10 cm/s) is difficult to obtain in a tunnel because of secondary flows and boundary layers. In our experiments, we found that

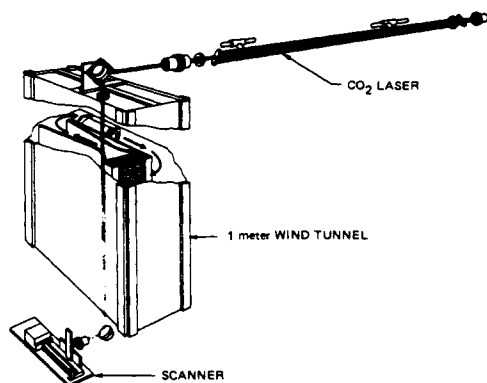


Fig. 17. Schematic of thermal blooming experiment utilizing a CW CO<sub>2</sub> laser and a closed cycle recirculating wind tunnel.

uniform flow at the cross section where the beam passed could be obtained by making the volume of the tunnel large compared to the propagation section ( $\sim 10$  times greater) and using flow straightening devices such as foam and metal grids. With a wind tunnel, an additional instrument is required to measure the wind velocity. (With translation of a cell or the laser beam the relative motion is measured in a straightforward manner by timing the translation distance.) The wind velocity is measured with a hot wire anemometer, but care must be exercised in these measurements because of the low wind velocities.

Most of the experiments were conducted with closed gas cells, with the variable absorption controlled by adding to air small amounts of absorbing gas such as propylene, propane, freon, or CO<sub>2</sub>. SF<sub>6</sub> is the highest absorbing gas at 10.6-μm wavelength, but it is so highly absorbing that it is difficult experimentally to control the amount of absorption. The closed gas cell has another advantage in that it can be operated at higher gas pressures. The gas pressure does not effect the distortion parameter (with fixed absorption), but it does reduce the role of thermal conduction. Thus by operating at 10 Atm, we can use lower velocities (thus higher distortion) without encountering thermal conduction as shown by the inequality in (27). A gas cell has another potential advantage in that a pivoted cell can be used to simulate a slewed beam. The following experiments were carried out with an experimental arrangement as shown in Fig. 14 with a total gas pressure of ten atmospheres [42].

Qualitative photographs of the distorted intensity pattern of the infrared CO<sub>2</sub> laser beam can be obtained using a heat-sensitive film called Kalvar film [43]. This film is sensitized by uv radiation and is developed thermally. The film is sensitized uniformly and then exposed to the distorted beam. The heating develops the film and shows the intensity pattern. The thermal distortion patterns of a collimated beam is shown in Fig. 18 for various values of the distortion parameter. With the vertical cell the natural convection effects are minimal even with wind velocities of 0.25 cm/s. Because of the 10-Atm gas pressure, thermal conduction also appears to be unimportant since conduction-dominated blooming would result in a symmetrically distorted beam pattern. The crescent-shaped beam patterns observed in Fig. 18 are those that have come to be associated with thermal blooming. The thermal distortion patterns of a focused beam are shown in Fig. 19 for various values of the distortion parameter, laser power, and wind velocity. For the collimated laser beam, we observe a truly crescent-shaped pattern and a definite narrowing of the

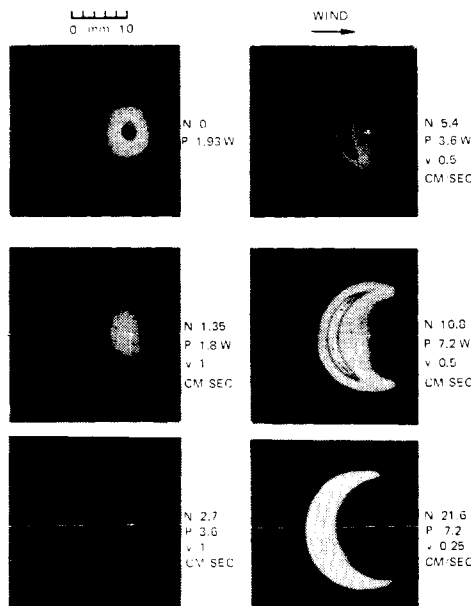


Fig. 18. Thermally distorted intensity patterns on Kalvar film with each contour labeled by the CO<sub>2</sub> laser power, transverse wind velocity and the calculated distortion parameter. The wind is incident from the left, the beam is initially collimated and propagated through the 1-m wind tunnel doped with absorber [44].

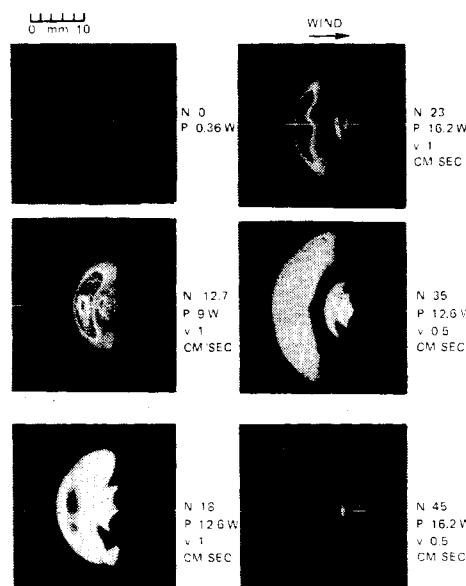


Fig. 19. Thermally distorted intensity patterns for an initially focused CW CO<sub>2</sub> laser beam. Each pattern is labeled by the laser power, transverse wind velocity and the distortion parameter calculated from (18) [44].

beam in the wind direction. With the focused beam, the thermally distorted intensity patterns are certainly different, and the influence of diffraction on the intensity contours are obvious. The diffraction effects cause the beam to break up into distinct areas in the focused-beam case, and this qualitative comparison supports the previous remarks made concerning the difference in thermal distortion for collimated and focused beams.

For the lowest values of velocity, tests were made to determine the role of natural convection by producing the same distortion parameter by doubling the laser power and also the wind velocity. If natural convection were important the

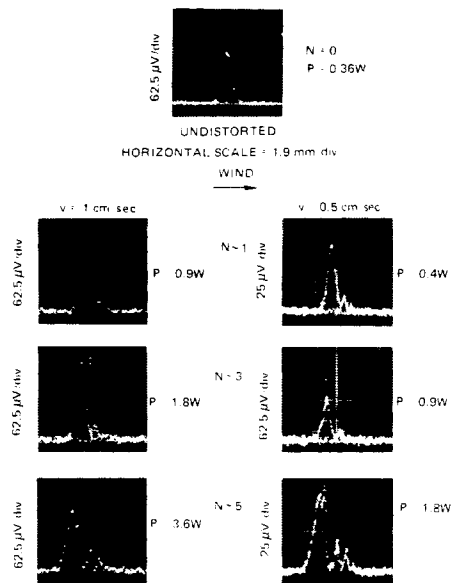


Fig. 20. Intensity contours of thermally distorted  $\text{CO}_2$  beam taken through the center of the beam parallel to the wind direction. The upper trace is the undistorted intensity contour. The left column data was obtained with a transverse velocity of 1 cm/s and various power level as marked. The right column was obtained with a velocity of 0.5 cm/s and one half the laser power as used for the left column data. Comparison of the two columns, for equal distortion conditions, show good agreement. (note scale changes and the comparison is made for normalized intensities) [44].

higher power would have less distortion because of the higher convection velocity with higher powers. Even for the 0.25 cm/s case there was only a 20 percent difference in the peak intensity compared to the case with doubled power and 0.5 cm/s case, which increases our confidence in the data being truly representative of forced convection. Quantitative data is obtained by scanning the laser beam with a  $35\text{-}\mu\text{m}$  diameter pin-hole apertured detector and some of this data was shown in Fig. 20. This is raw data which shows two important points. First the reproducibility of the experiment; each trace in Fig. 20 is a double trace showing two different runs, and the data are very close together, even down to the small scale structure. Secondly, the data shows that the thermal distortion scales as laser power divided by wind velocity. The data in the left column was obtained with a transverse velocity of 1 cm/s and the right column at 0.5 cm/s and half the power as the left set. In each case  $I_{\text{REL}}$  is the same within 10 percent for the same  $P/v$ . This shows that the thermal blooming scales as  $P/v$  and also shows that the laboratory simulation is behaving as it should for the convection dominated case. In other words for the high pressure vertical cell moving at 0.5 cm/s, the convection heat transfer dominates over natural convection and thermal conduction. Note also the scan of the undistorted laser-beam profile at the top of Fig. 20 which shows both the stability of the laser output as well as the symmetric, nearly Gaussian, intensity pattern.

Using data similar to that in Fig. 20, the peak intensity, and beam deflection were measured over a wide variety of experimental conditions. The relative intensity for these different focusing conditions are shown in Fig. 21 for fixed value of  $\alpha z$  of 0.41 and two velocities. Again the intensity is normalized with respect to the undistorted value at the detector. The collimated-beam data shows the tendency toward intensification as previously shown (the Fresnel number for this case is 5). The relative intensity decrease for the strongly and weakly

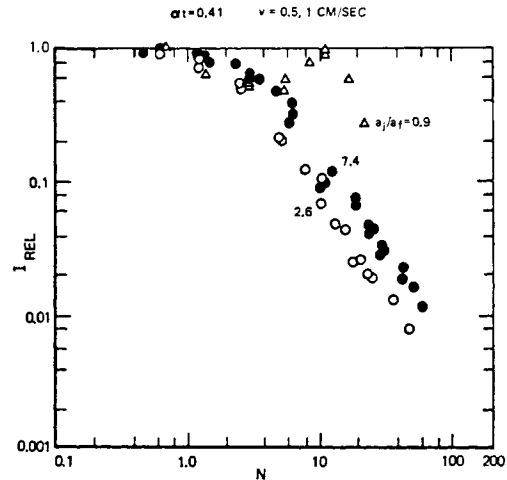


Fig. 21. Normalized peak intensity as a function of the distortion parameter for various degrees of focus. The  $\text{CO}_2$  laser beam was propagated through a vertical high pressure cell (10 Atm) traversed perpendicular to the beam and the distortion was measured with a pyroelectric detector [44].

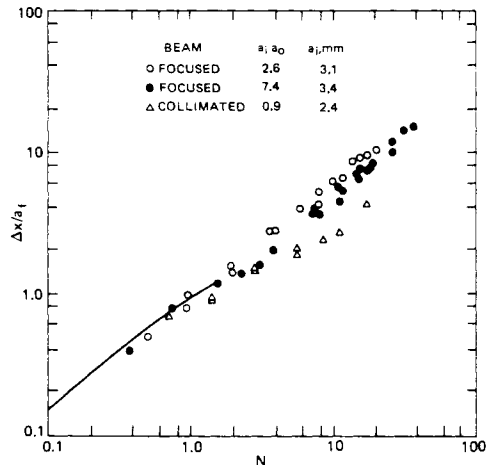


Fig. 22. Deflection of the peak intensity into the wind direction as a function of the distortion parameter  $N$ . The deflection is normalized by the initial laser beam radius [44].

focused beams agree with each other within approximately 50 percent for distortions of up to an  $N$  equal to 10 and within a factor of two beyond that. For the severe distortion of  $N$  greater than 10, the decrease in intensity is so severe that the experimental data is subject to larger errors. The laser-beam deflection for these same three cases is shown in Fig. 22, and the deflection appears to be relatively independent of the degree of focusing.

With the gas cell simulation, the absorption coefficient can be changed quite conveniently and the distortion was examined as a function of this variable. The variation in the peak intensity as a function of  $N$  for various values for  $\alpha z$  is shown in Fig. 23. This data is for a focused beam of  $a_i/a_f$  equal to 7.4, i.e., strong focusing. The data shows that there is an additional dependence of the distortion on  $\alpha z$  other than that expressed by  $N$ . This can be explained by the fact that for focused beams more distortion occurs close to the focus because of the beam size dependence of the distortion; however, for large  $\alpha z$  the attenuation itself reduces the intensity at the focus and therefore less distortion is encountered. This qualitatively explains the results shown in Fig. 23. It should

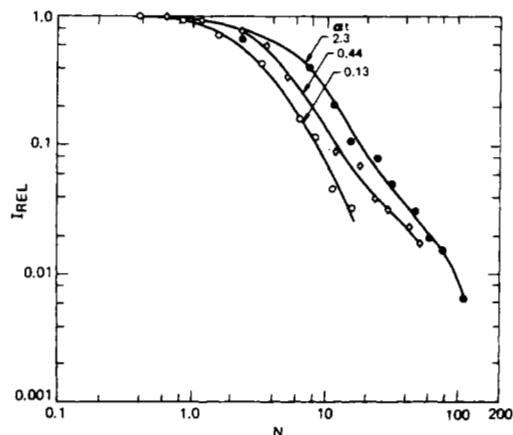


Fig. 23. Normalized peak intensity of thermally distorted  $\text{CO}_2$  laser beam as a function of the absorption coefficient of the gas, plotted as a function of the distortion parameter  $N$  [44].

be noted that a factor of 20 increase in  $\alpha z$  results in a reduction of the blooming by a factor of 3 to 4 even for severe distortion. For most cases of comparison,  $\alpha z$  will not vary this much, and for qualitative analysis of the effects of blooming, this additional dependence on  $\alpha z$  can be neglected or can be modeled by an additional dependence on  $\alpha z$ .

#### D. Summary of CW Blooming Solution Simulation Experiments

The results of the laboratory simulation experiments can be used to verify sophisticated computer codes used for predicting the thermal distortion of high-power laser radiation in the atmosphere. In addition, the results of the parametric studies can be used to develop simplified models of the thermal blooming for predicting the thermal distortion that will be extremely useful in system tradeoff studies. The laboratory data can be used to predict the loss in intensity to be encountered in the atmosphere by calculating the nondimensional parameters for the case of interest, including  $N$ ,  $F$ , and  $\alpha z$  for the case of uniform wind, and in addition the slewing number for the case of a slewed beam. The loss in intensity can then be determined by using Figs. 15 and 21 or Fig. 23 depending on the degree of focusing and linear absorption. (An analytic expression such as that shown in Fig. 13 could also be used in place of the experimental data). The beam deflection can be obtained in a like manner. The beam deflection may be more important for cases where the wind is not constant but variable, since this would represent the amount of beam wander that could be anticipated.

Less experimental work has been done on slewed laser beams than with a uniform wind. Based on the agreement between computer code results and the experiments for uniform wind, we can rely on the numerical results for comparing the scaling of slewed beams. Fig. 13 shows comparison of the thermal distortion with different slew rates for the same beamshapes, and we observe less than a 20 percent difference in distortion for factors of two change in slew rate.

The thermal distortion plots of  $I_{\text{REL}}$  versus  $N$  have an important interpretation if one considers the case of a fixed range, absorption, wind velocity, and focusing. In this case  $I_{\text{REL}}$  versus  $N$  is then a plot of  $I_{\text{REL}}$  versus total laser power. Thus the intensity on target will continue to increase with laser power as long as  $I_{\text{REL}}$  does not decrease faster than  $N^{-1}$  (equivalently 1/power). From Figs. 21 and 23 it can be

seen that the peak intensity in the focal plane continues to increase until the slope of the curve equals minus one. Beyond this value of laser power,  $I_{\text{REL}}$  decreases more rapidly than  $1/N$ , and the peak intensity actually decreases with increasing power because of the influence of the nonlinear thermal distortion effect. Thus we can define an optimum value of  $N$  or equivalently laser power, for a given set of atmospheric conditions. This leads to an optimum laser power which is sometimes referred to as the critical power and also a critical value of  $N$ . This result was also shown in Fig. 12. Based on the computer-code work and the experiment, the critical value of  $N$  is  $\sim 4$  for an infinite Gaussian beam and small  $\alpha z$ .

The concept of characterizing steady thermal blooming by a single parameter  $N$  with its dependence on absorption, slew, focusing, etc., is appealing from the standpoint of simplifying a rather complex nonlinear problem. In addition, a single-analytic expression can be used to fit the dependence of the thermal distortion on  $N$  such as that shown in Fig. 13. Different initial beam shapes have a different functional dependence on  $N$ , but the data can still be represented by an analytic expression. This type of scaling cannot be expected to hold for all degrees of focusing, slewing, or absorption, but errors in predicting the loss in intensity to within a factor of two or less can be expected for focusing ratios from 2 to 10. Absorption times, path length of from 0 to 2, and slew velocity ratios from 1 to 10, cover a wide range of experimental conditions.

#### V. TRANSIENT THERMAL BLOOMING

The thermal distortion of laser beams can be reduced by using a pulsed-laser source where the laser-pulse duration is short compared to the time required to form the thermal lens. Even if the absorbed laser power is transferred instantaneously to translational energy, there is still a finite time required for the distortion to develop. The distortion is the result of density changes (not temperature) which are propagated transverse to the beam by acoustic waves. Thus the time required to fully establish a thermal lens is the acoustic transit time across the laser-beam radius. For times shorter than this the strength of the lens is less than that associated with a longer pulse with the same absorbed laser energy. In this section we derive the governing equations for transient blooming and present perturbation solutions of the problem. Again the perturbation type solution gives us insight into the magnitude of the effect, and the nondimensional analysis allows us to relate laboratory experiments to atmospheric conditions. The problem can be divided into two time regimes, depending on whether the laser pulse is 1) longer than or 2) shorter than the acoustic transit time across the laser beam. In the former case, we are also assuming that the pulse is shorter than any other heat transfer rate.

#### A. Governing Equations

The equations that determine the density changes, and thus the thermal distortion, are the continuity, momentum, and energy equations as given in [45]

$$\begin{aligned} \partial \rho' / \partial t + \rho_0 \nabla' v' &= 0 \\ \rho_0 \partial v' / \partial t + \nabla P' &= 0 \\ \rho_0 c_p \partial T' / \partial t - P_0 / \rho_0 \partial \rho' / \partial t &= \alpha I \end{aligned} \quad (29)$$

where the prime terms represent perturbations to the quantities and the subscript 0 refers to the ambient or unperturbed value. These equations can be rearranged to give a single

equation for the density perturbation in the form of a wave equation

$$\left( \frac{\partial^2}{\partial t^2} - C_s^2 \nabla^2 \right) \frac{\partial \rho}{\partial t} = (\gamma - 1) \alpha \nabla^2 I \quad (30)$$

with  $C_s$  the acoustic velocity in the medium. The index change is related to the density by the Dale Gladestone law (6) and the intensity change is given by (5) for a collimated beam. Transient thermal distortion can be analyzed theoretically in the two time regimes, separated by the acoustic transit time across the laser beam as discussed in the following sections.

### B. Long-Time Blooming

If the laser pulse is long compared to the  $a/C_s$  time then the first term on the left-hand side of (30) is negligible and the equation for the density takes the form

$$\rho - \rho_0 = - \int_0^t \frac{(\gamma - 1)}{C_s^2} \alpha I dt', \quad t \gg a/C_s. \quad (31)$$

This can be written in terms of specific heats and density by recognizing that  $C_s = (\gamma P/\rho)^{1/2}$ ,  $\gamma = C_p/C_v$ , and the gas constant  $R = C_p - C_v$ . Substituting the density change into (6) and using (5), we obtain

$$\frac{I(r, z, t)}{I(r, 0, 0)} = \exp - \alpha z \exp \frac{2\mu_T \alpha I_0 t z^2}{\rho c_p a^2} [ + e^{-r^2/a^2} - r^2/a^2 e^{-r^2/a^2} - r^2/a^2 e^{-2r^2/a^2} ].$$

We can define a nondimensional parameter for the long-time transient blooming

$$T_{lc} = \frac{-2\mu_T \alpha I_0 t z^2}{\rho c_p a^2} g(\alpha z) \approx \frac{-2\mu_T \alpha I_0 t z^2}{\rho c_p a^2}, \quad \alpha z \ll 1 \quad (32)$$

with  $g(\alpha z)$  given by (18). Thus to first order in thermal distortion the intensity is given by

$$\frac{I(r, z, t)}{I(r, 0, t)} e^{-\alpha z} = \exp - T_{lc} [ + e^{-r^2/a^2} - r^2/a^2 e^{-r^2/a^2} - r^2/a^2 e^{-2r^2/a^2} ]. \quad (33)$$

The above expression is applicable for predicting the change in intensity for cases where the blooming is not too strong. For stronger blooming conditions where the change in intensity is appreciable, we must again resort to computer codes to solve the nonlinear problem. Even for the strong thermal blooming the nondimensional parameter is the appropriate scaling parameter and can be used for scaling purposes.

Shown in Fig. 24 are the radial intensity contours as a function of the distortion parameter  $T_{lc}$ . The beam radius is normalized by the original beam radius. We note that the centerline intensity decreases exponentially with  $T_{lc}$ . The long-time pulse intensity decreases at a faster rate as a function of the laser beam intensity than the CW wind dominated case. This is the result of the symmetric spreading of the pulsed beam as compared to the tendency toward focusing in the wind plane for the CW wind dominated case. The beam spreading for the CW wind case is one-dimensional with the spreading occurring only in the transverse dimension.

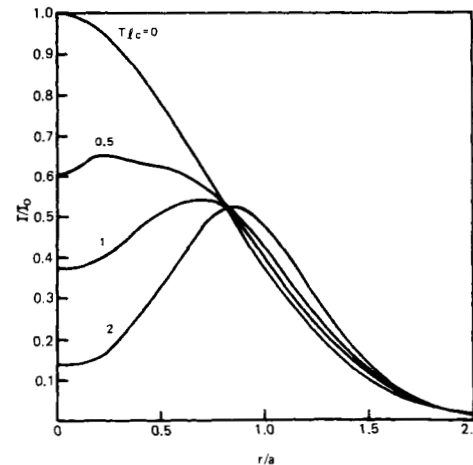


Fig. 24. Transient thermally distorted radial intensity profiles for a pulsed laser beam. The intensity is normalized by the undistorted peak intensity and the radius by the  $e^{-1}$  initial beam radius.  $T_{lc}$  is the nondimensional long time distortion parameter given in (32).

### C. Short-Time Transient Blooming

The more important case of transient blooming is encountered when the laser pulse is short compared to the hydrodynamic time  $t_p < t_H$ . For this case, it is anticipated that the thermal blooming will be less compared to the long-time blooming with the same pulse energy, since the pulse length is shorter than the lens-formation time. In this time regime, equation (30) can be written as

$$\frac{\partial^3 \rho}{\partial t^3} = (\gamma - 1) \alpha \nabla^2 I.$$

If we assume that the laser intensity is a square pulse in time,

$$\rho - \rho_0 = \frac{(\gamma - 1) \alpha \nabla^2 I t^3}{6}.$$

Again, using equation (6) to relate the index of refraction to the gas density, and (5) to calculate the intensity change based on the index of refraction we obtain, for an initial Gaussian, collimated beam

$$\frac{I(r, z, t)}{I(r, 0, t)} + \exp - T_{sc} \left\{ \left( 1 - \frac{2r^2}{a^2} + \frac{1}{2} \frac{r^4}{a^4} \right) e^{-r^2/a^2} + \left( \frac{1}{2} \frac{r^4}{a^4} - \frac{r^2}{a^2} \right) e^{-2r^2/a^2} \right\}$$

with the short pulse nondimensional distortion parameter given by

$$T_{sc} = \frac{8(-\mu_T) C_s^2 I_0 t^3 \alpha z^2}{3\mu_0 \rho c_p a^4} g(\alpha z)$$

with  $g(\alpha z)$  given by (18) and is equal to unity for small  $\alpha z$ .  $T_{sc}$  can be rewritten in terms of the energy in the pulse

$$T_{sc} = \frac{8(-\mu_T) C_s^2 E \alpha z^2 t^3 g(\alpha z)}{3\pi \rho c_p t_p a^6} \quad (35)$$

where  $E$  is the total energy in the pulse whose duration is  $t_p$ .

Plotted in Fig. 25 are the radial profiles of the short-pulse thermally bloomed patterns as a function of  $T_{sc}$ . The radius is normalized with respect to the undistorted  $e^{-1}$  beam radius. We note that the distortion for short pulses is different than that associated with the long-duration laser pulses as shown in

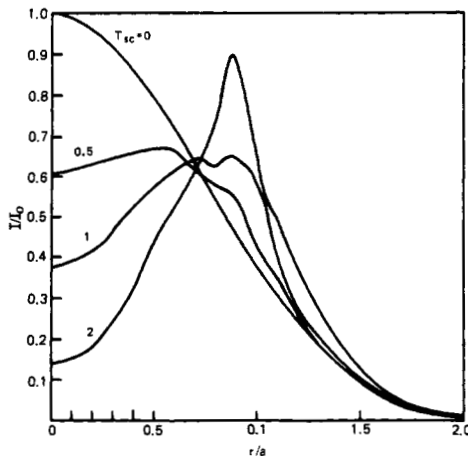


Fig. 25. Transient thermally distorted intensity profiles for short-pulse laser beams where the pulse duration is much less than the acoustic transit time across the beam. The intensity is normalized by the undistorted peak intensity and the radius by the initial  $e^{-1}$  beam radius.  $T_{sc}$  is the nondimensional short time distortion parameter given by (35).

Fig. 24. The centerline intensity, predicted by the perturbation analysis, does fall off exponentially with the distortion parameter just as the long-term pulse blooming did. However, the short-pulse intensity pattern off-axis is enhanced considerably. This is due to the refractive effects of the density gradients caused by the acoustic wave moving out from the beam center. For a  $T_{sc}$  of two we note that the peak intensity located off-axis is nearly equal to the undistorted centerline intensity.

Ulrich and Wallace [45] have reported numerical solutions for the transient thermal distortion for both the long-term and short-term distortion. They pointed out that the numerical results agree with the analytic results in the extreme time regimes. The computer code results for the intermediate cases, were also calculated by Ulrich and Wallace, where there is no analytic solution. Comparison of the perturbation solution centerline intensity calculated with the perturbation solution agrees quite well with those shown by Ulrich and Wallace, and qualitatively the radial profiles were the same for both calculations.

For comparison of the long- and short-pulse blooming we can express the short-pulse-distortion parameter in terms of the long-time-pulse-distortion parameter and the hydrodynamic time. This gives

$$T_{sc} = \frac{4}{3} T_{lc} (t_p/t_H)^2 (t/t_p)^2 \quad (36)$$

where  $t_H$  is the hydrodynamic time equal to  $a/C_s$ . If we evaluate the parameters at the end of the laser pulse where  $t = t_p$ , we see that the short-pulse-distortion parameter is reduced by the square of the ratio of pulselength to hydrodynamic time relative to the long-pulse distortion. This is for conditions which have the same beam size, pulse energy, absorption, range, i.e., everything the same except pulselength. Thus (36) points out in a very straightforward manner the advantage of propagating a laser pulse which is shorter than the acoustic transit time across the laser beam.

#### D. Influence of Focusing on Transient Blooming

The perturbation solutions derived for the single-pulse blooming were for collimated beams. Just as in the CW case, we can derive a perturbation parameter for the focused beam by assuming that the focusing can be represented by a simple

geometric expression for the beam radius at any axial position.

$$a/a_i = 1 - (1 - a_f/a_i) z/z_f.$$

Using this expression and performing the double axial integrations, the long-time- and short-time-distortion parameters are given by

$$T_s \text{ or } l = T_{sc} \text{ or } l c g_{s,l}(a_i/a_f)$$

where

$$g_l = \frac{x^2 - 1 - 2 \ln x}{2(1 - 1/x)^2} \quad (37)$$

$$g_s = \frac{x^4 - 1 - 4 \ln x}{8(1 - 1/x)^2} \quad (38)$$

where  $x = a_i/a_f$ .

In the limit of strong focusing, i.e.,  $x \gg 1$  the above expressions reduce to

$$g_l \approx x^2/2, \quad x \gg 1.$$

$$g_s \approx x^4/8, \quad x \gg 1.$$

Thus we observe that the influence of beam focusing on the thermal distortion of pulsed lasers is much stronger than for CW thermal blooming. (In the case of CW blooming recall that the focused distortion parameter was the product of  $N_c$  times  $x$ ). Thus the long-term and short-term distortion parameters are, for strongly initially focused Gaussian beams

$$T_l = \frac{-\mu_T E a z^2}{\rho c_p \pi a_i^4} \left( \frac{a_i}{a_f} \right)^2 t \quad (39)$$

$$T_s = \frac{-\mu_T c_s^2 E a z^2}{3 \rho c_p \pi a_i^6 t_p} \left( \frac{a_i}{a_f} \right)^4 t^3. \quad (40)$$

An important concept introduced by Ulrich [46] is that of saturation of the on-axis accumulated energy fluence for short pulse thermal blooming. He pointed out that after a certain time, labeled the saturation time  $t_s$ , the on-axis intensity dropped to one-tenth of its initial value. Thus after this time no significant further energy is deposited on-axis in the focal plane, regardless of how long the pulse is. Thus if the pulse length is made equal to  $t_s$ , this will maximize the on-axis energy deliverable, and will also be the most efficient propagation condition. The saturation time has been written conveniently by Gebhardt [40] as

$$t_s = 0.04 \left[ \frac{8\mu_0 \rho_0 c_p}{\mu_T c_s^2 \alpha} \right]^{1/2} \frac{\lambda^2 z}{a E_p^{1/2}}. \quad (41)$$

It is possible to express this concept in terms of a saturation pulse energy. If the pulse length is fixed, simply evaluate the above expression with  $t_s = t_p$  and solve for the saturation energy. In order to calculate severe pulsed thermal blooming, numerical computer codes must be used. Several authors have addressed this problem. The short term thermal distortion of a collimated pulsed laser beam was analyzed numerically by Ulrich and Wallace [45]. Aitken *et al.* [47] developed computer code modeling that included focusing and Ulrich [46] showed computer-code results which demonstrated the concept of saturation of energy deliverable. Additional computer code results, taking into account triangular-shaped temporal laser pulses as well as different initial beam geometries other than Gaussian were presented by Fleck *et al.* [48]. The computer code calculation for CW thermal blooming were more

important than in the pulse case for accurate prediction of the distortion because of the diffraction effects encountered in the CW laser blooming case. For pulsed blooming, the distortion increases the beam dimension in all directions and diffraction effects do not play as significant a role. Therefore, we anticipate that the analytic perturbation solutions should give the correct parametric dependence and a good insight into the distortion, even for severe distortion conditions.

### E. Transient Blooming Experimental Results

The long-time transient blooming problem has been investigated experimentally by Longaker and Litvak [49], Kenemuth *et al.* [50], and also by Buser and Rohde [51].

Longaker and Litvak [49] used a 1.06- $\mu\text{m}$  neodymium-laser pulse to examine the thermal distortion in absorbing solids, liquids, and gases. Short  $Q$ -switched pulses were used in some cases but the thermal distortion was examined on a long-time basis. They used an interferometer to examine the density perturbations and examined the thermal distortion as a function of laser pulse energy. The thermal distortion was characterized as a negative focal-length lens and was found to be linear with laser pulse energy as predicted by theoretical models. Longaker and Litvak did not examine the self-induced distortion of the laser beam itself, but confined their measurements to the disturbance of the medium.

Kenemuth *et al.* [50] utilized a 72-W CW CO<sub>2</sub> laser which was shuttered on in 60  $\mu\text{s}$  and propagated through a 559-cm long cell containing various pressures of CO<sub>2</sub> gas. In addition to the experiment, Kenemuth *et al.* also presented a theoretical model of the transient behavior derived from the eikonal equations. Comparison of their data and theory showed good quantitative agreement for the on-axis intensity measurements for times less than 200 ms. This time constraint was determined by their experimental conditions, where beyond this time convective flow dominated the heat transfer. Both their eikonal theory and the perturbation theory presented here predict that initially the intensity decreases exponentially with time which was verified by the experiments of Kenemuth *et al.* [50].

Buser and Rohde [51] also examined the transient behavior of thermal blooming in the long-time regime. They presented a theoretical model which took into account thermal conduction heat transfer which becomes important for small diameter laser beams. Shown in Fig. 26 is the measured on-axis and  $e^{-1}$  intensity as a function of time. Also shown are the theoretically predicted transient blooming intensities for cases neglecting as well as including thermal conduction. It is observed that the data in early times agree well with the theory and that for the longer times conduction is important and again the data agrees with the predicted model.

The measurement of short-pulse thermal blooming, where the pulse is short compared to the acoustic transit time, is the more difficult experimental problem. The laser-beam intensity must be measured, typically on a microsecond time scale. Thermal blooming on this time scale has been examined experimentally by Kleiman and O'Neil [52], Smith *et al.* [53] and O'Neil *et al.* [54].

Kleiman and O'Neil [52] examined the thermal distortion of 1.06- $\mu\text{m}$  wavelength radiation propagating through a 1-m absorption cell. The laser beam was slightly focused with a  $1/e$  radius of 0.74 cm entering the cell and a 0.24-cm radius leaving the cell. The hydrodynamic time (based on the mean radius) was quoted as 10  $\mu\text{s}$ . The laser pulse duration was

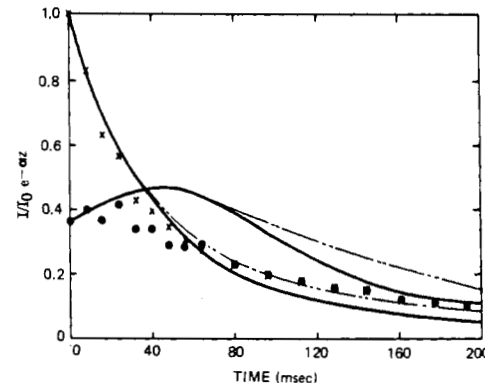


Fig. 26. Normalized intensity as a function of time from [51]. Both the on-axis peak and the intensity at the original  $e^{-1}$  laser beam radius are plotted and compared with the theoretical model (solid curve) for an initial Gaussian and also with the model including thermal conduction heat transfer (dashed curve).

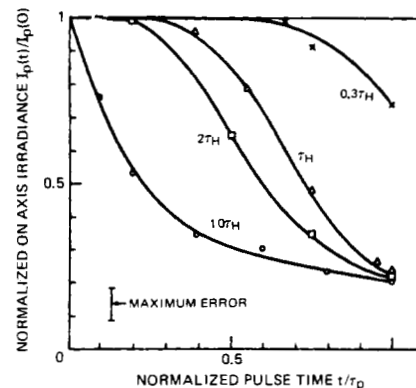


Fig. 27. Normalized on axis intensity as a function of time normalized with respect to the pulse duration. Each set of data is marked by pulse duration in fractions of the hydrodynamic time [52].

experimentally varied from 3 to 100  $\mu\text{s}$  so that careful examination of influence of laser-pulse duration on thermal blooming could be carried out, spanning the interesting range of pulses less than and greater than the hydrodynamic time. Shown in Fig. 27 are the on-axis peak intensity normalized with respect to the undistorted intensity as a function of time with time normalized with respect to the total laser-pulse duration. Each curve drawn through the experimental data is marked by the laser-pulse duration in fractions of a hydrodynamic time. This data dramatically shows the difference in short-time- and long-time-thermal distortion as well as the transition between the two time regimes. For  $t_p > t_H$  all three of the curves approach the same final relative intensity, showing that the hydrodynamics are not important and that the reduction of the on-axis intensity due to blooming is dependent only on the total energy in the beam, and independent of the temporal history. Thus  $t_H$  is the appropriate scaling parameter. For the short-duration laser pulse,  $t_p < t_H$  the relative on axis intensity decreases as the cube of time again in agreement with the theoretical modeling as predicted by the perturbation parameter  $T_s$ .

Smith *et al.* [53] also demonstrated experimentally the effects of the hydrodynamics on the thermal distortion of pulsed laser beams. Using a 0.2- $\mu\text{s}$  pulse from a TEA laser they compared the thermal distortion propagating through an absorbing gas cell with absorber added to air with that encountered by propagating through a cell filled with helium and

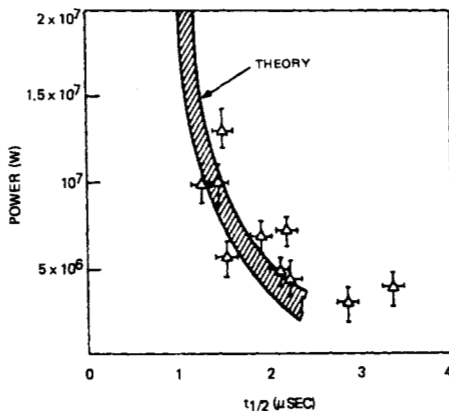


Fig. 28. Time required for the power contained in a central aperture to decrease to  $\frac{1}{2}$  its initial value as a function of laser power. The cross-hatched area is the theoretically predicted value with the uncertainty due to location of the aperture position [54].

the same absorption. The acoustic velocity in helium is approximately 3 times faster in helium than in air. Thus they altered the acoustic transit time and fixed the other parameters such as the laser beam parameters and the absorption in their experiment and showed that the distortion was more severe for propagation in a medium with the faster hydrodynamic time as compared to that with the slower hydrodynamic time.

The thermal blooming of a laser pulse whose duration is short compared to the hydrodynamic time was also reported by O'Neil *et al.* [54] utilizing a CO<sub>2</sub>-laser pulse propagated through a 10-m cell seeded with absorber (propane). Their measurements were reported for pulses which were one-half the hydrodynamic time based on the focal spot size. In this regime, they reported that exact hydrodynamic calculations of the density change was in good agreement with the perturbation type analysis as previously discussed, and they used the perturbation approach for comparison with their experimental data. Shown in Fig. 28 is the data from [54] which shows the time required for the laser power on-axis to be reduced to one-half its incident value. The hydrodynamic time at the focus for their experiment was 5 μs. The cross-hatched area represents the values predicted by the theoretical model with the range of absorption coefficients used in the experiments. One interesting aspect of the experiment is the observed lack of sensitivity of the distortion on the absorption coefficient which was varied from  $0.8 \times 10^{-3}$  to  $2.4 \times 10^{-3}$ . This insensitivity to absorption was predicted by the theory and is explained by the fact that a decrease in absorption (which would tend to decrease the blooming) is compensated for by an increase in the laser power reaching the focal region (which tends to increase the blooming).

#### F. Multiple-Pulse Thermal Blooming

We have observed in the previous section that if the laser-pulse duration is short compared to the hydrodynamic time, the thermal distortion is less than that encountered by a longer duration pulse with the same energy and propagation conditions. Thus from a thermal blooming standpoint, the shorter the laser pulse the better; however, the amount of energy that can be transmitted with a single pulse is limited by gas breakdown or the ionization of the air [5]. Thus in order to transmit greater fluences, trains of short-duration pulses must be used. The basic concept of multiple-pulse propagation to minimize thermal blooming is to propagate short pulses, suf-

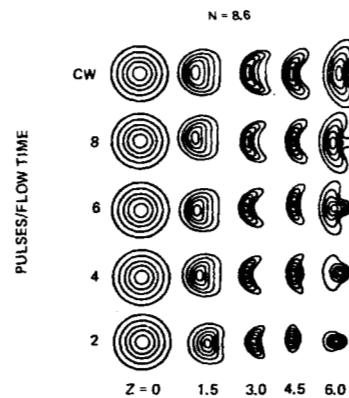


Fig. 29. Intensity contours for multiple-pulse laser beam as a function of pulses per flow time and at different ranges in kilometers. The average power is the same for all cases [55].

ficiently short as not to be bloomed, and to fix the repetition rate of the pulse train at a value where the heating of the air path by previous pulses does not severely distort subsequent laser pulses. Thus the repetition rate for optimum propagation is a function of the beam size, slew rate or wind velocity, and also the energy absorbed by the air from individual pulses. In this section, we examine the problem of multiple-pulse thermal blooming and show the appropriate nondimensional scaling parameters for predicting the thermal distortion of a train of laser pulses.

1) *Theoretical Modeling:* The multiple-pulse thermal blooming has been examined using numerical computer code techniques by a number of authors [55]–[59] and their results are discussed in this section.

Wallace and Lilly [55] theoretically evaluated the propagation characteristics of a train of pulses using a numerical computer-code analysis. In their analysis they assumed that each pulse was sufficiently short compared to the hydrodynamic times so that no  $t$ -cubed blooming occurred on the individual pulses themselves. The distortion of the laser pulse was caused by the heating of the air path by previous pulses where the heating was assumed to occur at constant pressure. The density gradients (and thus index of refraction gradients) were calculated by summing the density disturbance from all previous pulses; the index of refraction disturbance of the individual pulses are displaced with respect to each other because of transverse flow or slewing of the laser beam. An important parameter in multiple-pulse blooming is the number of pulses per gas transit time across the beam. We designate this parameter as

$$N_p = \frac{2a}{v} (\text{PRF})$$

where  $a$  is the  $e^{-1}$  radius and PRF is the pulse repetition frequency. (Wallace and Lilly define  $N_p$  in terms of the  $e^{-2}$  beam radius.)  $N_p$  is thus the number of pulses per flow time (PPFT).

Shown in Fig. 29 are contours of constant irradiance for a fixed time at various axial positions  $z$  in kilometers as a function of pulses per flow time. For these calculations the average power was fixed at 80 kw, the  $1/e^2$  initial radius of 25 cm, an absorption coefficient of  $2.0 \times 10^{-6} \text{ cm}^{-1}$ , a velocity  $10^3 \text{ cm/s}$  and the pulse repetition frequency was a variable for 40, 80, 120, and 160 pulses/s. Based on these numbers the CW distortion parameter given by (18) is 8.6. The data in Fig. 29 was for a fixed time of 0.05 s and shows the time evolution to steady state. At the range of 1.5 and 3.0 km all the distur-

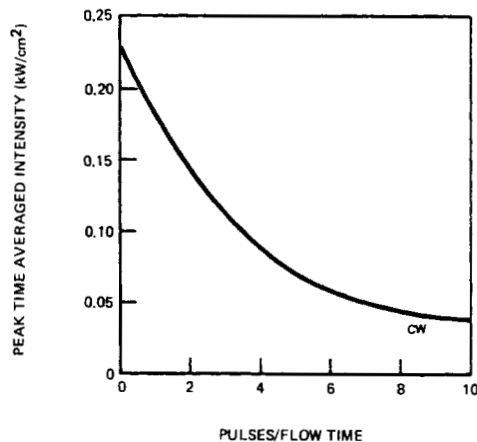


Fig. 30. Peak intensity as a function of pulses per flow time for a multiple-pulse thermally bloomed laser beam [55].

bances are nearly equal because there is considerable pulse overlapping for all cases, and the blooming of the pulsed beams is effectively the same as CW. At the 4.5-km range, the beam size is smaller, and for 2 PPFT there is little overlap and thus the distortion is less for that case. For the higher repetition-rate cases the contours again are nearly identical at the 4.5-km range. At the focal plane,  $z = 6.0$  km, there are noticeable differences observed as a function of repetition rate, showing dramatically the advantage of multiple-pulse laser sources relative to CW for propagating higher average irradiances. Quantitative comparison of the peak average irradiance deliverable in the focal plane is shown in Fig. 30 for the same experimental conditions as those for Fig. 29 as a function of the PPFT. As pointed out by Wallace and Lilly, if the wind conditions are such that there are two PPFT, the pulsed laser can deliver four times the peak intensity as compared to a CW beam with the same average power.

Lilly and Miller [56] have studied the multiple-pulse propagation of collimated and focused beams. In the case of collimated multiple-pulse lasers it has been observed that at low repetition frequencies the thermal distortion can lead to an enhancement in the peak intensity. This phenomena, first observed experimentally, is treated theoretically by Lilly and Miller, and their results are in agreement with the experimental data. The data is discussed in more detail in the next section.

Lilly [58] has done a parametric analysis of the steady-state multiple-pulse thermal blooming in an attempt to find analytic expressions to model the thermal distortion. He identifies the following nondimensional parameters as important; Fresnel number,  $\alpha z$ ,  $N_p$ , slew number, and  $N$  (equation (18)). He shows that for a limited range of the various nondimensional variables, he can define a scaling law for the peak intensity as a function of these parameters raised to different exponents. These exponents are determined from the numerical results and are given by Lilly in tabular form for the various ranges of the nondimensional parameters.

Fleck *et al.* [59] have examined the more complicated problem of the combined effects of  $t$ -cubed blooming and overlap blooming for a train of pulses. Because of the complexity of this problem it is not possible to make a general conclusion as to which is the more important effect. Fleck's concluding remark concerning this problem is that in some cases the overlapping effects may be more important than the  $t$ -cubed blooming effects on single pulses.

2) *Experimental Data on Multiple-Pulse Blooming:* Laboratory simulations of multiple-pulse overlap blooming are re-

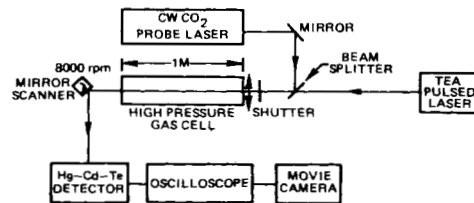


Fig. 31. Schematic diagram of experimental setup for examining multiple-pulse thermal blooming [61].

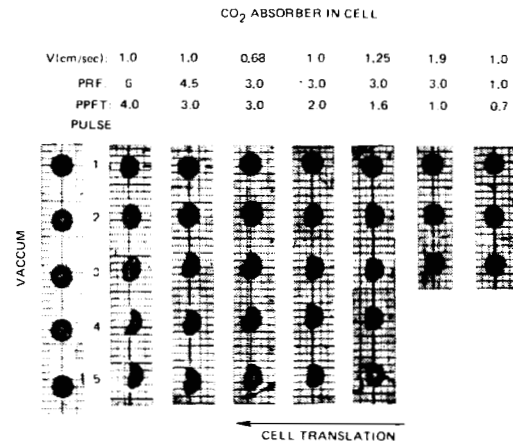


Fig. 32. Intensity contours for multiple-pulse thermal blooming as a function of the pulse number and PPFT [60].

ported in [60]-[62]. In these studies the laser pulses were sufficiently short that the  $t$ -cubed blooming could be ignored. Consequently, the overlap blooming problem was the topic of study. In [60] and [61] the collimated multiple-pulse blooming problem was investigated whereas [62] reports the thermal distortion of a train of pulses of a focused beam. These experiments are described below.

Laboratory simulation of multiple-pulse thermal distortion of laser beams has been carried out by Gebhardt *et al.* [60] and also by Buser *et al.* [61] utilizing the experimental setup shown in Fig. 31. The pulsed laser was a TEA laser operating in a TEM<sub>00</sub> mode with  $\sim \frac{1}{2}$  joule per pulse, a beam radius of 0.3 cm, and capable of operating at repetition rates of 10 pps. As shown in Fig. 31 the train of pulses is directed through the 1-m long translated absorption cell, used to simulate an atmospheric path. A 0.2-W CW probe beam is reflected off a salt wedge and passed through the cell, coaxial with the pulsed beam. The probe beam is swept across the face of a Hg-Cd-Te detector with a spinning mirror; the distorted intensity profiles are displayed on an oscilloscope and recorded with a fast-framing movie camera. By using a CW probe beam, the distortion can be monitored continuously without the problems associated with synchronizing and monitoring of the pulses themselves. In the experiments there appeared to be a slight misalignment between the probe beam and the pulsed-laser beam which lead to some experimental error, but did not affect the qualitative data or the trends in the data characteristic of multiple-pulse thermal blooming.

A qualitative picture of the thermal blooming of a train of pulses was obtained by exposing heat sensitive paper to the laser pulses located at the exit of the absorption cell. Shown in Fig. 32 are the thermally bloomed beam patterns for a variety of propagation conditions, the top exposure being the first pulse through the medium, followed in descending order by successive pulses in the train. The cell translation velocity

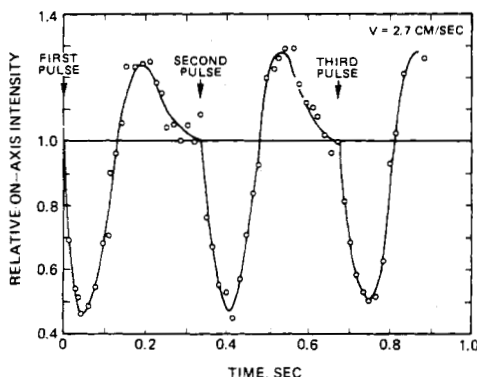


Fig. 33. Relative peak intensity as a function of time as recorded by the low-power CW probe beam. The location of the individual pulses responsible for the distortion are marked with an arrow [61].

and laser PRF are indicated above each column, along with the number of PPFT  $N_p$  as given by (41). It is evident from the distorted beam patterns that this definition of  $N_p$  is consistent with the time required to reach steady-state thermal distortion. After the number of pulses in the train equals  $N_p$ , the steady state is reached and all subsequent pulses suffer the same thermal distortion. Also in the last two columns with 1 and 0.7 PPFT, the thermal distortion is observed to be negligible, and the beam size is the same as the vacuum case, shown in the first column.

We now describe the probe-beam results. Fig. 33 shows the relative on-axis intensity of the low intensity probe beam as a function of time. The arrival time of the individual pulses are marked on Fig. 33. By measuring the intensity of the probe beam at each instant of time it is possible to determine the peak intensity that could be transmitted for a succeeding pulse. It is interesting to note that the intensity of the probe pulse is actually greater than the undistorted beam intensity for times corresponding to  $0.1 < t < 0.3$  s after each pulse. Therefore, if a second pulse were transmitted during this time under these experimental conditions the peak intensity could be greater than that in the absence of thermal blooming. The peak enhancement occurs at a PPFT of  $\sim 1.6$  and has a magnitude of 25 percent. This enhancement is a result of the motion of a negative thermal lens relative to the beam path, such that the "lens" now deflects a portion of the beam toward the center, e.g., it appears to act as a positive lens. This enhancement while not anticipated in the original experiments is predicted by a perturbation type solution for a collimated beam and also shown by the numerical analysis of Lilly and Miller [56]. The theoretical model for a focused beam predicts no enhancement. For the focused beam case, the enhancement mechanism is apparently washed out because of the variation in beam size as a function of range.

In scaling the multiple-pulse thermal blooming of a train of short pulses it is necessary to specify the thermal distortion of the individual pulses and the PPFT. Thus the nondimensional parameters are the long time-distortion parameter based on the energy of a single pulse and the number of pulses causing the blooming

$$T_{lc} = \frac{-2\mu_T \alpha E z^2}{\rho c_p \pi a^4} \quad (42)$$

$$N_p = (\text{PRF}) 2a/v.$$

For a collimated beam these two nondimensional parameters should completely characterize the blooming. The magnitude

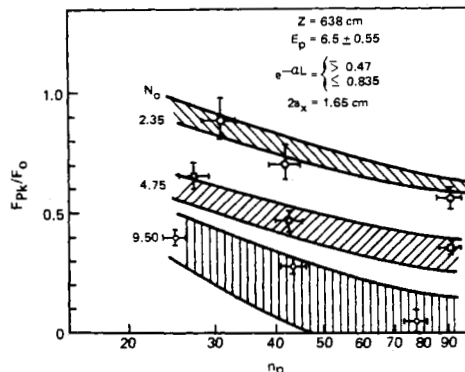


Fig. 34. Peak energy density of a multiple-pulse laser as a function of the distortion parameter and the pulses per flow time  $N_p$  [62].

of the initial drop in intensity is determined by  $T_{lc}$  and the recovery of the intensity by  $N_p$ . The enhancement magnitude will probably depend upon the strength of the thermal lens, specified by  $T_{lc}$  and the Fresnel number, which is a measure of the diffraction effects. The degree of enhancement in focusing will be limited by diffraction spreading and it is expected to behave in a manner similar to that observed for thermal blooming of a CW collimated beam, as shown in Fig. 9. In order to scale the thermal distortion of a focused beam an additional parameter, the Fresnel number must be specified.

O'Neil *et al.* [62] examined the steady-state thermal distortion of a focused train of CO<sub>2</sub>-laser pulses propagated through an absorbing gas cell. The 10.6 μm wavelength laser had a pulse duration of 5 μs, a pulse energy of 5–10 J and a beam size of 2 × 4 cm with a uniform intensity distribution. The repetition rate was varied from 1 to 200 pps and the transverse velocity was simulated by translating the beam across the stationary absorbing gas cell. The distorted beam integrated energy-density profiles were measured with a 64-element pyroelectric array. Plotted in Fig. 34 is the peak energy density of the distorted beam, normalized with respect to the undistorted energy density (the energy was averaged over one 0.1-cm element of the array) as a function of the distortion parameter  $n_p$  for a variety of pulse overlap numbers. According to [62] the distortion parameter which they use is

$$n_p = \frac{4\pi(\mu - 1)\alpha Ez}{\rho c_p Ta^2 \lambda}$$

which is equivalent to  $T_{lc}$  times the Fresnel number times  $\pi$ . The cross-hatched curves are the calculated theoretical values with the uncertainty due to laser beam motion which modifies the experimentally determined overlap number. Each curve in Fig. 34 is marked by the overlap number. The conclusion reached is that the theory and experiment agree within experimental error. Again it is obvious from the data that an increase in the average irradiance delivered to the focal plane can be made if sufficient beam clean out occurs between pulses.

The above discussion and the experiments described were for the case where the self-induced distortion of individual pulses is negligible. The ultimate problem is to calculate the thermal distortion for a train of pulses where each individual pulse is also distorted, i.e., the pulses are in the  $t$ -cubed blooming regime. This problem has been treated and reference to the theoretical results of Fleck *et al.* [48] were cited. Further theoretical and experimental work is required to predict the thermal distortion when both  $t$ -cubed blooming and overlap blooming are important and competing effects.

## VI. OTHER EFFECTS

The self-induced thermal blooming can be influenced by different conditions of the propagation path which can be encountered and a number of these situations are discussed in this section. One important area is the kinetics of the absorption and how the absorbed laser power is transferred to the air. Interesting effects can occur both for molecular absorbers as well as aerosols. Other circumstances introduced by the interaction geometry or atmospheric conditions can also complicate the problem such as atmospheric turbulence, stagnation zones, and transonic flow and these are also discussed in this section. Since the thermal distortion is a self-induced thermal lens, it is of interest to determine if the distortion can be countered by altering the initial conditions at the laser source. There are two techniques that can be used; amplitude shaping and phase correction. With amplitude shaping the thermal distortion is controlled by varying the intensity profile to obtain more favorable density gradients for propagation. Phase compensation can be applied to the beam prior to propagation in an attempt to precondition the beam. Both of these techniques are discussed in this section.

### A. Kinetic Cooling

Kinetic cooling is an effect that is unique to CO<sub>2</sub>-laser radiation propagation in the atmosphere. It is a transient effect whereby the laser energy absorbed by CO<sub>2</sub> molecules in the air is stored in the upper absorbing level-first-vibrational-level of N<sub>2</sub> manifold. The cooling occurs because the lower absorbing level (the 100 vibrational symmetric stretch mode of the CO<sub>2</sub> molecule) is repopulated by equilibrating collisions of the ground state atoms of CO<sub>2</sub> at the expense of translation energy. This unique kinetic process was first predicted by Wood *et al.* [6] and first shown experimentally by Gebhardt and Smith [8]. Because of its uniqueness and potential importance for high-power long-range propagation of CO<sub>2</sub>-laser radiation this effect is discussed in more detail.

A detailed theoretical treatment of the transient kinetics considering a large variety of vibrational level relaxation channels for the atmospheric constituents, is given by Wood *et al.* [6]. Shown in Fig. 35 is the vibrational-energy-level diagram for a standard atmosphere at sea level with 30 percent relative humidity with the collisional relaxation times for the various transitions marked in seconds [6]. Experimental data reported by Sica [10] shows that the T<sub>g</sub> relaxation rate is in error with a correct value of  $0.8 \times 10^{-3}$  s for the 30-percent relative humidity condition. This will have a significant influence on the kinetic cooling time for atmospheric conditions where water vapor is an important collisional deactivation partner of the upper level of the absorbing transition.

A qualitative understanding of the cooling process can be obtained by considering the energy level as composed of four groups: 1) the ground level with no vibrational energy, 2) the 100 CO<sub>2</sub> vibrational level which is absorbing at 10.6-μm wavelength, 3) the 001 asymmetric stretch level of CO<sub>2</sub> as well as the ν = 1 vibrational level of nitrogen, and 4) parasitic molecules which collisionally relax group 3, such as water and oxygen. When CO<sub>2</sub>-laser radiation is propagated through air, a fraction of the laser power is absorbed by the 100 vibrationally excited CO<sub>2</sub> molecules raising that molecule to the 001 vibrational level which is in equilibrium with the first vibrational level of nitrogen. Equilibrating collisions will repopulate the 100 vibrational level at the expense of the kinetic or translational energy of the CO<sub>2</sub>-ground state atoms. This corresponds to a

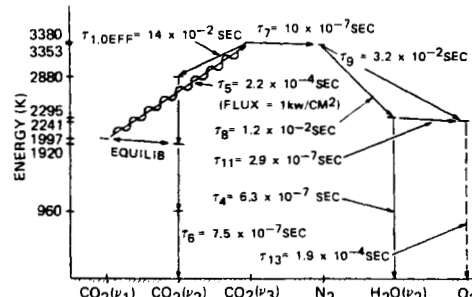


Fig. 35. Energy-level diagram showing vibrational levels of CO<sub>2</sub> and other atmospheric gases. Typical rates for the vibrational relaxation to different levels are shown for sea level pressure and 30 percent relative humidity [6].

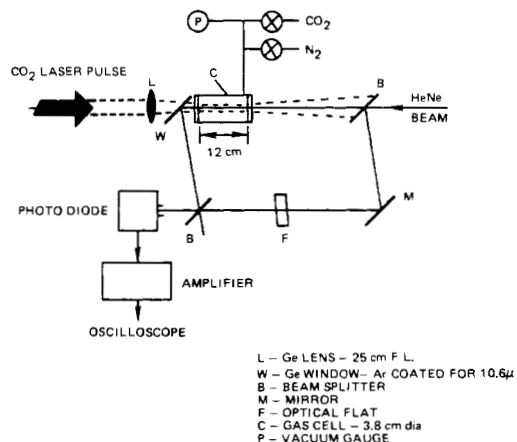


Fig. 36. Schematic of experimental apparatus for the kinetic cooling experiment [8].

decrease in the gas temperature and therefore a cooling. This cooling persists until the energy stored in the upper level relaxes by collisions with other atoms. For the 30 percent relative humidity 15°C atmospheric conditions, according to Sica, this time corresponds to  $0.8 \times 10^{-3}$  s.

The first experiment demonstrating this concept was presented by Gebhardt and Smith using the apparatus shown in Fig. 36. The kinetic cooling was observed in a mixture of CO<sub>2</sub> and nitrogen. A TEA laser pulse was propagated through the cell and the density changes were observed using a Mach-Zehnder interferometer as shown in Fig. 36. Shown in Fig. 37 are oscilloscope traces, recording the intensity change caused by a shift in interference fringes as observed on the center of the beam propagation path with a pin-hole apertured photomultiplier. The interference pattern was adjusted prior to each experimental run for maximum sensitivity by rotating an optical flat to change the optical path of one arm of the interferometer. Each trace is marked by the percentage of CO<sub>2</sub> gas in the cell. It is noted that not only does the magnitude of the cooling decrease with increased CO<sub>2</sub>, but also the duration, since for a mixture of CO<sub>2</sub> and N<sub>2</sub> the collisional relaxation of the upper absorbing level is through CO<sub>2</sub>. For pure CO<sub>2</sub> we see only heating effects.

The TEA laser pulse duration was less than 1 μs; for this experiment this time is instantaneous and the observed effects on the density can be considered an instantaneous absorption. (However, a longer duration pulse would encounter these density changes and therefore would be focused for positive

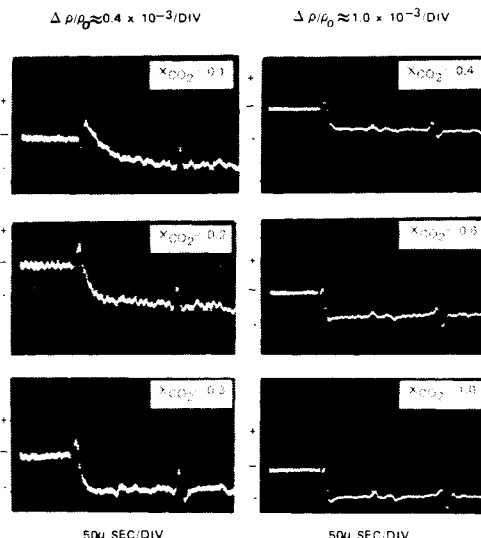


Fig. 37. Photodiode signals showing the interferometrically determined density changes in a mixture of  $\text{CO}_2$  and  $\text{N}_2$  following the irradiation of the mixture with the pulse from a  $\text{CO}_2$  TEA laser of  $\sim 1 \mu\text{s}$  and  $0.5 \text{ J}$  [8].

density increases). These experimental observations show the physics of the kinetic cooling and show proof of the concept. For atmospheric conditions the cooling would persist for longer times and, in order to be beneficial, would occur during the laser beam propagation, either pulsed or CW.

The influence of kinetic cooling on a CW beam with a cross-wind has been calculated by Wallace and Camac [34] under more realistic conditions and the intensity contours predicted by their computer code are shown in Fig. 38. For the conditions shown, the relative humidity is low, the absorption is due to  $\text{CO}_2$ , and the relaxation time of the upper absorbing level is twice the flow time across the initially parallel Gaussian beam. The strength of the distortion in terms of our nondimensional parameters is  $N_c = 0.5$ . Several interesting aspects of the distortion of the beam when cooling occurs can be noted. First, the wind is from left to right and the beam is refracted in the direction of the wind, opposite to that which occurs in the case of heating. Second, the beam is expanded in the direction of the wind and compressed in the direction transverse to the wind, again the opposite of the case with heating. The net effect is an increase in the peak intensity. For long atmospheric propagation paths this may prove to be an extremely important and advantageous effect in that the focusing effect due to kinetic cooling could balance the diffraction spreading, making it possible to propagate high-power beams over long ranges, not only in the absence of beam expansion due to thermal blooming but the channeling effects of kinetic cooling.

#### B. Turbulence and Blooming

Atmospheric turbulence can have two effects on the thermal blooming; turbulent spreading can cause changes in the intensity contour and directly influence the self-induced effect or turbulent motion of the atmosphere can influence the temperature gradients and thereby alter the thermal blooming.

The first effect is due to atmospheric index of refraction gradients which cause distortion of the beam even in the absence of thermal blooming. The second is the mechanical motion of the atmosphere due to turbulence and the influence that those velocity fluctuations have on the thermal distortion.

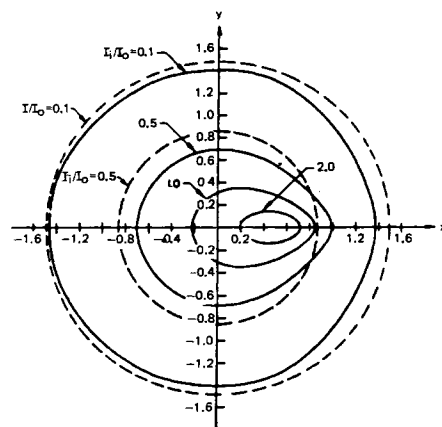


Fig. 38. Intensity contours of CW laser beam showing the effects of kinetic cooling [7].

First we consider turbulent induced spreading and thermal blooming. This is a highly complicated transient problem. Turbulent induced spreading alone has been the subject of extensive studies. Yura [63] and Lutomirski and Yura [64] have shown that the time average mean value of turbulent induced beam spread is given by

$$a_t = 2z/k\rho_0 \quad (43)$$

with

$$\rho_0 = \begin{cases} \infty, & z < z_c \\ (0.5k^2 C_N^2 z)^{-3/5}, & z_c < z < z_i \\ (0.76z^{1/2} C_N l_0^{-1/6} k)^{-1}, & z > z_i \end{cases}$$

where  $a_t$  is the turbulent induced beam radius,  $\rho_0$  is referred to as the radial coherence length,  $C_N^2$  is the refractive index structure constant of the turbulence and is a measure of the strength of the turbulence,  $L_0$  is the outer scale size of the turbulence,  $l_0$  is inner scale size of the turbulence. The qualifications on the range are given as

$$\begin{aligned} z_c &= (0.4k^2 C_N^2 L_0^{5/3})^{-1} \\ z_i &= (0.4k^2 C_N^2 l_0^{5/3})^{-1} \end{aligned} \quad (44)$$

There probably is no such thing as a typical atmospheric turbulence condition, but a moderate turbulence is given by [65] a  $C_N^2 10^{-15} \text{ cm}^{-2/3}$ ,  $l_0 = 0.1 \text{ cm}$ , and  $L_0 = 10 \text{ m}$ .

Thus for a given set of atmospheric conditions the beam spread due to turbulence can be calculated using (43). We also know how to calculate the thermal distortion in the absence of turbulence. The problem with the combined effect is that atmospheric turbulence is a transient phenomena with fluctuations that have a wide-frequency spectrum and it is not known how to handle the combined effects analytically. If the frequency were very fast compared to the time required to establish the steady-state thermal distortion then turbulence spreading would increase the beam size and the thermal distortion could be calculated based on the larger turbulent spread-laser beam. For low frequencies, the turbulence would cause spreading of the thermally bloomed beam and the blooming would be determined by the initial laser beam size. For intermediate frequencies, the combined effect is a transient problem and can not be treated analytically. Gebhardt

[66] has analyzed high-power-laser propagation and assumed that turbulence was sufficiently fast that it resulted in an effectively larger beam. He then calculated the thermal blooming based on the larger beam radius. This assumption has been justified for a number of cases. The explanation for why this works is given in detail in the analysis of the combined effects of thermal blooming and beam jitter.

Numerical computer simulation of the combined effects of thermal blooming and atmospheric turbulence have been carried out by Brown [67], Bradley [68] and Fleck *et al.* [48].

According to Fleck *et al.* [48] turbulence was included as a random statistical fluctuation on the index of refraction for each increment of the propagation path and this random phase distortion was added onto that due to blooming. A random "phase screen" of turbulence was added numerically and evaluated in time along with blooming. Their code capability thus allowed them to combine the two effects as they are realized in atmospheric propagation. However, it is not clear from their results how to handle the two effects simultaneously by an analytic method. Brown [67] in his analysis compared this type of an approach with the analytically tractable approach of the square root of the sum of the squares of the combined effects of blooming and turbulence and found that they agreed reasonably well. In the section describing the combined effects of blooming and beam jitter, a phenomenon close to that of turbulence, we will show why this approach is valid. The second important aspect of atmospheric turbulence is the influence of the mechanical or velocity turbulence on thermal blooming discussed in the following paragraphs.

An experimental and theoretical analysis of mechanical (velocity) turbulence on thermal blooming was reported by Gebhardt *et al.* [69] where they simulated the mechanical turbulence in a laboratory scale experiment with a 2 m long cell. The mechanical turbulence was generated by opposing spray bars in the cell as depicted schematically in Fig. 39. The mechanical turbulence does not simulate real atmospheric turbulence, but control of the turbulent eddy size was possible and experimentally it was verified that it was homogeneous and isotropic. It was found that the influence of turbulence could be characterized by a parameter

$$\Gamma = 4K_H/\bar{u}a$$

where  $K_H$  is the turbulent eddy diffusion coefficient equal to  $u'l_c$  where  $u'$  is the rms velocity fluctuation and  $l_c$  is the characteristic scale length of the turbulence.  $\bar{u}$  is the average transverse velocity coefficient and  $a$  is the laser beam radius.  $\Gamma$  is the ratio of the heat transfer from the beam caused by eddy diffusion to that by the wind or convection.  $K_H$  was measured in the experiment with a hot wire anemometer, and typical data for thermal blooming as a function  $\Gamma$  is shown in Fig. 40. These are oscilloscope traces through the center of the beam with each trace marked by the appropriate  $\Gamma$  and other conditions fixed.

The results of the experiment showed that the mechanical turbulence can reduce the thermal distortion for a sufficiently large  $\Gamma$ , but that  $\Gamma$  must be greater than 10 to have an appreciable effect. Even though the mechanical turbulence in the cell does not simulate the real atmosphere, the laboratory experiments along with the diffusion model developed in [69] can be used to provide a qualitative estimate of the relative importance and effect of velocity turbulence on atmospheric propagation.  $K_H$  is taken to be  $u'l_c$  where  $u'$  is atmospheric

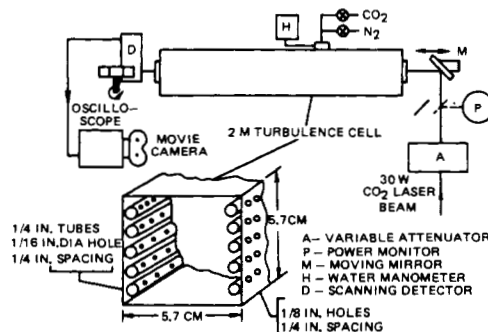


Fig. 39. Experimental apparatus used for the mechanical turbulence and thermal blooming experiment [69].

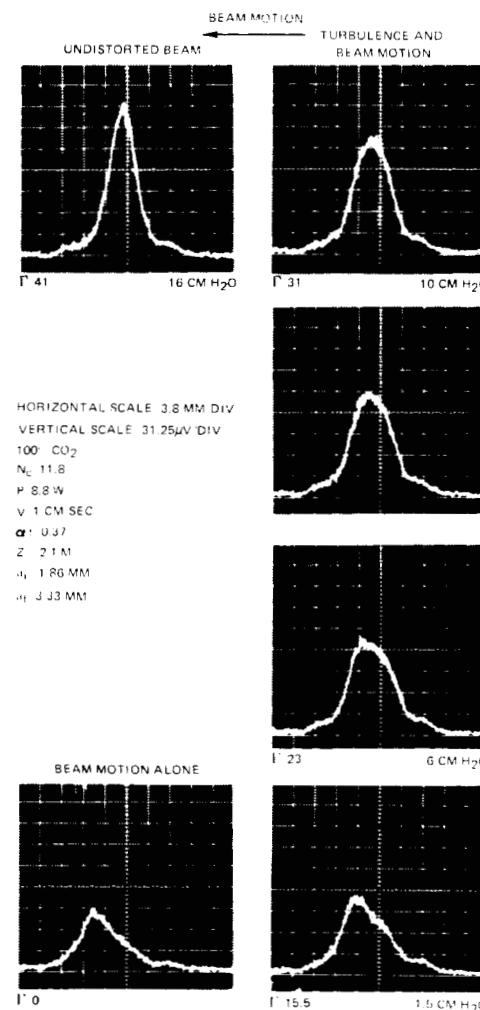


Fig. 40. Intensity contours parallel to the wind for fixed distortion conditions but variable mechanical turbulence strength [69].

mixing velocity and  $l$  is the scale of the turbulence. Thus

$$\Gamma = \frac{4u'l_c}{\bar{u}a}. \quad (46)$$

In order for the diffusion theory to apply, the turbulent scale size cannot be larger than the beam radius. Said simply, a turbulent eddy that is larger than the beam size does not re-

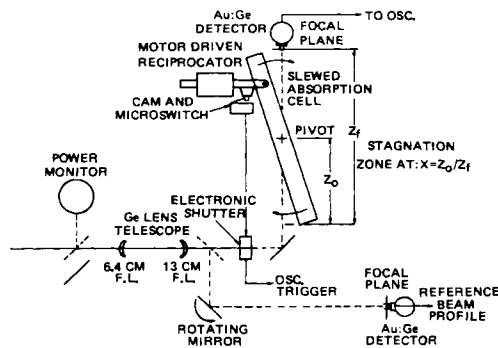


Fig. 41. Experimental apparatus used in the stagnation zone experiment [73].

duce the temperature rise in the laser beam. Thus  $\Gamma$  is approximately equal to  $4u'/\bar{u}$ . For normal atmospheric conditions, the mixing velocity is  $\sim 10$  percent of the wind velocity and thus  $\Gamma$  will be on the order of unity. From the experiments we see that for this size  $\Gamma$ , the effects of mechanical turbulence can be ignored.

There are circumstances where mechanical turbulence could play an important role [70]. One example is the thermal distortion in a stagnation zone. The stagnation zone, discussed in detail below, is a region of zero net motion between the laser beam and the air. In this case, the heat transfer due to eddy diffusion could limit the strength of the thermal lens. This has to be analyzed in terms of the transient nature of the stagnation zone and has not been treated in detail as of yet.

### C. Stagnation Zones

The self-induced thermal distortion is most serious when there is no forced flow or motion of the laser beam relative to the propagation path. This can occur in laboratory environments or on extremely quiet atmospheric conditions. Stagnation zones can also occur when a laser beam is being slewed in the same direction as the wind. The motion due to slew then cancels the wind velocity at one axial point and in this region of the air path there is no net motion. This potentially serious situation was first identified as a problem by Hayes [71] and also by Hogge and Butts [72].

One technique for simulating a stagnation zone in the laboratory is to propagate a CW laser beam through a pivoted absorption cell; the pivot point locates the center of the stagnation zone. A schematic of such an experiment used by Berger *et al.* [73] is shown in Fig. 41. This also enables us to get a physical feel for the problem. The stagnation zone is a transient thermal blooming problem; initially we can consider that, when the beam is turned on, the stagnation zone extends from the laser to the focal plane. As the cell pivots the heated gas is swept out of the extreme ends and the stagnation zone shrinks in length. That portion of the beam that has been traversed by the new gas is effectively in steady state. The region that has not been swept out with new gas continues to heat up and thermal distortion increases in strength in that region. There is a balancing effect since the length of the stagnation zone is shrinking but the magnitude of the temperature rise is increasing. As will be seen, these two effects tend to balance one another and a quasi-steady-state is reached.

Using the apparatus shown in Fig. 41, the thermal distortion of a CW CO<sub>2</sub>-laser beam was examined as a function of pivot rate and pivot position. A typical set of data from [73], showing the relative on-axis intensity as a function of time and

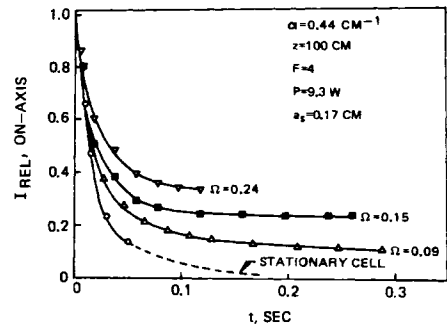


Fig. 42. The relative on-axis intensity as a function of time and slew rate with a stagnation zone located at the mid point of the cell [73]. (The intensity in the figure is not the peak, but the intensity at  $x = y = 0^\circ$ , all other  $I_{RCL}$  in this paper refer to the peak.)

slew rate with the stagnation zone located at the mid-point of the absorption cell is shown in Fig. 42. From the data we observe that the relative intensity decreases with time but arrives at a quasi-steady-state value. As you might expect the quasi-steady-state is approached more rapidly as the slew rate is increased. The experimental parameters are listed in the table in the figure where  $a_s$  is the beam radius at the stagnation zone.

This fairly complicated distortion situation has been successfully modeled by Berger [74] where he was able to predict rather accurately the quasi-steady-state intensity for a wide variety of experimental conditions. He found the scaling parameter by assuming that the stagnation zone could be described by a length equal to  $\Delta z_s = 4a_s/\Omega t$ , and that the strength of the lens is given by the transient blooming parameter. After some manipulation he found a single parameter which could describe the thermal distortion.

$$N_{sz} = \frac{-4\mu_T \alpha P z_f}{\pi \mu_0 \rho c_p a_s^3 \Omega} \omega(x) \quad (47)$$

where  $\omega(x)$  the weighting function which is a function of the position of the stagnation zone,  $x = z_s/z_f$  and the Fresnel number

$$\omega(x) = [x(1-x) + (F(1-x)^2)] \exp(-\alpha z_s) R(x)$$

with

$$R(x) = \begin{cases} 0.5 + 5x, & 0 < x < 0.1 \\ 1, & 0.1 < x < 0.9 \\ 0.5 + 5(1-x), & 0.9 < x < 1.0 \end{cases}$$

The parameter  $R(x)$  corrects for the fact that stagnation zones occurring at the extremities of the propagation path are one sided. With this single parameter Berger [74] found that he could fit the experimental data of Berger *et al.* [73] as shown in Fig. 43. It is noted that the vertical cell data agrees very well with the analytic model and that most of the horizontal data lie above that predicted by the model. This is attributed to the influence of natural convection on the thermal blooming in the stagnation zone and if this were corrected the agreement would be better than the results shown in Fig. 43. Good agreement is obtained in spite of the fact that the model neglects the contribution of the steady-state paths which occur on either side of the stagnation point. This is indicative of the strength of the stagnation zone itself.

Computer code simulation of the transient effects of a stagnation zone have been carried out by Fleck *et al.* [48] and Berger *et al.* [75] where they compared the transient computer code results with the experimental results of [73].

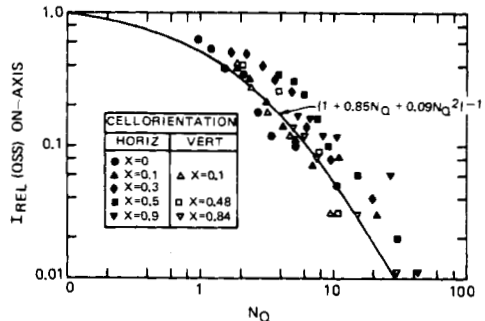


Fig. 43. The quasi-steady-state relative on-axis intensity as a function of the distortion parameter  $N_Q$ . The solid curve is an empirical fit to the experimental data [74].

Fleck *et al.* [48] showed good agreement between code results and experiment when taking into account the finite shutter time of the beam in the experiment as well as the refractive effects of the cell windows. In the experiments the laser beam focal spot was larger than calculated using a diffraction limited Gaussian beam and when Fleck *et al.* tried to account for this by assuming longer wavelength radiation or by focusing the beam beyond the detector plane they found poor agreement with the data. The reason for the poorer agreement is unclear.

Berger *et al.* [75] also compared transient computer code results with the experimental results of [73]. The main problem encountered was in modeling the laser beam turn-on time used in the experiment. For almost all of the cases compared the computer code results agreed with the experimental data indicating that all of the important parameters were considered in the calculations.

There are other important aspects of the stagnation zone which are being studied and will have important impact on determining the seriousness of this problem. There are two potential circumstances that can alter the effects of the stagnation zone: 1) axial motion of the zone and 2) noncoplanar geometry. The first effect can arise because the laser beam has a variable slew rate thus changing the axial location where the net velocity is zero. The second effect arises because the laser beam and focal plane do not always occur in a two-dimensional plane; thus there is a component of slew in the plane transverse to the wind and the direction of the propagation beam. These effects can alter the overall influence of stagnation zones and must be accounted for in a final analysis of the seriousness of stagnation zones on high-power laser propagation in the atmosphere. Another aspect is a comparison of multiple-pulse laser propagation with CW laser propagation when a stagnation zone is present. The presence of such a zone could reduce the advantage of pulsed versus CW laser operation.

#### D. Transonic Flow

Almost all CW thermal blooming problems are associated with the heating process occurring at constant pressure, which is a valid approximation for low wind speeds. However, for a rapidly slewed beam or as wind speeds approach Mach 1 the effects of compressibility become important, and the density changes near sonic velocities, caused by the addition of a small amount of energy due to absorption of laser power, can become large compared to those calculated ignoring compressibility. This problem was first analyzed by Hayes [76] and Hogge [77] with a one-dimensional treatment of the problem using the linearized hydrodynamic equations to predict the

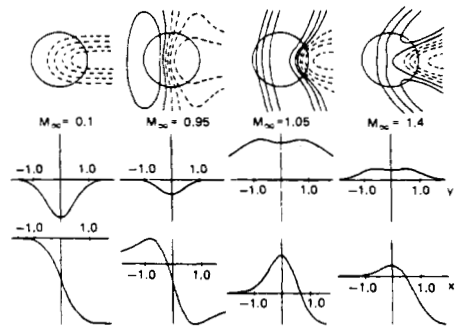


Fig. 44. Normalized steady-state density distributions as a function of the Mach number [80].

density changes. In addition, the problem of the density changes caused by heating near Mach 1 flows was also analyzed by Bradley [78] and Ellinwood and Mirels [79]. Subsequent calculations by Wallace and Pasciak [80], and Fleck *et al.* [48] have shown the importance of the two dimensionality of the problem for predicting the density gradients. A simple experiment was performed by Brown and Smith [81], which showed that shock waves predicted in the one-dimensional analysis are not observed in the experiments because of the two-dimensional flow and alternation of the flow pattern.

A first estimate as to the importance of transonic flow can be obtained by calculating the change in stagnation temperature caused by absorption of laser radiation

$$\Delta T_0 = \frac{\alpha I 2a}{\rho V c_p} \quad (49)$$

and comparing this with the stagnation temperature difference between that at the flow Mach number and that corresponding to Mach 1 flow. If the temperature change is sufficient to equal that difference, then the density changes caused by the transonic flow can be greater than those due to heat addition at constant pressure. The flow can be either less than or greater than Mach 1 since the addition of heat always drives the flow to Mach 1. It is interesting to note that in this transonic region, not only can the magnitude of the density change be larger, but also the sign can be different and complex in shape as shown by Wallace and Pasciak [80].

The most complete theoretical discussion of the influence of transonic flow on thermal distortion has been given by Wallace and Pasciak [80] where they solved numerically the two-dimensional steady-state nonlinearized hydrodynamic equations combined with wave propagation equations and predicted the thermal distortion in the transonic-flow regime. The nonlinear equations are required to treat this problem in order to accurately and correctly calculate the density changes for flows close to Mach 1. Shown in Fig. 44 are density distributions for various Mach number flows from [80]. The upper series are density contours with the dashed contours showing density decrease and the solid contours represent density increases above ambient. The middle and bottom sketches in Fig. 44 are profiles transverse to the direction of wind and parallel with the wind, respectively. These profiles have been normalized to unity just to show the qualitative difference in the density changes and shows that both the magnitude and type of distortion encountered by laser beams in this flow regime should be quite different from that encountered for low Mach number flows. Wallace and Pasciak calculated the thermal distortion for both slewed laser beams where the transonic regime was reached because of slewing and also for

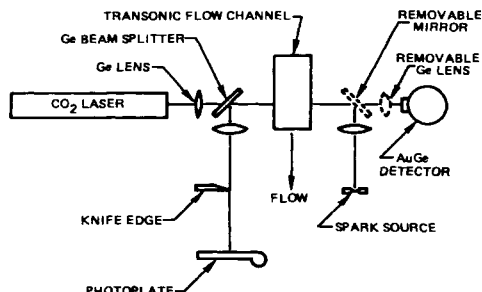


Fig. 45. Experimental apparatus used in the transonic thermal blooming experiment [81].

uniform wind near the transonic flow point along the whole path. For a 2-km path with an absorption of 0.2 km<sup>-1</sup> and a uniform velocity with a Mach number of 1.0001, their calculations show that a 25-kW CW beam with an initial radius of 35 cm is distorted rather severely with an increase in beam area of roughly a factor of two. If we had ignored compressibility effects, the distortion parameter given by (18) for these same conditions is  $\sim 10^{-2}$  and blooming would have been predicted to be negligible. For this highly unlikely case of  $M = 1.0001$  along the whole propagation path transonic effects are important. For the slewed beam case, the transonic regime only exists for a very short path length, and their conclusion is that the effect is small and negligible. This same conclusion was reached by Ellinwood and Mirels [79]. Also the calculations of Fleck *et al.* [48] show small distortion effects for slewed laser beams even with a portion of the path passing through the transonic regime.

The only experimental data on the influence of transonic flow was reported by Brown and Smith [81]. Using the apparatus shown in Fig. 45, they investigated experimentally the density changes caused by laser-beam heating of a gas at flow Mach numbers of 1.19. The gas was expanded through a nozzle and consisted of nitrogen seeded with SF<sub>6</sub> to increase the absorbed power. The laser was a quasi-CW CO<sub>2</sub> laser operating at  $\sim 500$  W. For the experimental conditions,

$$\Delta T_0 = \frac{\alpha I d}{\rho V c_p} \approx 18 \text{ K.}$$

For Mach 1.2 flow the stagnation temperature difference between Mach 1 and 1.2 is only 1.8 K. Thus under the experimental conditions we anticipate considerable interaction and based on one dimensional analysis we would predict the formation of a shock. Shown in Fig. 46 are Schlieren photographs of the flow field for various conditions. Fig. 46(a) is a Schlieren photo with flow but no laser beam to show the uniformity of the unperturbed flow field. Fig. 46(b) shows the conditions with no flow but with absorber in the gas to locate the position of the laser beam. Fig. 46(c) is  $M = 1.2$  flow with the schlieren knife edge vertical to show density gradients in the direction of flow and 46(d) is for the same flow and laser conditions but with the schlieren knife-edge horizontal to show the density gradients in the direction transverse to the flow. Even though the absorption was sufficiently great to alter the stagnation temperature by a significant amount, no shock waves were formed in the flow. Brown and Smith [81] results therefore showed that even under very adverse conditions shock waves are not formed; further experimental work is required to determine experimentally the distortion due to density gradients in the transonic regime and verify the theoretical predictions.

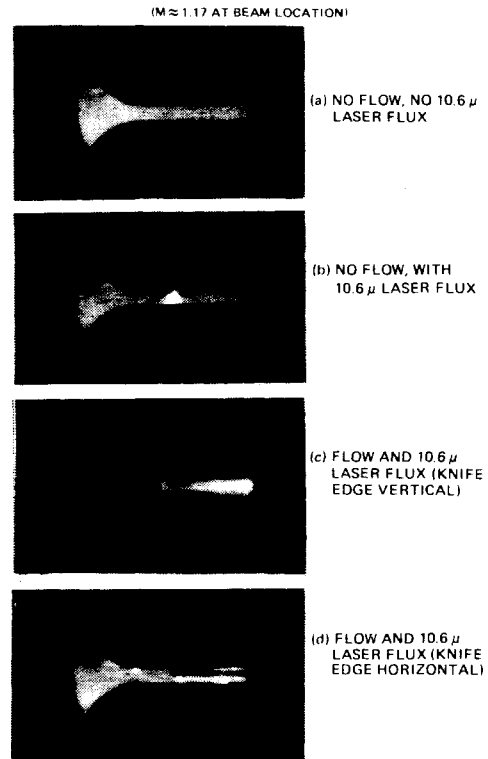


Fig. 46. Schlieren photographs of the laser induced density changes in a transverse flow at Mach number of 1.17 [81].

### E. Laser Beam Jitter

An important area of research involving thermal blooming is the modeling of the combined effects of thermal blooming with other propagation phenomena such as atmospheric turbulence or beam motion caused by jitter. Since thermal blooming is a nonlinear problem which depends on the laser intensity there can be a considerable increase in the complexity of the problem introduced by beam jitter. Beam jitter can arise from motion of the pointer/tracker, transients in the laser medium itself, or beam motion caused by atmospheric turbulence. The frequency and amplitude of the jitter motion can vary over a wide range of values and in order to predict the influence of jitter, a full four-dimensional computer code is required to analyze the problem. Gebhardt and Smith [82] have analyzed the problem and have performed laboratory experiments to investigate experimentally the combined effects of blooming and jitter and these are discussed below.

In analyzing the combined effects of jitter plus blooming there are two regimes of laser-beam jitter which can be modeled theoretically and these regimes are dependent on the jitter frequency relative to the characteristics thermal blooming frequency, or the inverse of the time required to reach steady state. The blooming frequency is  $V/2a$  where  $a$  is the laser-beam radius. For a collimated beam there is no problem defining a characteristic radius; however for a focused beam the blooming frequency varies with range and we arbitrarily use the undistorted focal spot radius as the characteristic dimension. This of course is one of the problems in analyzing the combined effects since the blooming frequency is a variable. If the jitter frequency is much less than the blooming frequency then the two effects can be treated separately. We can then calculate the thermal blooming independent of the effects of jitter. The common practice is to assign an effective increase in beam size due to blooming and add this increase to

that caused by jitter, calculating the final beam size as the square root of the sum of the squares, since the two effects, are independent. Thus the final laser-beam intensity is

$$I = \frac{P}{\pi a_f^2 + \pi a_B^2 + \pi a_j^2} \quad (50)$$

where  $a_B$  is the effective increase in beam radius due to blooming and  $a_j$  is the increase in beam radius due to jitter. Thus the relative intensity is

$$I(RSS) = \frac{1}{1 + (a_B/a_f)^2 + (a_j/a_f)^2} \quad (51)$$

where  $I(RSS)$  is the relative beam intensity normalized with respect to the undistorted, unjittered laser-beam intensity.

For the case of very-high-frequency jitter where the jitter frequency is much greater than the blooming frequency, the problem can also be handled analytically. In this case the jitter reduces the degree of focusing and the thermal blooming of the more weakly focused beam can be calculated. One simple analytic technique is to use the distortion parameter based on the jittered laser-beam size

$$N(a_j) = \frac{\mu_T P \alpha z^2}{\rho c_p \pi V(a_i^3)} \left( \frac{a_i}{a_{j+f}} \right) q \left( \frac{a_i}{a_{j+f}} \right). \quad (52)$$

It was shown in Fig. 13 that the thermally bloomed beam can be represented analytically by

$$I_{REL} = \frac{1}{1 + 0.06 N^2}. \quad (53)$$

We can, therefore, calculate the jittered-beam-blooming relative intensity

$$I(jBB) = \frac{1}{1 + 0.06 [N(a_j)]^2} \quad (54)$$

where  $I(jBB)$  is the intensity at the target normalized with respect to the laser-beam intensity in the absence of blooming but with jitter (i.e., not normalized with respect to the diffraction limited intensity but with the jittered beam intensity). Thus in these two extremes, the two effects can be handled analytically. The problem arises in the intermediate case where the jitter frequency is comparable to the blooming frequency. In this regime the problem is a transient one, and no simple analytic treatment is possible. The problem is further complicated for the focused case where the laser beam size is changing and it is possible to encounter both the low- and high-frequency regimes and no simple analytic treatment has been found.

Experiments were performed by Gebhardt and Smith [82] to examine the combined effects of laser-beam jitter and thermal blooming in a laboratory-scaled experiment. They examined the effects of both laser-beam jitter amplitude and frequency on the thermal distortion of a CW CO<sub>2</sub>-laser beam.

A schematic of the experimental apparatus is shown in Fig. 47 where the laser, wind tunnel, and beam diagnostics are similar to those discussed in describing previous thermal-blooming experiments. The beam jitter is provided by a pair of orthogonally mounted scanning mirrors which are electrically driven. The driving source is amplified thermal noise which was chosen because of its randomness and zero-mean. The noise was generated by a high-gain differential amplifier and passed through a tunable bandpass filter (effective  $Q$  of 15) before being applied to the scanning mirrors. The amplitude of jitter signals was measured using a visible He-Ne laser beam and measurement of the beam displacement at the end

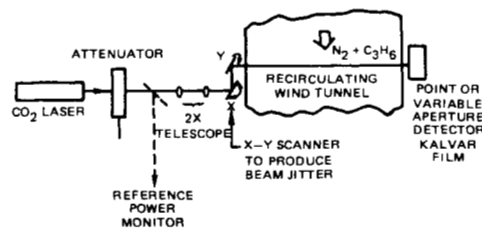


Fig. 47. Experimental apparatus used in the laser-beam jitter plus thermal blooming experiments [82].

$\alpha z = 0.36 - 0.51$
$t_B = \frac{1.7}{2(0.1)} = 8.5$
$a_i/a_f = \frac{0.27}{0.10} = 2.7$

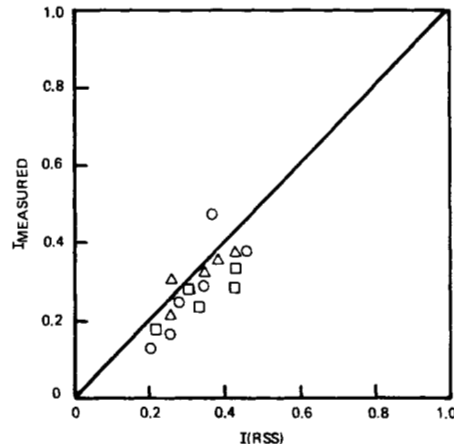


Fig. 48. Measured relative peak intensity as a function of the calculated intensity for combined laser-beam jitter and thermal-blooming effects [82].

of the wind-tunnel was photographic. In measuring the intensity of the jittered beam, the scan rate of the detector is set sufficiently slow so that an average intensity is measured.

The data can be analyzed in two ways: 1) measurement of the peak intensity and comparison with the *RSS* model or 2) measurement of the peak intensity and comparison with that predicted by the *JBB* model. Shown in Fig. 48 is a comparison of the measured relative intensity with that calculated using the *RSS* model. The data is marked by the various jitter frequencies. For this data, we measured the thermal blooming in the absence of jitter and used the measured value to calculate  $a_B$ ; this value was then used to calculate  $I(RSS)$ . The thermal blooming frequency is 8.5 based on the undistorted focused spot. For this data the experimental variable was laser power and the jitter amplitude was set at one value for the different jitter frequencies. Along the solid line, the *RSS* theory and experimental data agree. With the exception of two data points the measured value lies below that predicted by the *RSS* model. The most interesting aspect of the data is that the measured value of the intensity of the jittered and bloomed beam is independent of the jitter frequency. The frequency range covered is both lower and higher than the blooming frequency. Even if the blooming frequency is calculated based on the initial beam radius, the jitter-frequency range covered is still both lower and higher than this value.

The second technique for analyzing the data is the *JBB* modeling. Shown in Fig. 49 is the measured relative intensity as a function of the calculated thermal distortion parameter based on the jittered beam size.  $I_{REL}$  is normalized with re-

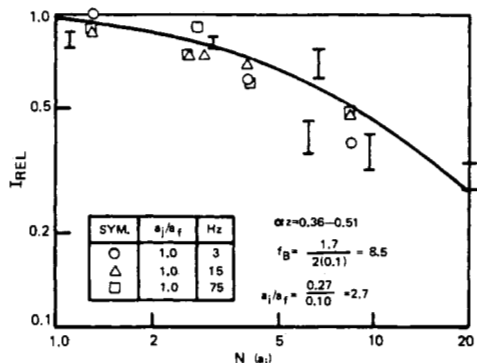


Fig. 49. The relative peak intensity as a function of the distortion parameter for thermal blooming plus beam jitter [82].

spect to the intensity in the absence of blooming but with beam jitter. The vertical bars represent the thermal-blooming data in the absence of jitter. Again no systematic trend of the data is observed as a function of jitter frequency.

In analyzing the experimental data, Gebhardt and Smith [82] showed that if the thermal blooming could be represented by a quadratic dependence on  $N$  such as (53) then the two models give identical answers. This says that the reduction of blooming caused by beam jitter is just compensated by the reduction of the intensity caused by jitter. Since the RSS-type of analysis is more simple to implement, it is probably the one to use in evaluating the combined effects of blooming and jitter.

One aspect of the combined blooming-jitter problem which has not been analyzed is the effects of the initial laser-beam shape. The analyses and experimental results presented above were for an initial Gaussian shaped beam. When a random-zero mean-jitter spectrum is imposed on a Gaussian, the resulting beam, on average is still Gaussian. Thus the basic shape is conserved. If the beam were initially a uniform amplitude beam and the jitter spectrum were imposed on it, the basic shape of the beam would be changed. Recall from Fig. 13 that the thermal distortion of a uniform beam was functionally different than that for a Gaussian beam. Thus when jitter is added to a laser beam with a shape other than Gaussian the thermal distortion itself will be different because of the change in beam shape. We would therefore anticipate that the simple analytic analysis applied above would not work and the distortion would then depend on jitter frequency and amplitude.

The results of the influence of beam jitter for the initial Gaussian shaped beam can be directly applied to the analysis of the problem of atmospheric turbulence and blooming. The experiments and theory have shown that the frequency of the motion of the beam does not influence the end result of the loss in intensity when combining beam motion and thermal blooming. This then explains why atmospheric turbulence effects can also be modeled by the RSS technique since the frequency spectrum of the atmospheric turbulence would not matter. This result was corroborated by the numerical computer code modeling of atmospheric turbulence discussed previously.

#### F. Aerosol Absorption Induced Blooming

In addition to molecular constituents, solid particles in the atmosphere also absorb and scatter laser radiation. For some laser sources where the molecular absorption is low, such as some lines of the DF chemical laser, or for a particularly high concentration of aerosols, the aerosol absorption can be greater than the molecular. In any case, it is important to de-

termine the contribution of aerosol absorption to thermal blooming. The aerosol absorption problem is different from the molecular absorption in several aspects. 1) Before thermal distortion can occur the absorbed energy must be transferred from the particle to the surrounding gas. This is somewhat analogous to the transfer of vibrational energy of a molecular absorber to translational energy. 2) The aerosols are distributed spatially far apart and the heating is not truly volumetric. 3) For sufficiently high laser-beam intensities, particles can reach the melting point and the absorbed power does not go completely into heating but a fraction of the energy is used in phase change. The latter effect is analogous to a saturation of molecular absorbers. Some aspects of the aerosol absorption problem have been analyzed both experimentally and theoretically and these are discussed in this section.

The problem of nonuniform heating of the propagation path caused by aerosol absorption has been treated by a simple analysis by Smith and Brown [83] and more rigorously by Lencioni and Kleiman [84]. Initially the particles are heated by absorption of laser radiation and conduction of heat from the particle produces a spherical region of air around the particle which expands at the thermal diffusion rate. The propagation path consists of hot spheres of air centered on the aerosol with the accompanying index of refraction change. If we neglect for the moment the time required to transfer the heat from the particle and assume that the observation time is long compared to the acoustic transit time across the laser beam (i.e., the heating is occurring at constant pressure), the problem is calculating the net effect on the laser beam propagating through the heated spheres. It has been shown [83], [84] that if a sufficient number of spheres are encountered, the net phase changes on the laser beam (and thus the thermal distortion) can be calculated from the volumetric absorption of the aerosols. Thus, in theory, the thermal distortion caused by aerosol absorption can be calculated in the same manner as for molecular absorption using the absorption per unit path length due to aerosols. This result is independent of the growth rate of heated spheres and therefore independent of the inner particle spacing and thermal diffusion time.

The short-time behavior of aerosol induced blooming effects were addressed by Lencioni and Kleinman [84] and by Chan [85]. In [84], it was assumed that the heat transfer from the particle to the surrounding air occurred on a fast time scale. After heating the air, the mass removal from the heated region (and thus index of refraction change) occurs at the acoustic velocity. The mass removed for the heated region surrounding the aerosol is contained in a positive density increase located at a distance of  $ct$  from the aerosol. This is analogous to the  $t$ -cubed blooming problem, but is occurring on a scale size of the order of the inner particle spacing. In the analysis of Lencioni and Kleiman, they showed that the integrating effect of the laser beam passing through this complex structure was again the same as that which occurs for a true volumetric absorber. In other words, neglecting the time required to transfer the absorbed power from the aerosol to the air, the aerosol absorber is again the same as molecular absorbers and  $t$ -cubed-type blooming would occur, with the characteristic time determined by the laser beam radius and independent of the aerosol inner particle spacing.

Chan [85], however, has shown that the time required for transfer of absorbed power from aerosols to the air can be important and lead to a delay in the effective heating rate. He showed that the temperature rise of the air for typical aerosol sizes and distributions could be delayed by tens of microsec-

onds due to the heat transfer time from the solid to the surrounding air. This effect then would be important for laser pulses of this length. What has not been analyzed theoretically is the combined effects of particle heat transfer time combined with the hydrodynamic equations to predict the thermal distortion caused by aerosols in the short-time regime.

A limited number of experiments have been reported concerning aerosol-induced blooming. Brown and Smith [86] examined aerosol induced blooming in a laboratory experiment comparing the thermal blooming of a CW CO<sub>2</sub>-laser beam caused by molecular absorption with that caused by carbon dust suspended in a gas cell. For their particular experiment the interparticle diffusion time was short compared to the laser beam transit time and they observed that qualitatively the blooming was the same for both cases. Quantitatively the distortion due to aerosols was slightly less than that caused by molecular absorption, but Brown and Smith [86] felt that the difference could be explained by experimental difficulties in obtaining a uniform carbon particle distribution in the cell. Since the time scale for reaching steady thermal blooming is long compared to inner particle thermal diffusion time (and certainly the hydrodynamic time) these results can not be used to evaluate the transient response of aerosol blooming.

An experiment to examine the transient response of aerosol induced blooming was performed by Smith [87] where he seeded a gas cell with carbon dust and propagated a TEA CO<sub>2</sub> laser pulse through the carbon-laden cell. The cell was located in one arm of a Mach-Zehnder interferometer in a setup very similar to that used in the kinetic cooling experiment shown in Fig. 36. A photomultiplier was used to monitor the density change in the gas caused by aerosol absorption. In the absence of aerosols there was no measurable change in gas density. The TEA laser pulse was  $\sim 1 \mu\text{s}$  in duration and, on the time scale of the experiment, can be considered an instantaneous heating source of the carbon particles. Shown in Fig. 50 are oscilloscope traces of the interferometer intensity monitored with a pin-hole-apertured photomultiplier showing the density change as a function of time for two different concentrations of carbon particles. The laser pulse was fired at  $t_0$  as marked on the oscilloscope. The rise time of the density change is independent of the concentration, and the time required to reach 90 percent of its maximum density change is 50  $\mu\text{s}$ . According to the theoretical model of Fader [88] the time required for an instantaneous volumetric heating source to reach this condition for a laser beam radius of 0.5 cm is 17  $\mu\text{s}$ . Thus the experimental results indicate that the finite time associated with the transfer of energy from the particles can increase the response time of the density changes relative to that of a molecular absorber with fast collisional deactivation. The experiment further shows that the response time of aerosol induced blooming is certainly much faster than the inner particle diffusion time as was predicted by the theoretical models [83], [84].

In summary, aerosol absorption can cause thermal blooming and, for CW laser beams, the distortion can be calculated just as for molecular absorbers. For time scales as short as a few microseconds, the thermal distortion is delayed by the combined effects of the rate of heat transfer from the particles and the hydrodynamics of the density change. This problem has not been fully analyzed. In addition, the aerosols can be vaporized at sufficiently high laser-beam intensities. If the vaporization temperature is reached then not all of the absorbed laser power contributes to thermal blooming since the latent

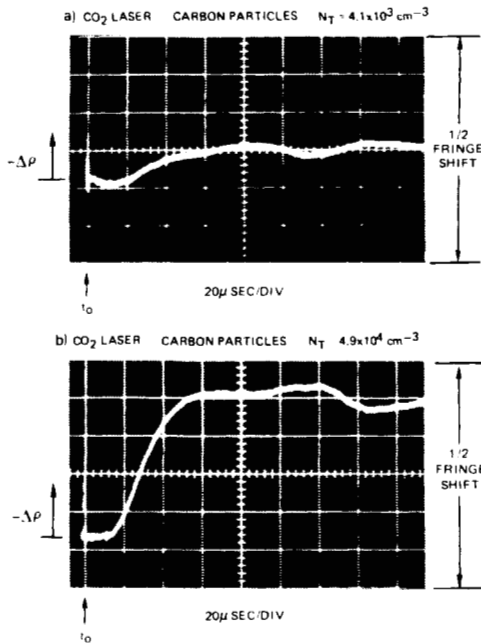


Fig. 50. Oscilloscope traces of the interferometrically determined density changes of a gas caused by aerosol absorption heating [87].

heat of vaporization must be subtracted out. This problem also requires further analysis.

#### G. Effects of Beam Shape

Since the thermal distortion is self-induced and is a result of the heating of the path by the laser-beam intensity, some interesting effects can be observed with different intensity profiles. For example, for a rectangular uniform-intensity laser beam, the thermal distortion in the CW case does not cause beam spreading but just a bending of the beam. However, in most cases of focused beams and with diffraction, the intensity profile evolves into an intensity pattern with gradients similar to a Gaussian, and beam shape effects are not as important as first thought. Further, since CW blooming is a result of the integral of the intensity across the beam, the gross effects of beam shape are integrated out.

Recall the computer code results shown in Fig. 13 which compared the thermal distortion of infinite Gaussians, truncated Gaussians, and uniform-intensity profiles. The distortion is certainly different for the three cases, but rather than being due to a gross beam-shape effect, it can be accounted for by an effective larger laser beam radius associated with the beams with more uniform intensity contours.

The initial intensity profile is most important when the thermal distortion is weighted near the transmitter. For these cases, laser-beam profiles that cause self focusing have been considered, such as a beam with an intensity which increases in the wind direction which tends to focus the laser beam. Transient thermal blooming may offer more potential for reducing the thermal blooming by optimizing the beam shape. An example of this is to propagate a collimated unstable resonator beam and follow this with a smaller beam that can be channeled in the gradients that tend to focus the beam. There are obviously many concepts that can be considered for producing different thermal blooming effects, especially in the transient regime. We will only consider the CW case in this section since beam-shape effects on transient blooming have not been treated in detail. In particular the experimental results of the thermal distortion of unstable

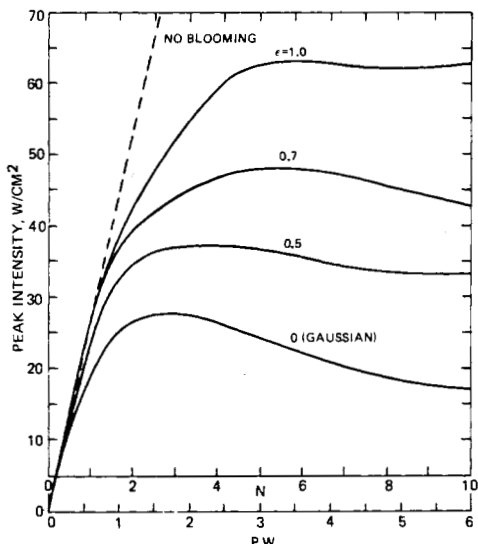


Fig. 51. Computed peak intensity as a function of laser power with each curve labeled by obscuration  $\epsilon$  normalized with respect to the  $e^{-1}$  beam radius [89].

resonator beams of different obscuration ratios are discussed in detail below.

The wave optics computer code was used to calculate the thermal distortion of an annular beam [89]. For these calculations an infinite Gaussian beam was used with different obscurations of the center portion  $\epsilon$  which is normalized with respect to the initial  $e^{-1}$  beam radius of the Gaussian. Shown in Fig. 51 is the peak intensity of the thermally distorted beam as a function of laser power (and also the distortion parameter  $N$ ) with each curve marked with different degrees of obscuration  $\epsilon$ . For these calculations the following parameters were used:

Medium Parameters	Initial Beam Characteristics
$\alpha = 4.5 \times 10^{-5} \text{ cm}^{-1}$	$a_0 = 0.43 \text{ cm}$
$\mu_0 = 1.0$	$R = 108 \text{ cm}$
$\mu_T = -1.4 \times 10^{-5} \text{ }^{\circ}\text{C}^{-1}$	$\lambda = 10.6 \text{ m}$
$\rho = 1.79 \times 10^{-2} \text{ g/cm}^3$	$\beta = 1.58$
$c_p = 0.86 \text{ J/g }^{\circ}\text{C}$	$\lambda_e = \beta\lambda$ (effective wavelength)
$t = 103 \text{ cm}$ (cell length)	
$z = 108 \text{ cm}$ (total length)	

(In these calculations, we have used the standard practice of increasing the laser wavelength to account for the laser beam quality.) The conditions were chosen to correspond to experimental conditions to be described. For a fixed laser power, the thermal distortion is observed to be less for larger obscurations. An interesting feature of an obscured Gaussian is that for the same power, the peak intensity in the focal plane is independent of the size of the central obscuration. Thus from Fig. 51 we see that the thermal distortion is significantly less for the obscured beams compared to the infinite Gaussian. This can be qualitatively explained in terms of the effective larger laser aperture size for the truncated beam and, at least qualitatively we would expect less distortion for larger diameter laser beams with the same laser power.

Experiments were performed by Gebhardt [89] to examine the CW thermal distortion of unstable resonator-type beams using the apparatus shown in Fig. 52. The unstable resonator beam is generated by reflecting the Gaussian shaped beam off

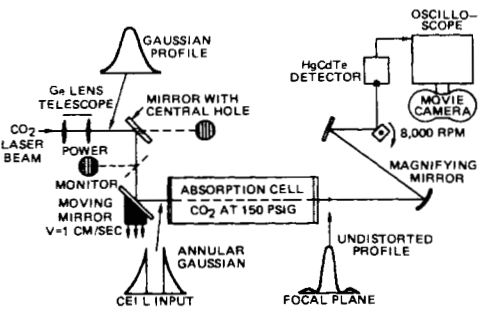


Fig. 52. Experimental apparatus used in the unstable resonator thermal blooming experiment [89].

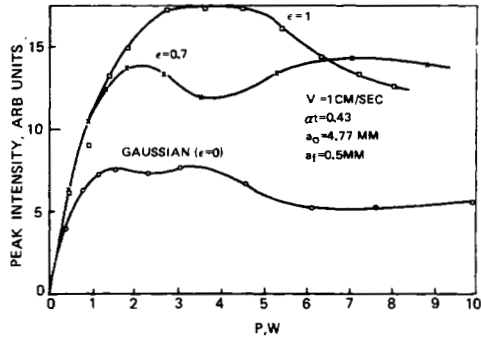


Fig. 53. Experimentally measured peak intensity as a function of laser power with different degrees of obscuration [98].

of a mirror with a variable diameter hole. The absorption cell was filled with 10 atm of CO<sub>2</sub>, and the intensity contour exiting the cell was measured with a mercury-doped-germanium detector with a pin-hole aperture. The beam was scanned across the detector and the output recorded on an oscilloscope. Shown in Fig. 53 is the measured peak laser intensity plotted as a function of laser power for three different obscurations. For these experimental conditions  $N = 1.53P$  with the power in watts. The general shape of the curves are similar to those previously observed with a peak in the intensity as a function of laser power. The annular peak intensities are greater than those of the Gaussian being 1.9 and 2.3 times higher for the  $\epsilon = 0.7$  and 1.0 respectively. Comparison of these peaks with the theoretical curves of Fig. 51 shows good agreement between the theory and experiment. The finer details of the data such as the cross over in the peak intensity for the two annular cases can probably be attributed to experimental errors. At a power level of 7 W the thermal distortion is quite severe and small changes in laser beam size or alignment can cause significant errors in peak intensity on the scale shown.

The reduction in thermal blooming with unstable resonator beams can be attributed to the effectively larger laser beam size. The distortion parameter scales as  $(\text{diameter})^{-2}$ , and by concentrating the laser power on the outer extremities of the beam radius, we reduce the air path heating and temperature gradients for the same transmitted laser power.

The effects of different beam shapes and a discussion of optimum beam shapes for minimizing thermal blooming were presented by Wallace *et al.* [90]. These results, described as preliminary, showed advantages to tailoring of the laser-beam intensity contours by using an intensity ramp with the intensity increasing in the wind direction and cylindrical focusing optics to counteract the defocusing of the beam in the direction transverse to the wind.

Another beam shape which has been considered theoretically is the uniformly illuminated aperture. If we compare the thermal distortion of this beam shape with that of a Gaussian truncated at the  $e^{-2}$  diameter equal to the uniform diameter, we find that the thermal distortion is less as shown in Fig. 13. This again can be explained in terms of an effective beam size; since the uniformly illuminated aperture has more power at the edges than the Gaussian, the temperature gradients are reduced compared to the Gaussian. In the near field of a uniformly illuminated aperture, the temperature gradient in the wind direction is linear, which does not cause distortion but rather just bending. However, from a practical standpoint, this uniform illumination lasts for only a few beam diameters and the focused beam rapidly evolves into an Airy pattern with a bell-shaped intensity pattern and this shape does lead to density gradients which deform the laser beam.

Again for the CW case, it does appear that the effects of laser-beam shape on the thermal blooming are of secondary importance. It is still possible to describe the thermal distortion by a simple parameter for various laser-beam shapes. An interesting exercise would be to determine the effective laser-beam size associated with each intensity profile, such that the distortion could be described by a single parameter independent of the beam shape.

#### H. Phase Compensation of Thermal Blooming

Since the intensity loss associated with thermal blooming is caused by a redistribution of the laser beam power, as distinguished from an absorption loss, it is reasonable to consider techniques to modify the laser source phase distribution to reduce the thermal blooming effect. The basic idea of using phase correction to reduce thermal blooming is to choose the phase at the transmitter such that it counteracts or cancels the beam-induced phase changes encountered along the path. The phase compensation technique is expected to be most effective when the dominant thermal distortion effects occur near the laser source, since the thermal lens can be considered as a thin lens, and its effect can be cancelled by the source correction. The thermal distortion of rapidly slewed CW beams or focused multiple-pulse laser beams is weighted close to the source and therefore should be amenable to phase correction.

The simplest form of phase correction is changing the radius of curvature of the laser beam at the source, or, said another way, changing the degree of focusing. Because the thermal distortion is self-induced, and the distortion depends on the laser intensity itself, it is possible that the optimum condition for obtaining the maximum intensity in the focal plane is not the strongly focused beam. This was demonstrated experimentally by Gebhardt and Smith [44] where they examined the thermal distortion of a CW CO<sub>2</sub> laser beam propagating in a CS<sub>2</sub> liquid cell as a function of the degree of focusing. The experimental techniques used are as described previously. Shown in Fig. 54 are the results of these experiments for two cases, the collimated beam and the strongly focused beam. All other experimental conditions, including the propagation conditions and the initial laser beam radius, were kept constant for these two cases except the focusing. As can be seen, for laser powers greater than 2 W the collimated-beam case can deliver a higher intensity to the focal plane than the strongly focused case. In fact for these propagation conditions, the maximum focal plane intensity was achieved with the collimated beam. Thus the simple concept of refocus can help alleviate the severity of

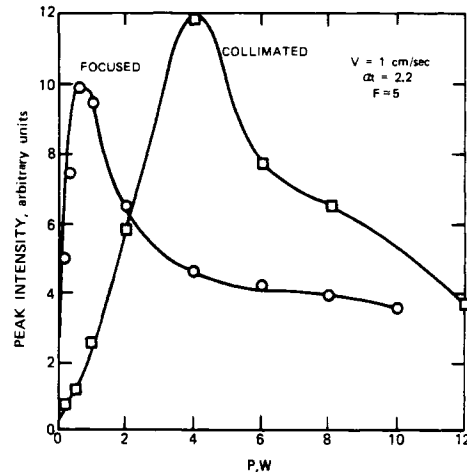


Fig. 54. Experimentally measured peak intensity as a function of laser power for a focused and collimated laser beam [44].

the thermal distortion. For the wind dominated thermal blooming the distortion is not symmetric, and we would not expect the refocusing to be the optimum correction. In the following paragraphs we discuss the phase distortion of CW beams and the optimum phase corrections for reducing thermal blooming.

The phase change of the laser beam is related to the index of refraction by

$$\delta\phi(x, y, z) = k \int_0^z \delta\mu(x, y, z') dz'. \quad (55)$$

For the CW wind-dominated thermal distortion we have previously derived the temperature change and related that to the index of refraction change. If we assume that the laser beam is a Gaussian, to first-order undistorted, and that the focusing can be approximated by a geometric decrease in beam size we obtain for the phase distortion

$$\delta\phi(x, y, z) = \frac{-\Delta}{2} e^{-y^2/a^2} [1 + \text{erf}(x/a)] \quad (56)$$

where erf is the error function and

$$\Delta = \pi FN_c \frac{\ln(a_i/a_f)}{(1 - a_i/a_f)} \quad (57)$$

is the total path integrated phase change across the beam. We have further assumed that  $\alpha z << 1$  in performing the axial integration.  $N_c$  is the collimated-distortion parameter given by (16). It is interesting to expand the phase distortion in a power series about the beam axis and identify the dominant terms of the thermal lens in terms of classical aberrations

$$\begin{aligned} \delta\phi(x, y) = \phi(0, 0) - \frac{\Delta}{\sqrt{\pi}} \left( \frac{x}{a} \right) + \frac{\Delta}{2} \left( \frac{y}{a} \right)^2 \\ + \frac{\Delta}{\sqrt{\pi}} \left[ \frac{1}{3} \left( \frac{x}{a} \right)^3 + \left( \frac{x}{a} \right) \left( \frac{y}{a} \right)^2 \right] - \frac{\Delta}{4} \left( \frac{y}{a} \right)^4. \end{aligned} \quad (58)$$

The linear term, which is associated with the effect of beam bending into the wind is generally referred to as distortion and in this case is pincushion distortion. The quadratic term is known as astigmatism and results in the spreading or blooming of the beam in the plane transverse to the wind. The third-order term is primary coma and the fourth-order term is spherical aberration.

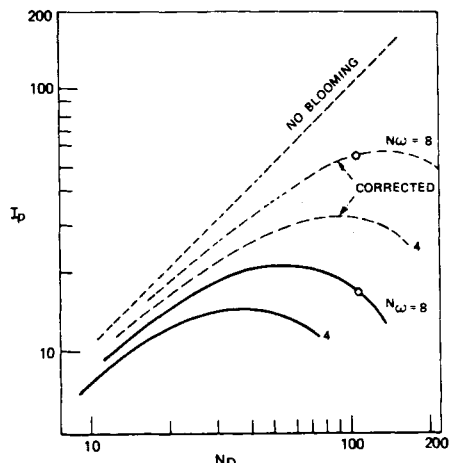


Fig. 55. Computed peak intensity as a function of a distortion parameter, and slew number  $N_\omega$  showing the effects of phase compensation for correcting thermal blooming [91].

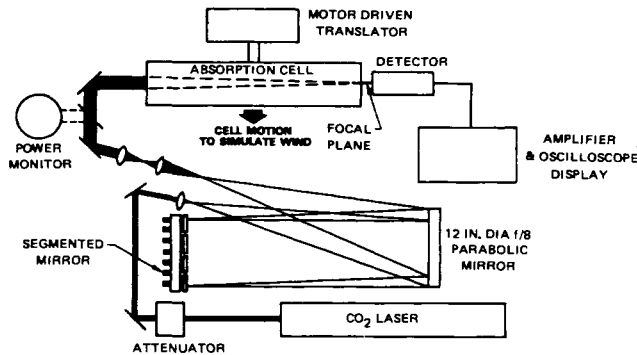


Fig. 56. Experimental apparatus used in the phase compensation of thermal-blooming experiment [92].

A theoretical treatment of phase correction of CW thermal blooming was presented by Bradley and Hermann [91] where they expressed the phase distortion in terms of Zernike polynomials, and examined the phase correction using a computer code. Shown in Fig. 55 is a plot of the peak intensity as a function of their distortion parameter  $N_D$  with and without the phase correction and two different cases of slew rates as obtained numerically. (Their parameter  $N_D$  is related to  $N$  given in (18) by  $N_D = \pi N$ ). As can be seen, phase compensation can lead to an increase in the peak intensity by a factor of two to three. This increase is due to both an increase in the peak at fixed power and also an increase in the critical power or the power where the maximum flux is achieved. It is also interesting to note that the phase correction is more effective for high slew rates. With higher slew rates, the distortion that occurs is closer to the transmitter and phase correction is more effective in correcting the thermal distortion.

Experimental investigations of the phase correction of CW thermal blooming was first reported by Gebhardt and Kendall [92] and by Bridges and Pearson [93] and Primmerman and Fouche [94]. Gebhardt and Kendall [92] used the apparatus shown in Fig. 56 where a moderate power laser was used in conjunction with a 20 segment micrometer adjustable mirror and a laboratory-scale simulation experiment. The segmented mirror was used to place on the beam a piecewise continuous phase contour, precalculated from the theoretical model. Shown in Fig. 57 are the photographs of the distorted beam

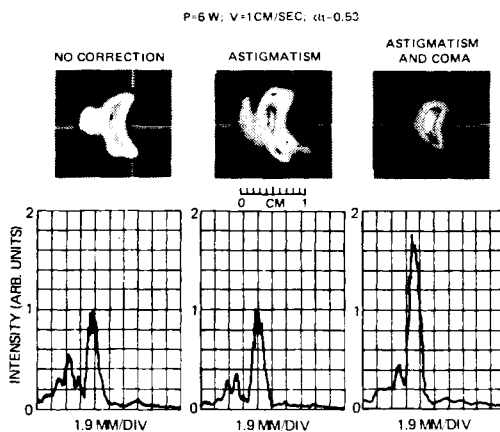


Fig. 57. Photographs of the thermally distorted intensity contours with various phase corrections added. The lower traces are the corresponding intensity profiles through the center of the beam parallel with the wind direction [92].

with different corrections as well as intensity profiles measured with a pin-hole detector through the center of the beam in the wind direction. The middle case was one with the astigmatism alone applied. As can be seen in the photograph the astigmatism correction did alter the contour of the distortion, but no increase in the peak flux was achieved. When coma was added to astigmatism, a factor of 1.8 increase in intensity was achieved, in qualitative agreement with that predicted by the theory. It was found that the relative coefficients of the phase distortion terms required for optimum correction were as given in (58); however, the magnitude of the correction was less than that given by (57). This is easily explained by recalling that the thermal lens is a distributed lens along the propagation path, and if the total phase distortion is placed on the beam at the transmitter this will overcompensate for the distortion away from the transmitter.

Bridges and Pearson [93] reported the use of a coherent optical adaptive techniques (COAT) system to correct for thermal blooming. For their experiment the thermal distortion was the result of a thin liquid cell close to the transmitter and did not simulate the distributed lens associated with atmospheric conditions. Their results showed that the closed-loop correction provided by the 18 element multidither adaptive aperture could correct for the thermal distortion which occurs in the near field. Corrections in peak irradiance of 2 to 4 times were observed in their experiments. Since the distortion was that associated with a thin cell (thin lens) located close to the aperture it is not unexpected that the correction could fully compensate for the thermal blooming. When the lens is distributed as in the atmosphere, corrections of 2 to 3 are more typical. An important aspect of Bridges and Pearson's experiment was the demonstration of a closed-loop correction of the nonlinear thermal blooming distortion. The intensity in the focal plane was monitored with a detector and the detected signal was used to optimize the phase correction. Eighteen elements of the adaptive mirror were individually dithered, and the multiple-loop was closed on the observed dither signal in the focal plane using a "hill climbing" servo system. Before this experiment it was not obvious that such a closed loop system would arrive at a unique stable state when correcting for a nonlinear distortion such as thermal blooming.

The phase correction of multiple-pulse thermal blooming has been investigated theoretical by Wallace and Pasciak [95]

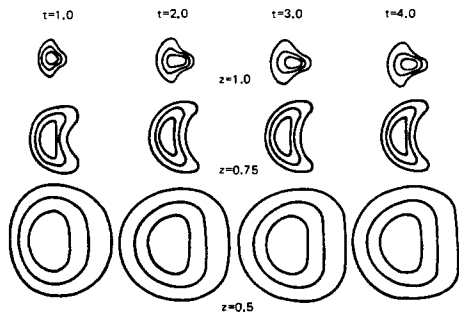


Fig. 58. Intensity contours for multiple-pulse blooming as a function of time and range for 4 PPFT [95].

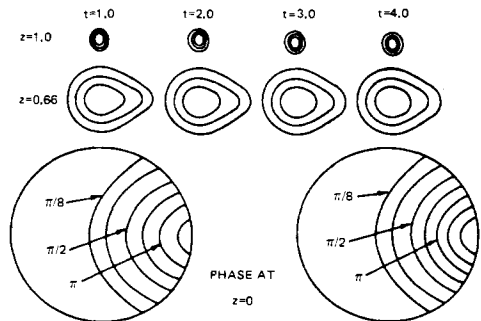


Fig. 59. Phase correction of multiple pulse thermal blooming. The initial and final phase contours are also shown [95].

and experimentally by Dunphy and Smith [96]. For focused multiple-pulse blooming, the strongest thermal distortion is the result of the overlap of pulses close to the transmitter. Because of focusing, the beam is smaller at the focus and the clean out of the beam path is most effective there. Thus the multiple-pulse mode of operation is well-suited to applying phase correction since more of the distortion is occurring in the near field.

In the analysis of Wallace and Pasciak [95] they calculated the temporal evolution of the thermal distortion of a train of laser pulses by numerically summing the density changes in the propagation path due to previous pulses and then calculating the change in laser beam intensity using the scalar wave equation. They neglected the thermal distortion of a single pulse which requires that  $T_S$  calculated for the individual pulse parameters be much less than one. Shown in Fig. 58 are calculated intensity contours at different fractions of the propagation range (the contours correspond to 0.6, 0.3 and 0.1 times the peak intensity) and as a function of time, normalized by the  $(2w/v)$  flow time; where  $w$  is the  $e^{-2}$  laser-beam radius. For this calculation the propagation range was 2 km,  $\alpha$  was  $0.2 \text{ km}^{-1}$ , the wind velocity was 10 m/s the  $e^{-1}$  beam radius was 18 cm, with a CO<sub>2</sub>-laser power of 75 kw with a repetition rate of 80 pps. The thermal distortion is sufficient to reduce the intensity to 0.47 times the undistorted value in the steady state. Wallace and Pasciak [95] then calculated the integrated phase distortion introduced by the thermal distortion and applied the conjugate of this phase to the multiple-pulse laser beam. Shown in Fig. 59 are the phase contours (initial and final at  $t = 1$  and 4) as well as the corrected intensity contours; the propagation conditions are the same as for Fig. 58. As can be seen in the figure the phase correction eliminates the crescent-shaped distortion and almost complete correction of the distortion is achieved. The amount of phase correction depends, of course on the strength

of the thermal lens, the number of PPFT and the strength of the focusing.

Dunphy and Smith [96] showed experimentally that the thermal distortion of a multiple-pulse laser beam could be compensated by a relatively simple deformable mirror. The laboratory experiment was performed with a 10-pps TEA CO<sub>2</sub> laser and one meter long absorption cell similar to the apparatus previously described and used in the multiple pulse blooming experiment. The deformable mirror was constructed from a 2 in diameter copper mirror with a portion of the mirror machined out leaving a thin section of the surface. A single actuator was attached to this section and the phase deformation was accomplished by pulling on the section. The diameter of the membrane was made equal to the  $e^{-1}$  diameter of the initial laser beam. The deformation was shifted off-axis to produce a phase contour on the original beam similar qualitatively to that shown in Fig. 59.

In the experiment the thermal distortion reduced the peak intensity to 0.75 times its undistorted value for 4 PPFT. With phase correction the intensity was increased to 0.93 times its undistorted value. The maximum phase distortion applied to the mirror was 0.35 times the calculated phase distortion using a computer code for the experimental laboratory distortion conditions. This experimental program showed that a simple deformable mirror could be used for phase correction of multiple-pulse thermal blooming and as in the CW case the optimum phase correction is less than the total phase distortion imposed by thermal blooming.

The full potential for phase correction of thermal blooming has probably not been realized. For CW beams that are strongly focused, the distortion is distributed along the path and factors of two or three increase in peak intensity may be realized. For highly slewed laser beams, the phase correction of CW blooming may be even greater. For multiple-pulse lasers the phase correction should be able to correct for more of the thermal distortion compared to CW correction because of the geometry of the focus and the decrease in pulse overlap with range.

## VII. DISCUSSION

We have presented data and analysis of the self-induced thermal distortion for a wide variety of conditions, beginning with a discussion of CW laser beam blooming based on the form of heat transfer of the power absorbed in propagating medium. In the absence of forced convection laser beams of the multikilowatt level are severely limited in propagating over tens of meters of path because of the inefficiency of conduction and buoyancy in removing heat from the beam. However, we can also see from the studies that CW thermal distortion can be alleviated with a sufficient transverse flow or introduction of mechanical turbulence.

One important aspect of CW thermal blooming studies is the scaling laws. By determining proper scaling, we can predict the thermal distortion for a wide variety of conditions based on the laboratory scale experiments and/or computer code results. For accuracies of a factor of 2, we have found that the CW blooming can be characterized by a single-distortion parameter, within certain limits of slew rate, absorption, and degree of focusing as discussed in the text. Ongoing programs for scaling the thermal distortion can reduce these errors significantly. One such study by Breaux [97] has found that the scaling is more accurate using the integral of the phase distortion along the path as the scaling parameter, combined with the other parameters, rather than  $N$  which requires one

more path integration. For more accurate predictions of thermal blooming, further studies of scaling are required.

The value of the data and accuracy which can be achieved with laboratory scale experiments of thermal blooming have been demonstrated. In scaling the experiments to atmospheric conditions it is important to simulate the nondimensional parameters such as  $N_C$ ,  $F$ ,  $\alpha z$ , and slew rate for CW propagation. In addition, it is important that the forced convection heat transfer be dominant over thermal conductions and natural convection. In addition the temperature rise in the laboratory experiment must be kept small in order for the simulation to be valid. These same conditions apply to multiple pulse propagation simulation with the addition of the nondimensional parameters which are applicable to this case. For these cases, the transient parameters  $T_{IC}$ , PPFT, and Fresnel number are most important. For multiple-pulse simulation, the characteristic conduction or natural convection time must be long compared to the inner pulse spacing; otherwise, these effects can influence the experimental results. Laboratory scaled experiments under careful control of the parameters have proven to be a valuable asset in predicting the effects of nonlinear thermal blooming on the propagation of high power CW and multiple-pulse lasers.

Pulsed-laser radiation can be used to reduce the thermal distortion relative to a CW beam for a given amount of energy transmitted. This is true for pulses that are short compared to the acoustic transit time across the beam and experimental studies have confirmed this. Thus short-pulsed blooming could be the answer to the problem of propagating large energy fluxes through absorbing medium except for other nonlinear effects such as gas breakdown. The breakdown threshold of atmospheric air is a complex problem depending on wavelength, aerosol concentration, etc., and will be the subject of another article, but suffice to say breakdown limits the energy flux deliverable by a single laser pulse. This limit is the reason for the interest in multiple-pulse propagation and the pulse-overlap thermal-blooming problem. The experiments and theory show that the thermal distortion of a train of pulses can be substantially less than that encountered by CW laser beams of the same average power for certain conditions of pulse repetition rate and wind velocity. The philosophy of reducing the thermal distortion with a train of pulses is, very simply, that each pulse is made shorter than the acoustic transit time across the beam, and the repetition rate is determined by the wind clean out time. The multiple-pulse thermal blooming requires three scaling parameters; these are the single-pulse distortion  $T_l$ , the pulses per flow time,  $N_p$ , and the Fresnel number  $F$ . No single parameter scaling has been found for multiple-pulse blooming.

Lilly [58] has done a systematic study of the multiple-pulse-laser propagation and has found power-law solutions for the relative intensity as a function of five nondimensional parameters. The exponents for the various parameters are determined from curve fits to computer code data. However, the values of the exponent have to be varied considerably depending on the range of the five parameters. The five nondimensional parameters are: the Fresnel number, attenuation number, PPFT, slew number, and the distortion number for the focused beam. One interesting aspect of the multiple-pulse blooming which has not been investigated thoroughly is the optimization of the laser pulse length relative to the repetition rate. This tradeoff then involves the optimization of the combined effect of short-pulse blooming and pulse-overlap blooming.

In addition to the problems of CW and multiple-pulse thermal blooming in a uniform wind or slew, there are additional complications of the problem which must be considered in order to predict the distorted laser beam intensity. These can involve such effects as the kinetics of the absorption, both molecular and aerosol, a combination of thermal blooming and beam motion such as induced by turbulence or beam jitter, nonuniformity of the meteorological conditions (wind magnitude and direction including stagnation zones, absorption, mechanical turbulence), and details of the laser beam shape. In spite of all these potential complications, the experimental results presented and the code calculations show that the thermal distortion can be calculated and, in most cases, can be described by analytic expressions and scaling laws.

In the kinetics, we have the unique effect of kinetic cooling of the air path caused by a CO<sub>2</sub> laser beam, a transient effect which can have advantageous effects such as focusing of the beam as opposed to the thermal blooming. Molecular absorption can also be saturated, or the absorbing species depleted. This usually involves a rather high intensity. For example for CO<sub>2</sub>-laser irradiation the saturation flux for CO<sub>2</sub> molecules in the atmosphere is of the order of  $5 \times 10^5$  W/cm<sup>2</sup> [98]. This is the intensity required to reduce the absorption by a factor of two. Another possible kinetic process is the so called  $\pi$  pulse propagation where the absorbing transition is driven coherently with no net absorption. This is a very special case and requires a specially phased laser pulse and absorbing transition [99]. In general, it will not be applicable for atmospheric propagation conditions. The aerosol absorption has several effects that are analogous to the molecular absorption. The time to transfer heat from the aerosol to the air is similar to a kinetic effect of transfer of energy from a vibrational mode to translational energy. The vaporization of aerosols is also analogous to saturation of molecules, at least as far as the aerosol contribution to the nonlinear effects is concerned.

The combination of random laser-beam motion and thermal blooming has been analyzed on a computer code and also experimentally for Gaussian shaped beams. Both computer code and experiment have shown that either the root sum square or thermal distortion of the larger beam can be used to obtain an analytic expression for the combined effects. This is independent of the time scale of the beam motion relative to the thermal blooming. This result is probably valid only for Gaussian beams and may not necessarily hold for other laser-beam shapes.

Variations of the meteorological conditions along the path can have a significant impact on the thermal distortion. One of the most important cases involves the stagnation zone where there is no net motion between the beam and the air for a portion of the path. It has been shown that for a stationary zone, the intensity reaches a quasi-steady-state, and further, an analytic expression for this intensity has been found. The stagnation zone is so important that the contribution of the other portions of the path can usually be neglected in calculating the distorted intensity. One important area that is presently being studied [100] is the influence of axial motion of the stagnation zone that would occur with a variable slew rate. In this case the stagnation zone is not fixed and, therefore, its effect may be reduced. Another area, treated on the computer code by Fleck [39] is the influence of noncoplanar slew, i.e., slew components in two planes. Fleck has shown for this geometry that this is a very important effect in reducing the thermal distortion due to stagnation zones.

In spite of all the complications, it appears that for the most cases, we can predict the self-induced thermal distortion of CW and pulsed laser beams if we know the initial conditions and the relevant parameters of the propagation path. Further studies are required to perform sensitivity-type studies such as the effects of variable wind along the propagation path, and also optimization studies, such as the tradeoff between  $t^3$  blooming and overlap or multiple pulse versus CW beams. These studies are greatly simplified when analytic expressions can be obtained to describe the nonlinear effects.

#### ACKNOWLEDGMENT

The author has had the pleasure of working with a number of people on the thermal blooming problem and he gratefully acknowledges their contribution to this article. Among these are F. G. Gebhardt, P. J. Berger, R. T. Brown, J. R. Dunphy, and M. C. Fowler and L. A. Newman.

#### REFERENCES

The list of references does not represent a complete bibliography of thermal blooming, but hopefully a sufficient number to include all aspects of the problem that have been treated to date.

- [1] *Infrared Components*, Brochure No. 67 cm, Santa Barbara Research Center, Goleta, CA, 1967.
- [2] R. A. McClatchey and J. E. A. Selby, "Atmospheric attenuation of HF and DF laser radiation," (Environmental Research Paper 400), Air Force Cambridge Res. Labs., Lincoln, MA, May 23, 1972.
- [3] W. B. Heath, "DF and HF emission in the infrared," Ph.D. dissertation, Ohio State Univ., Columbus, (University Microfilms, Ann Arbor, MI), 1976.
- [4] D. C. Smith and R. G. Meyerand, Jr., "Laser radiation induced gas breakdown," in *Principles of Laser Plasmas*. New York: Wiley, 1976.
- [5] D. C. Smith, "High power laser propagation—Gas breakdown," unpublished.
- [6] A. D. Wood, M. Camac, and E. T. Gerry, "Effects of  $10.6\mu$  laser induced air chemistry on the atmospheric refractive index," *Appl. Opt.*, vol. 10, no. 8, pp. 1877-1884, Aug. 1971.
- [7] J. Wallace and M. Camac, "Effects of absorption at  $10.6\mu$  on laser-beam transmission," *J. Opt. Soc. Amer.*, vol. 60, no. 12, pp. 1587-1594, Dec. 1970.
- [8] F. G. Gebhardt and D. C. Smith, "Kinetic cooling of a gas by absorption of  $\text{CO}_2$  laser radiation," *Appl. Phys. Letts.*, vol. 20, no. 3, pp. 129-132, Feb. 1972.
- [9] E. L. Breig, "Limitations on the atmospheric thermal effects for high-power  $\text{CO}_2$  laser beams," *J. Appl. Phys.*, vol. 62, no. 4, pp. 518-528, Apr. 1972.
- [10] L. Sica, "Interferometric observations of kinetic cooling," *Appl. Phys. Letts.*, vol. 22, no. 8, pp. 396-398, Apr. 1973.
- [11] R. C. C. Leite, R. S. Moore, and J. R. Whinnery, "Low absorption measurements by means of the thermal lens effect using an He-Ne laser," *Appl. Phys. Letts.*, vol. 4, no. 7, pp. 141-143, Oct. 1964.
- [12] J. P. Gordon, R. C. C. Leite, R. S. Moore, S. P. S. Porto, and J. R. Whinnery, "Long-transient effects in lasers with inserted liquid samples," *J. Appl. Phys.*, vol. 36, no. 1, pp. 3-8, Jan. 1965.
- [13] K. E. Rieckhoff, "Self-induced divergence of CW laser beams in liquids—A new nonlinear effect in the propagation of light," *Appl. Phys. Letts.*, vol. 9, no. 2, pp. 87-88, July 1966.
- [14] R. C. C. Leite, S. P. S. Porto, and T. C. Damen, "The thermal lens effect as a power-limiting device," *Appl. Phys. Letts.*, vol. 10, no. 3, pp. 100-101, Feb. 1967.
- [15] J. R. Whinnery, D. T. Miller, and F. Dabby, "Thermal convection and spherical aberration distortion of laser beams in low-loss liquids," *IEEE J. Quantum Electron.*, vol. QE-3, pp. 382-383, Sept. 1967.
- [16] S. A. Akhmanov, D. P. Krindach, A. P. Sukhorukov, and R. V. Khoklov, "Nonlinear defocusing of laser beams," *JETP Lett.*, vol. 6, no. 2, pp. 39-42, July 1967.
- [17] W. R. Callen, B. G. Huth, and R. H. Pantell, "Optical patterns of thermally self-defocused light," *Appl. Phys. Letts.*, vol. 11, no. 3, pp. 103-105, Aug. 1967.
- [18] H. Inaba and H. Ito, "Observation of power-dependent distortion of an infrared beam at  $10.6\mu\text{m}$  from a  $\text{CO}_2$  laser during propagation in liquids," *IEEE J. Quantum Electron.*, vol. QE-4, pp. 45-48, Feb. 1968.
- [19] R. L. Carman and P. L. Kelley, "Time dependence in the thermal blooming of laser beams," *Appl. Phys. Letts.*, vol. 12, no. 8, pp. 241-243, Apr. 1968.
- [20] E. A. McLean, L. Sica, and A. J. Glass, "Interferometric observation of absorption induced index change associated with thermal blooming," *Appl. Phys. Letts.*, vol. 13, pp. 369-380, Dec. 1968.
- [21] S. A. Akhmanov, D. P. Kindach, A. V. Migulin, A. P. Sukhorukov, and R. V. Khoklov, "Thermal self-action of laser beams," *IEEE J. Quantum Electron.*, vol. QE-4, no. 10, Oct. 1968.
- [22] F. W. Dabby and H. A. Haus, "Steady-State solutions for thermal focusing of light beams," *J. Appl. Phys.*, vol. 40, no. 1, pp. 439-440, Jan. 1969.
- [23] F. W. Dabby, R. W. Boyko, C. V. Shank, and J. R. Whinnery, "Short time-constant thermal self-defocusing of laser beams," *IEEE J. Quantum Electron.*, vol. QE-5, pp. 516-520, Oct. 1969.
- [24] F. G. Gebhardt and D. C. Smith, "Effects of wind on thermal defocusing of  $\text{CO}_2$  laser radiation," *Appl. Phys. Letts.*, vol. 14, no. 2, pp. 52-54, Jan. 1969.
- [25] R. L. Carman, A. Mooradian, P. L. Kelley, and A. Tufts, "Transient and steady state thermal self-focusing," *Appl. Phys. Letts.*, vol. 14, no. 4, pp. 136-139, Feb. 1969.
- [26] A. J. Glass, "Thermal blooming in gases," *Opto-Electronics*, vol. 1, no. 4, pp. 174-178, 1969.
- [27] D. C. Smith, "Thermal defocusing of  $\text{CO}_2$  laser radiation in gases," *IEEE J. Quantum Electron.*, vol. QE-5, pp. 600-607, Dec. 1969.
- [28] P. M. Livingston, "Thermally induced modifications of a high power CW laser beam," *Appl. Opt.*, vol. 10, no. 2, pp. 426-436, Feb. 1971.
- [29] M. Born and E. Wolf, *Principles of Optics*. New York: Pergamon Press, 1959, p. 120.
- [30] F. G. Gebhardt and D. C. Smith, "Effects of diffraction on the self-induced thermal distortion of a laser beam in a crosswind," *Appl. Opt.*, vol. 11, no. 2, pp. 244-248, Feb. 1972.
- [31] F. G. Gebhardt and D. C. Smith, "Effects of wind on thermal defocusing of  $\text{CO}_2$  laser radiation," *Appl. Phys. Letts.*, vol. 14, no. 2, pp. 52-54, Jan. 1969.
- [32] R. J. Hull, P. L. Kelley, and R. L. Carman, "Self-induced thermal lens effect in  $\text{CCl}_4$  in the presence of beam motion," *Appl. Phys. Letts.*, vol. 17, pp. 539-541, Dec. 15, 1970.
- [33] In the early computer code work on wave optics calculations of steady-state thermal blooming, the following people were involved in this type of analysis: J. Wallace at AVCO-Everett Research Laboratory, Everett, MA; L. C. Bradley, and J. Herrmann at M.I.T. Lincoln Laboratory, Lexington, MA; P. M. Livingston and H. Breaux at Ballistic Research Laboratory, Aberdeen, MD; C. B. Hogge at AFWL Albuquerque, NM; J. N. Hayes, P. B. Ulrich, and A. H. Aitken at Naval Research Laboratory, Washington, DC; W. Brown at Hughes Research Labs, Mal, CA; and F. G. Gebhardt and D. C. Smith, United Aircraft Research, East Hartford, CT.
- [34] J. Wallace and M. Camac, "Effects of absorption at  $10.6\mu$  on laser-beam transmission," *J. Opt. Soc. Amer.*, vol. 60, no. 12, pp. 1587-1594, Dec. 12, 1970.
- [35] L. C. Bradley and J. Herrmann, "Numerical calculation of light propagation in a nonlinear medium," *J. Opt. Soc. Amer.*, vol. 61, p. 668, Apr. 1971.
- [36] F. G. Gebhardt and D. C. Smith, Ann. Rep. on Army Contract DAABO7-70-C-0204 UAR Rep. K921004-4, Apr. 1971.
- [37] J. N. Hayes, P. B. Ulrich, and A. H. Aitken, "Effects of the atmosphere on the propagation of  $10.6\mu$  laser beams," *Appl. Opt.*, vol. 11, no. 2, pp. 257-260, Feb. 1972.
- [38] D. C. Smith and F. G. Gebhardt, "Saturation of the self-induced thermal distortion of laser radiation in a wind," *Appl. Phys. Letts.*, vol. 16, no. 7, pp. 275-278, Apr. 1, 1970; also F. G. Gebhardt and D. C. Smith, Quart. Rep. on Army Contract DAABO7-70-C-0204, United Aircraft Rep. J921004-2, Nov. 16, 1970.
- [39] J. A. Fleck, J. R. Morris, and M. D. Feit, "Time-dependent propagation of high energy laser beams through the atmosphere: II," Lawrence Livermore Lab., Livermore, CA, Rep. UCRL 52071, May 18, 1976.
- [40] F. G. Gebhardt, "Multiple pulse propagation model," United Technologies Research Cent., East Hartford, CT, Rep. UTRC-R20, Aug. 1975.
- [41] F. G. Gebhardt, J. H. McCoy, and D. C. Smith, "Variable attenuator for  $\text{CO}_2$  laser radiation," *IEEE J. Quantum Electron.*, vol. QE-5, no. 9, pp. 471-473, Sept. 1969.
- [42] F. G. Gebhardt and D. C. Smith, "Investigation of self-induced thermal effects of  $\text{CO}_2$  laser radiation propagating in absorbing gases," *Annu. Rep. Army Contract DAABO7-70-C-0204*, Apr. 1971.
- [43] J. F. Forner and D. C. Lowenthal, "A photographic recording medium for  $10.6\mu$  laser radiation," *Appl. Opt.*, vol. 6, p. 471, Sept. 1969.
- [44] F. G. Gebhardt and D. C. Smith, "Investigation of self-induced

- thermal effects of CO<sub>2</sub> laser radiation propagating in absorbing gases," *Annu. Rep. Army Contract DAAB07-70-C-0204*, UAR Rep. L921004-8, Apr. 1972.
- [45] P. B. Ulrich and J. Wallace, "Propagation characteristics of collimated, pulsed laser beams through an absorbing atmosphere," *J. Opt. Soc. Amer.*, vol. 63, no. 1, pp. 8-12, Jan. 1973.
- [46] P. B. Ulrich, "Requirements for experimental verification of thermal-blooming computer results," *J. Opt. Soc. Amer.*, vol. 63, no. 7, pp. 897-898, July 1973.
- [47] A. H. Aitken, J. N. Hayes, and P. B. Ulrich, "Thermal blooming of pulsed focused Gaussian laser beams," *Appl. Opt.*, vol. 12, no. 2, pp. 193-197, Feb. 1973.
- [48] J. A. Fleck, Jr., J. R. Morris, and M. J. Feit, "Time-dependent propagation of high energy laser beams through the atmosphere," Lawrence Livermore Lab., Livermore, CA, Rep. UCRL-51825, June 2, 1975.
- [49] P. R. Longaker and M. M. Litvak, "Perturbation of the refractive index of absorbing media by a pulsed laser beam," *J. Appl. Phys.*, vol. 40, no. 10, pp. 4033-4041, Sept. 1969.
- [50] J. R. Kenemuth, C. B. Hogge, and P. V. Avizonis, "Thermal blooming of a 10.6μ laser beam in CO<sub>2</sub>," *Appl. Phys. Letts.*, vol. 17, no. 5, pp. 220-223, Sept. 1, 1970.
- [51] R. G. Buser and R. S. Rohde, "Transient thermal blooming of long laser pulses," *Appl. Opt.*, vol. 14, no. 1, pp. 50-55, Jan. 1975.
- [52] H. Kleiman and R. W. O'Neil, "Thermal blooming of pulsed laser radiation," *Appl. Phys. Letts.*, vol. 23, no. 1, pp. 43-44, July 1, 1973.
- [53] D. C. Smith, R. T. Brown, F. G. Gebhardt, and P. J. Berger, "Effects of particulate matter on atmospheric propagation of CO<sub>2</sub> laser radiation," Rep. on Navy Contract N00014-72-C-0469, UAR rep. M921503-3, July 1973.
- [54] R. W. O'Neil, H. Kleiman, and J. E. Lowder, "Observation of hydrodynamic effects on thermal blooming," *Appl. Phys. Letts.*, vol. 24, no. 3, pp. 118-120, Feb. 1, 1974.
- [55] J. Wallace and J. Q. Lilly, "Thermal blooming of repetitively pulsed laser beams," *J. Opt. Soc. Amer.*, vol. 64, no. 12, pp. 1651-1655, Dec. 1974.
- [56] J. Q. Lilly and T. G. Miller, "Target intensity enhancement for repetitively pulsed laser beams," AIAA Paper 75-718 presented at AIAA 10th Thermophysics Conference, Denver, CO, May 1975.
- [57] L. C. Bradley and J. Herrmann, "Short pulse computer code-JSL-1," M.I.T. Lincoln Lab., Lexington, 1973.
- [58] J. Q. Lilly, "Simplified calculation of laser beam propagation through the atmosphere," Tech. Rep. RH-76-8, U. S. Army Missile Command, Redstone Arsenal, AL, Jan. 1976.
- [59] J. A. Fleck, Jr., J. R. Morris, and M. D. Feit, "Time dependent propagation of high energy laser beams through the atmosphere: II," Rep. UCRL-52071, Lawrence Livermore Lab., Livermore, CA, May 1976.
- [60] F. G. Gebhardt, P. J. Berger, D. C. Smith, B. Burdick, and R. Tripodi, "Reduction of thermal blooming by beam optimization," Final Rep. on Army Contract DAAB07-74-C-0028, United Aircraft Rep. UARN921769-4, Oct. 1974.
- [61] R. G. Buser, R. S. Rohde, P. J. Berger, F. G. Gebhardt, and D. C. Smith, "Transient thermal blooming of single and multiple short laser pulses," *Appl. Opt.*, vol. 14, no. 11, pp. 2740-2746, Nov. 1975.
- [62] R. W. O'Neil, H. Kleiman, and H. R. Zwicker, "Experimental determination of single and multiple pulse propagation," Pre-Print 183 from NATO AGARD Conf. on Optical Propagation in the Atmosphere, Oct. 1975.
- [63] H. T. Yura, "Atmospheric turbulence induced laser beam spread," *Appl. Opt.*, vol. 10, no. 12, pp. 2771-2773, Dec. 1971.
- [64] R. F. Lutomirski and H. T. Yura, "Propagation of a finite optical beam in an inhomogeneous medium," *Appl. Opt.*, vol. 10, no. 7, pp. 1652-1658, July 1971.
- [65] R. S. Lawrence and J. W. Strohbehn, "A survey of clean-air propagation effects relevant to optical communications," *Proc. IEEE*, vol. 48, p. 1523, Oct. 1970.
- [66] F. G. Gebhardt, "High power laser propagation," *Appl. Opt.*, vol. 15, no. 6, pp. 1479-1493, June 1976.
- [67] W. D. Brown, Jr., Hughes Research Lab., private communication.
- [68] L. C. Bradley, "Simulation of atmospheric index fluctuations," M.I.T. Lincoln Lab., Cambridge, MA, unpublished Rep.
- [69] F. G. Gebhardt, D. C. Smith, R. G. Buser, and R. S. Rohde, "Turbulence effects on thermal blooming," *Appl. Opt.*, vol. 12, no. 8, pp. 1794-1805, Aug. 1973.
- [70] H. Breaux, private communication.
- [71] J. H. Hayes, U. S. Naval Research Laboratory Washington, DC, private communication.
- [72] C. B. Hogge and R. R. Butts, "Propagation effects of a slewed beam with transverse wind null spots," Air Force Weapons Laboratory, Kirkland AFB, NM, Rep. AFWL-TR-73-76, 1973.
- [73] P. J. Berger, F. G. Gebhardt, and D. C. Smith, "Thermal blooming due to a stagnation zone in a slewed beam," Final Tech. Rep. on Navy Contract N00014-73-C-0454, UTRC Rep. N921724-12, Oct. 1974.
- [74] P. J. Berger, "Thermal blooming of a slewed laser beam containing a stagnation zone: Analytical model for the quasi-steady-state," UTRC Rep. UTRC75-39, June 1975.
- [75] P. J. Berger, P. B. Ulrich, J. T. Ulrich, and F. G. Gebhardt, "Transient blooming a a slewed laser beam containing a region of stagnant absorber," *Appl. Opt.*, vol. 16, no. 2, pp. 345-354, Feb. 1977.
- [76] J. N. Hayes, "Thermal blooming of rapidly slewed laser beams," *Appl. Opt.*, vol. 13, no. 9, pp. 2072-2074, Sept. 1974.
- [77] C. B. Hogge, Air Force Weapons Laboratory, Kirkland AFB, NM, private communication.
- [78] L. C. Bradley, "Thermal blooming in the transonic regime," M.I.T. Lincoln Lab., Lexington, MA, Rep. LTP-24, Jan. 1974.
- [79] J. W. Ellinwood and H. Mirels, "Density perturbations in transonic slewing laser beams," *Appl. Opt.*, vol. 14, no. 9, pp. 2238-2242, Sept. 1975.
- [80] J. Wallace and J. Pasciak, "Thermal blooming of a rapidly moving laser beam," *Appl. Opt.*, vol. 15, no. 1, pp. 218-222, Jan. 1976.
- [81] R. T. Brown and D. C. Smith, "Laser propagation through an absorbing transonic flow," *Appl. Phys. Letts.*, vol. 25, no. 9, pp. 500-503, Nov. 1, 1974.
- [82] F. G. Gebhardt and D. C. Smith, "Influence of beam jitter on thermal blooming," Final Tech. Rep. on Navy Contract N00014-75-C-0469 UTRC Rep. R76-922050-12, Mar. 1976.
- [83] D. C. Smith and R. T. Brown, "Laser particle interaction," Final Rep. Navy Contract N00014-72-C-0469, UTRC Rep. N921503-16, Oct. 1974.
- [84] D. E. Lencioni and H. Kleiman, "Effects of Aerosol particle heating on laser beam propagation," M.I.T. Lincoln Lexington, MA, Rep. LTP-27, July 1974.
- [85] C. H. Chan, "Effective absorption for thermal blooming due to aerosols," *App. Phys. Letts.*, vol. 26, no. 11, pp. 628-630, June 1, 1975.
- [86] R. T. Brown and D. C. Smith, "Aerosol-induced thermal blooming," *J. Appl. Phys.*, vol. 46, no. 1, pp. 402-405, Jan. 1975.
- [87] D. C. Smith, "Transient response of aerosol induced thermal blooming of laser beams," unpublished.
- [88] W. J. Fader, "Density perturbations caused by weak absorption of a laser pulse," *J. Appl. Phys.*, vol. 47, no. 5, pp. 1975-1978, May 1976.
- [89] F. G. Gebhardt, "Investigation of self-induced thermal effects of CO<sub>2</sub> laser radiation propagating in absorbing gases," Final Rep. on Army Contract DAAB07-70-C-0204, UTRC Rep. M921004-12, Nov. 1973.
- [90] J. Wallace, I. Itskan, and J. Camm, "Irradiance tailoring as a method of reducing thermal blooming in an absorbing medium," *J. Opt. Soc. Amer.*, vol. 64, no. 8, pp. 1123-1128, Aug. 1974.
- [91] L. C. Bradley and J. Herrmann, "Phase compensation for thermal blooming," *Appl. Opt.*, vol. 13, no. 2, pp. 331-334, Feb. 1974.
- [92] F. G. Gebhardt and J. S. Kendall, post deadline paper 14A-9 presented at the 1973 IEEE/OSA Conf. on Laser Engineering and Applications, Washington, DC; J. S. Kendall, J. P. Waters, F. G. Gebhardt and A. I. Chalfant, "Final report on multi-segmented mirrors," on Navy Contract N00014-72-C-0470, United Aircraft Research Lab., East Hartford, CT, Rep. M911455-3, July 1973.
- [93] W. B. Bridges and J. E. Pearson, "Thermal blooming compensation using coherent optical adaptive techniques (COAT)," *Appl. Phys. Letts.*, vol. 26, no. 9, pp. 539-543, May 1, 1975.
- [94] C. A. Primmerman and D. G. Fouche, "Thermal-blooming compensation: Experimental observations using a deformable mirror system," *J. Opt. Soc. Amer.*, vol. 65, no. 10, p. 1212, Oct. 1975.
- [95] J. Wallace and J. Pasciak, "Compensating for thermal blooming of repetitively pulsed lasers," *J. Opt. Soc. Amer.*, vol. 65, no. 11, pp. 1257-1260, Nov. 1975.
- [96] J. R. Dunphy and D. C. Smith, "Multiple pulse thermal blooming and phase correction," *J. Opt. Soc. Amer.*, vol. 67, no. 3, pp. 295-298, Mar. 1977.
- [97] H. Breaux, private communication.
- [98] An estimate of the saturation intensity for CO<sub>2</sub> in the atmosphere can be obtained from the expressions,  $I_s = h\nu/\sigma T_l$  where  $h\nu$  is the photon energy,  $\sigma$  the absorption cross section, and  $T_l$  is the limiting lifetime of the absorbing transition, i.e., the longer of the upper or lower level lifetimes. From [8]  $h\nu/\sigma$  was measured to be approximately 0.4 J/cm<sup>2</sup> and from [6]  $T_l = 7.5 \times 10^{-7}$  s. Thus,  $I_s = 5 \times 10^5$  W/cm<sup>2</sup> at atmospheric pressure.
- [99] The self-induced transparency effect was first discussed by S. L. McCall and E. L. Hahn "Self-induced transparency by pulsed coherent light," *Phys. Rev. Lett.*, vol. 18, pp. 908-911, May 22, 1967. A review of coherent propagation and some of the problems in realizing these effects such as level degeneracy, are discussed in Chapter 5 of L. Allen and J. H. Eberly, *Optical Resonance and Two-Level Atoms*. New York: Wiley, 1975.
- [100] M. C. Fowler, private communication.

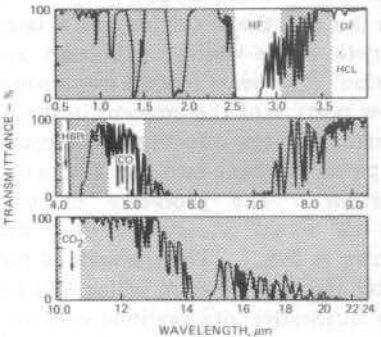


Fig. 2. Broad-band atmospheric transmission as a function of wavelength from [1]. Data was taken over a 10-km path; the light sections denote the wavelength ranges where there are potential high-power lasers.

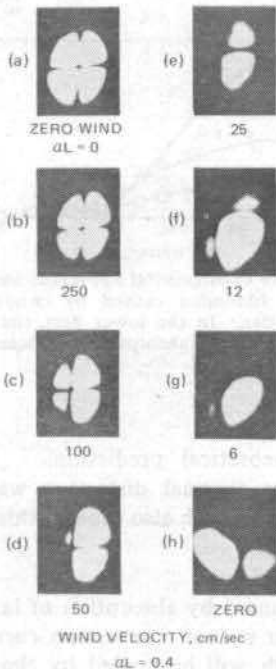


Fig. 7.  $\text{CO}_2$  laser beam burn patterns which show the distortion with varying wind velocities incident from the right [31].

## EXPERIMENT

## THEORY

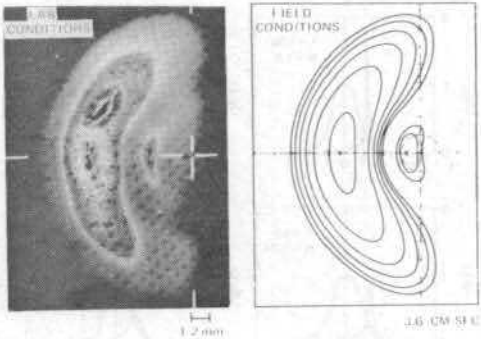


Fig. 10. Comparison of laboratory [36] and computer code results [35] under closely matching dimensionless scaling conditions. The equal intensity contours from the computer code are for 0.09, 0.14, 0.23, 0.36, 0.57, and 0.9 times the peak and the distortion parameter given by (18) is 16. In the laboratory scaled experiments, the Kalvar film photograph shows an inner bright contour which is roughly 0.5 times the peak irradiance and the distortion parameter is 13.

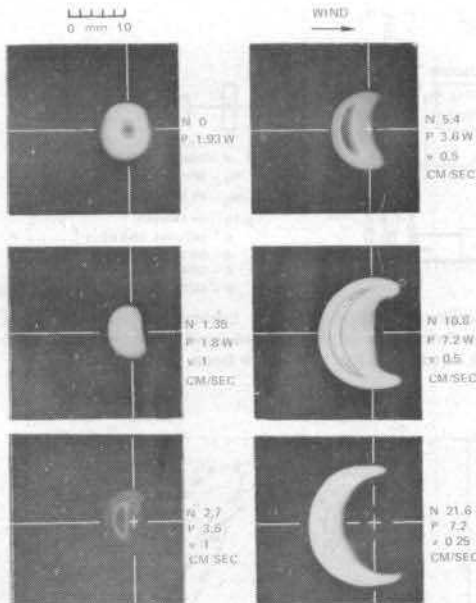


Fig. 18. Thermally distorted intensity patterns on Kalvar film with each contour labeled by the  $\text{CO}_2$  laser power, transverse wind velocity and the calculated distortion parameter. The wind is incident from the left, the beam is initially collimated and propagated through the 1-m wind tunnel doped with absorber [44].

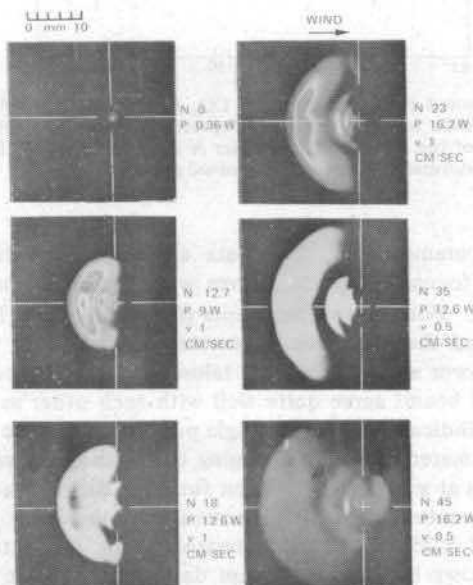


Fig. 19. Thermally distorted intensity patterns for an initially focused CW  $\text{CO}_2$  laser beam. Each pattern is labeled by the laser power, transverse wind velocity and the distortion parameter calculated from (18) [44].

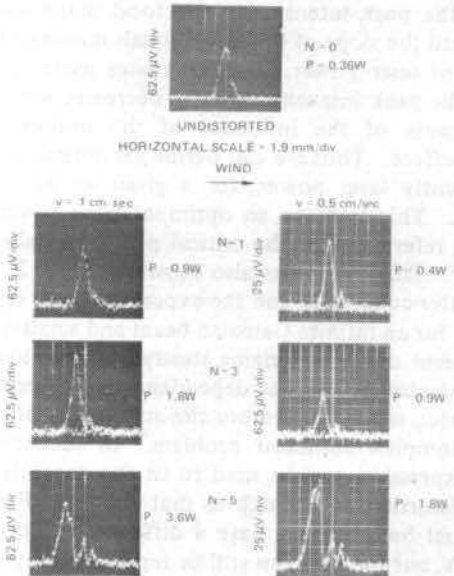


Fig. 20. Intensity contours of thermally distorted  $\text{CO}_2$  beam taken through the center of the beam parallel to the wind direction. The upper trace is the undistorted intensity contour. The left column data was obtained with a transverse velocity of 1 cm/s and various power level as marked. The right column was obtained with a velocity of 0.5 cm/s and one half the laser power as used for the left column data. Comparison of the two columns, for equal distortion conditions, show good agreement. (note scale changes and the comparison is made for normalized intensities) [44].

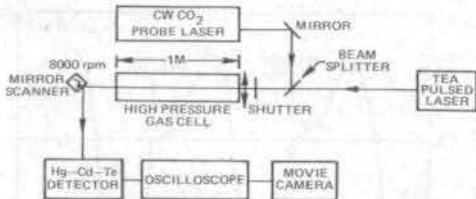


Fig. 31. Schematic diagram of experimental setup for examining multiple-pulse thermal blooming [61].

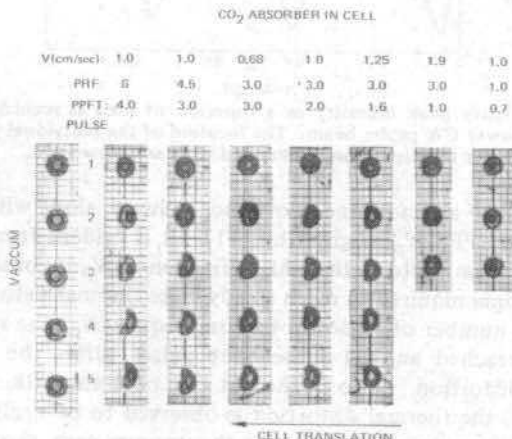


Fig. 32. Intensity contours for multiple-pulse thermal blooming as a function of the pulse number and PPFT [60].

$$\Delta \rho / \rho_0 \approx 0.4 \times 10^{-3} / \text{DIV}$$

$$\Delta \rho / \rho_0 \approx 1.0 \times 10^{-3} / \text{DIV}$$

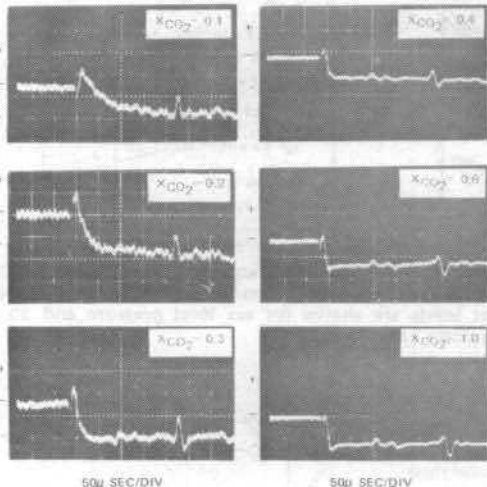


Fig. 37. Photodiode signals showing the interferometrically determined density changes in a mixture of  $CO_2$  and  $N_2$  following the irradiation of the mixture with the pulse from a  $CO_2$  TEA laser of  $\sim 1 \mu s$  and 0.5 J [8].

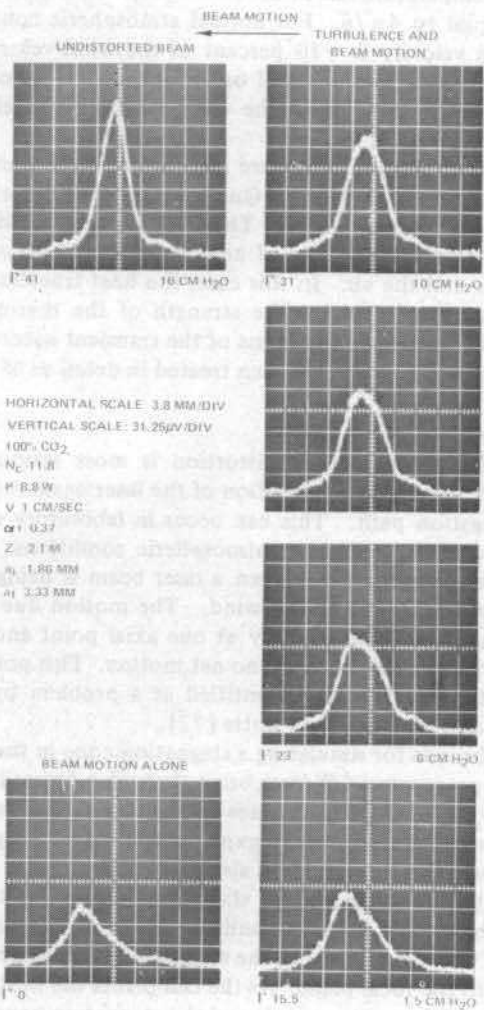
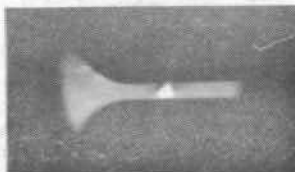


Fig. 40. Intensity contours parallel to the wind for fixed distortion conditions but variable mechanical turbulence strength [69].

$IM \approx 1.17$  AT BEAM LOCATION!



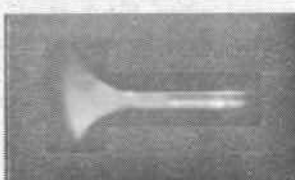
(a) NO FLOW, NO  $10.6 \mu$   
LASER FLUX



(b) NO FLOW, WITH  
 $10.6 \mu$  LASER FLUX



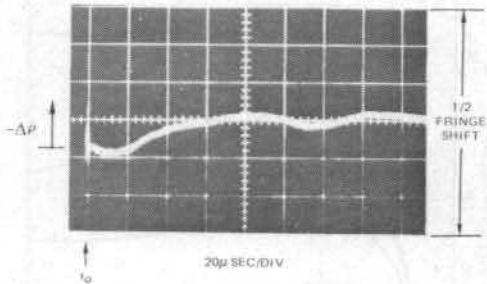
(c) FLOW AND  $10.6 \mu$   
LASER FLUX (KNIFE  
EDGE VERTICAL)



(d) FLOW AND  $10.6 \mu$   
LASER FLUX (KNIFE  
EDGE HORIZONTAL)

Fig. 46. Schlieren photographs of the laser induced density changes in a transverse flow at Mach number of 1.17 [81].

a) CO<sub>2</sub> LASER CARBON PARTICLES  $N_T = 4.1 \times 10^3 \text{ cm}^{-3}$



b) CO<sub>2</sub> LASER CARBON PARTICLES  $N_T = 4.9 \times 10^4 \text{ cm}^{-3}$

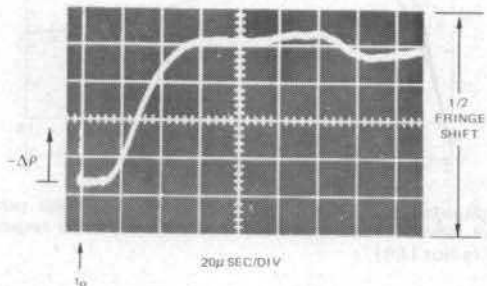


Fig. 50. Oscilloscope traces of the interferometrically determined density changes of a gas caused by aerosol absorption heating [87].

P=6W, V=1CM/SEC., m=0.5J

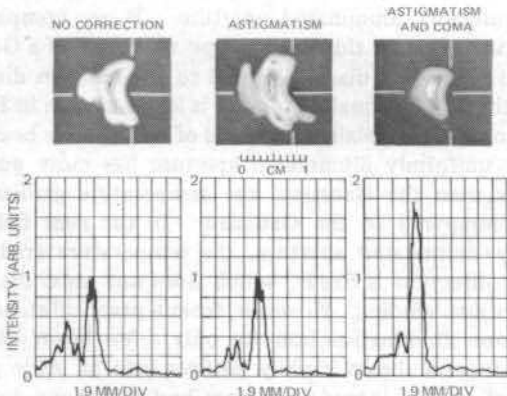


Fig. 57. Photographs of the thermally distorted intensity contours with various phase corrections added. The lower traces are the corresponding intensity profiles through the center of the beam parallel with the wind direction [92].